Application of Pulse-Decay Technique to Characterize Whole Cores

by

Jalal Hamid

A Thesis Presented to the

FACULTY OF THE COLLEGE OF GRADUATE STUDIES

KING FAHD UNIVERSITY OF PETROLEUM & MINERALS

DHAHRAN, SAUDI ARABIA

In Partial Fulfillment of the
Requirements for the Degree of

MASTER OF SCIENCE

In

PETROLEUM ENGINEERING

April, 2000

INFORMATION TO USERS

This manuscript has been reproduced from the microfilm master. UMI films the text directly from the original or copy submitted. Thus, some thesis and dissertation copies are in typewriter face, while others may be from any type of computer printer.

The quality of this reproduction is dependent upon the quality of the copy submitted. Broken or indistinct print, colored or poor quality illustrations and photographs, print bleedthrough, substandard margins, and improper alignment can adversely affect reproduction.

In the unlikely event that the author did not send UMI a complete manuscript and there are missing pages, these will be noted. Also, if unauthorized copyright material had to be removed, a note will indicate the deletion.

Oversize materials (e.g., maps, drawings, charts) are reproduced by sectioning the original, beginning at the upper left-hand corner and continuing from left to right in equal sections with small overlaps.

Photographs included in the original manuscript have been reproduced xerographically in this copy. Higher quality 6" x 9" black and white photographic prints are available for any photographs or illustrations appearing in this copy for an additional charge. Contact UMI directly to order.

Bell & Howell Information and Learning
300 North Zeeb Road, Ann Arbor, MI 48106-1346 USA
800-521-0600

Application of Pulse-Decay Technique to Characterize Whole Cores

BY

JALAL HAMID

A Thesis Presented to the

DEANSHIP OF GRADUATE STUDIES

KING FAHD UNIVERSITY OF PETROLEUM & MINERALS

DHAHRAN, SAUDI ARABIA

In Partial Fulfillment of the
Requirements for the Degree of

MASTER OF SCIENCE

In

PETROLEUM ENGINEERING

APRIL 2000

KING FAHD UNIVERSITY OF PETROLEUM AND MINERALS
DHAHRAN, SAUDI ARABIA

DEANSHIP OF GRADUATE STUDIES

This thesis, written by **Mr. Jalal Hamid** under the direction of his Thesis Advisor and approved by his Thesis Committee, has been presented to and accepted by the Dean of the Graduate Studies, in partial fulfillment of the requirements for the degree of **MASTER OF SCIENCE** in **PETROLEUM ENGINEERING.**

Thesis Committee

H. Y. Al-Yousef
Dr. Hasan Y. Al-Yousef
Thesis Advisor

Dr. Khalid A. Al-Fossail
Member

M. A. Aggour
Dr. Mohamed A. Aggour
Member

A. A. Almajed
Dr. Abdulaziz A. Al-Majid
Department Chairman

Dr. Abdallah M. Al-Shehri
Dean, College of Graduate Studies

Date: 22/5/2000

Dedication

I dedicate this work to my loving parents, brother and sister

May Allah Almighty bless them

Acknowledgement

In the name of Allah, Most Gracious, Most Merciful

First and the foremost, all praise to Allah, the Almighty Who gave me the opportunity, courage and patience to carry out this work.

I would like to express my deepest gratitude to my thesis advisor, Dr. Hasan Y. Al-Yousef for his constant support and guidance throughout the course of this research. Working with him was indeed a learning experience. I am also grateful to my thesis committee members, Dr. Khalid A. Al-Fossail and Dr. Mohamed A. Aggour, for their valuable suggestions and comments.

I am also indebted to Dr. AbdulAziz Al-Majed, Chairman Petroleum Engineering Department and all the other faculty members for their support. Many thanks are also due to all the laboratory staff members in Petroleum and Gas Engineering Section, Research Institute as well as in the Petroleum Engineering Department for their cooperation and help during the experimental work. Acknowledgement is also due to King Fahd University of Petroleum and Minerals for providing support to this work.

Last but not least, special thanks are due to my family members for their encouragement and understanding throughout my academic career, and to all my friends in and out of campus who shared my happiness and were partners in tough times.

Table of Contents

List of Tables

List of Figures

THESIS ABSTRACT

Name of Student :	**JALAL HAMID**
Title of Study :	**Application of Pulse-Decay Technique to Characterize Whole Cores**
Major Field :	**Petroleum Engineering**
Date of Degree :	**April 2000**

The application of pulse-decay method has been extended from linear core plugs to full diameter whole cores. A mathematical model, which incorporates the slippage effects, has been developed to solve the problem of transverse, unsteady compressible fluid flow through whole cores. Experimental set-up has also been constructed for performing pulse-decay experiments on whole cores. A numerical model adopting a curvilinear grid has been developed to solve the governing non-linear flow equation. Based on this numerical solution, a data analysis computer program has also been developed which calculates the permeability and Klinkenberg factor from measured pulse-decay experimental data using non-linear regression technique. Pulse-decay experiments were conducted on sandstone samples under the conditions where the data were influenced by gas slippage effects, using gas as the pore fluid. A technique has also been presented for the estimation of permeability and Klinkenberg factor from multiple pressure pulse-decay tests. The obtained results are compared with the conventional steady-state values. The proposed method is much faster and easier to perform as compared to the conventional steady-state method and can also help detect core heterogeneity.

MASTER OF SCIENCE DEGREE

KING FAHD UNIVERSITY OF PETROLEUM AND MINERALS
DHAHRAN, SAUDI ARABIA

APRIL 2000

ملخص الرسالة

اسم الطالب : جلال حامد

عنوان الرسالة : تطبيق أسلوب التلاشي النبضي لوصف العينات الصخرية الكاملة

التخصص : هندسة البترول

تاريخ التخرج : إبريل ٢٠٠٠م

لقد تم في هذه الدراسة تعميم تطبيق التلاشي النبضي من حالة العينات الصخرية الخطية إلى العينات الصخرية كاملة القطر . لقد طوِّر نموذج رياضيٌ يدمج تأثيرات انزلاق الموائع إلى صخور المكمن بغرض حل مشكلة إعتراض السوائل غير منتظمة السريان والقابلة للانضغاط خلال سريانها عند العينات الصخرية . لقد أنشأ لهذا الغرض جهاز تجريبي لأداء تجارب التلاشي النبضي على العينات الصخرية . وقد تم لهذا الخصوص تبني نموذج رقمي يتألف من خلايا ذات منحنيات خطية لحل معادلة السريان الغير خطية . بناءاً على نتائج هذا النموذج فقد أمكن تحليل هذه النتائج بإعداد برنامج حاسب آلي يمكن من حساب النفاذية ومعامل كلنكنبرغ إعتماداً في الأساس على نتائج القياسات التجريبية للتلاشي النبضي باستخدام التراجع اللاخطي .

لقد أجريت تجارب التلاشي النبضي على عينات من صخور رملية عند الظروف التي تتأثر بها النتائج بتأثيرات إنزلاق الغاز ، وذلك باستخدام الغاز كمائع يملأ المسامات الصخرية . لقد قُدِّمَ أيضاً في هذه الدراسة أسلوبٌ لتقدير النفاذية ومعامل كلنكنبرغ من اختبارات الضغط المتضاعف لتلاشي النبضات ، ولقد قورنت النتائج مع القيم الإعتيادية للسريان المنتظم .

إن الطريقة المقترحة في هذه الدراسة تعتبر أكثر سرعة وأسهل في الأداء ، مقارنة بالطرق الإعتيادية للسريان المنتظم ويمكن أيضاً أن تساعد في اكتشاف عدم التجانس في الصخور.

درجة ماجستير العلوم في هندسة البترول

جامعة الملك فهد للبترول والمعادن

الظهران ، المملكة العربية السعودية

ابريل ٢٠٠٠م

CHAPTER 1

INTRODUCTION

Permeability is the property of a porous material that characterizes the ease with which a fluid may be made to flow through the material by an applied pressure gradient. The measurement of permeability of a porous rock or stratum, is thus a measurement of the fluid conductivity of the particular material. Permeability of the reservoir rocks is one of the major factors of concern to petroleum engineers and hydrogeologists in the production of fluids, where high permeability of the reservoir rock is desired. Similarly, fluid flow through relatively impermeable ($< 10^{-18}$ m^2 or 10^{-6} darcy) rock formations is also important to the recovery of natural resources, to understanding certain types of natural faulting, to earthquake prediction and to nuclear waste isolation.[16]

Single-phase permeability measurements can be subdivided into four major categories: those utilizing flowing liquid or gas under steady-state or unsteady-state (transient) conditions. Traditionally, permeability can be determined by a steady state, flow rate measurement. Liquid permeabilities are determined by the steady-state displacement technique where the flow rate through a core sample is monitored as a function of applied constant

pressure gradient. Darcy's Law is then applied using flow rate and pressure drop data to compute permeability.

A similar method is used for the gas flow, however, Klinkenberg[24] has reported variations in permeability as determined using gases as the flowing fluid from that obtained using liquid. These variations were ascribed to "slippage" at the fluid-solid boundary, a phenomenon that occurs when the pore sizes of rock approach the mean free path of gas. The amount of gas slippage is a function of the mean pressure of the flowing gas and of the particular rock specimen. The variation can be represented by the following linear relationship between the computed values of the gas permeability and the reciprocal of the mean pressure:

$$k_g = k_\infty \left(1 + \frac{b}{P_m} \right) \tag{1.1}$$

where k_g is the permeability of the porous medium to gas calculated according to Darcy's Law at P_m, the mean pressure of flow, k_∞ is the permeability of the porous medium to liquid and b, Klinkenberg Factor, is a constant which varies with the type of rock, type of gas and the permeability. To avoid the problem of obtaining pore-pressure-dependent gas permeabilities, permeability values are determined at different mean pressures and are then plotted against the reciprocal of mean pressure as a straight line, as indicated by the above-mentioned relationship. When this line is extrapolated to infinite mean pressure ($1/P_m$) intercept, the liquid

permeability is obtained while by dividing the slope of the line by the intercept, one can get the Klinkenberg Factor, b.

During the steady-state measurements, large volumes of fluid are passed through the sample before rate and pressure stability is achieved. The steady-state method is well suited for highly permeable rocks ($k > 1$ md) and for samples with low mineral fines content.[1]

For low-permeability cores, however, the conventional steady-state displacement methods are not feasible because the achievement of the steady-state condition is questionable, the flow rates are difficult to measure and control, measurements can last for a long time and thus, increases error accumulations, i.e., stabilization times can be prohibitively long. To complicate the situation, low-permeability rocks are usually sensitive to stress, fluid velocities and throughputs; they often contain sensitive clay minerals and fines and are susceptible for damages caused by floods.[7]

As numerous low-quality reservoirs worldwide still present a considerable potential for hydrocarbon production, a method for determining permeability with precision and reasonable speed can thus, be quite important when one is to characterize a low-permeability reservoir. Hence, considerable attention was paid to the investigation of these rocks and devising a simple and fast permeability-measurement method.

In a rock saturated with fluid, the diffusion of pressure gradient in the pore fluid is much faster than the steady-state flow of fluid itself. On the

premise that the pressure measurements are made more conveniently and accurately than the rate measurements, Brace *et al.*[3] suggested an unsteady-state technique, known as the transient flow or pressure-pulse technique, for the determination of permeability in tight cores. The transient method is essentially a measurement of the pressure gradient diffusion.

In this method, the core is confined in a cell, and two vessels are attached to both ends of the cell (Figure 1.1a). The upstream vessel is pressurized and then allowed to equilibrate with the core and the downstream vessel; the pressure-decay with time is closely monitored. As indicated by Brace *et al.* and subsequently discussed by other investigators, the pressure-decay characteristics are dependent upon dimensions of the sample and vessels, fluid characteristics and the sample permeability, i.e., the decay will be slower for samples with lower permeability and vice versa. The pressure-time behavior of the vessels (Figure 1.1b) is then used with analytical solutions to calculate permeability. This technique is relatively simple and enables very fast and accurate permeability measurements particularly in low-permeability samples. Several modifications to this technique have since been proposed and are discussed in chapter 2.

Existing methods of permeability determination include **a)** "core plug" analysis in which measurements are made on small (1 to 2 inches long) cylindrical samples drilled from the whole core and, **b)** "whole core" analysis in which measurements are made through full diameter cores.

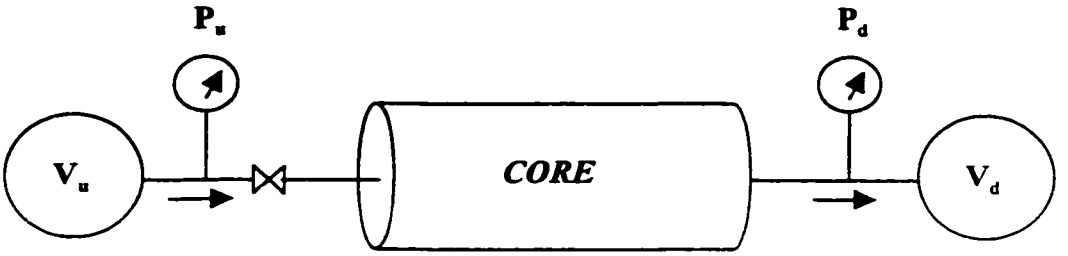

Figure 1.1a: Pulse-Decay Test Method

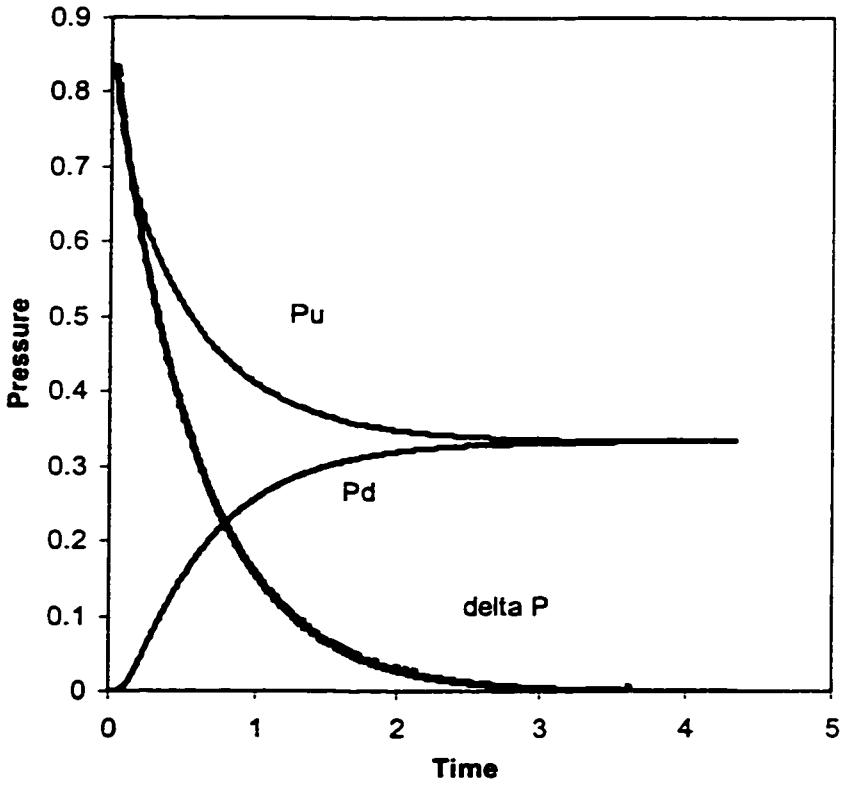

Figure 1.1b: Pressure-Time Data from Pulse-Decay Test Method

Geological formations are not usually homogeneous with regard to lithology and structure. Measurements of permeability in core samples of inhomogeneous rocks are susceptible to errors resulting from inadequate sample size and shortcomings inherent in the existing techniques (Figure 1.2).[15] In non-uniform formations, plug analysis simply employs too small a sample to be representative of the formation. Furthermore, the measurement may be unreliable where large permeability anisotropies exist.[15]

Whole core samples are much more representative of the formation since the sample is both larger in volume and more nearly complete in vertical continuity and thus, permit considerable permeability averaging. Besides this, on oriented whole core samples, orthogonal measurements can be made to determine directional permeability. Whole core techniques may, nevertheless, produce inaccurate and thoroughly misleading data. The measurements are susceptible to error in the vertically veined or fractured samples.

The aim of this study is to apply the pressure pulse-decay technique on whole cores for permeability determination and compare the results with that of conventional steady-state techniques.

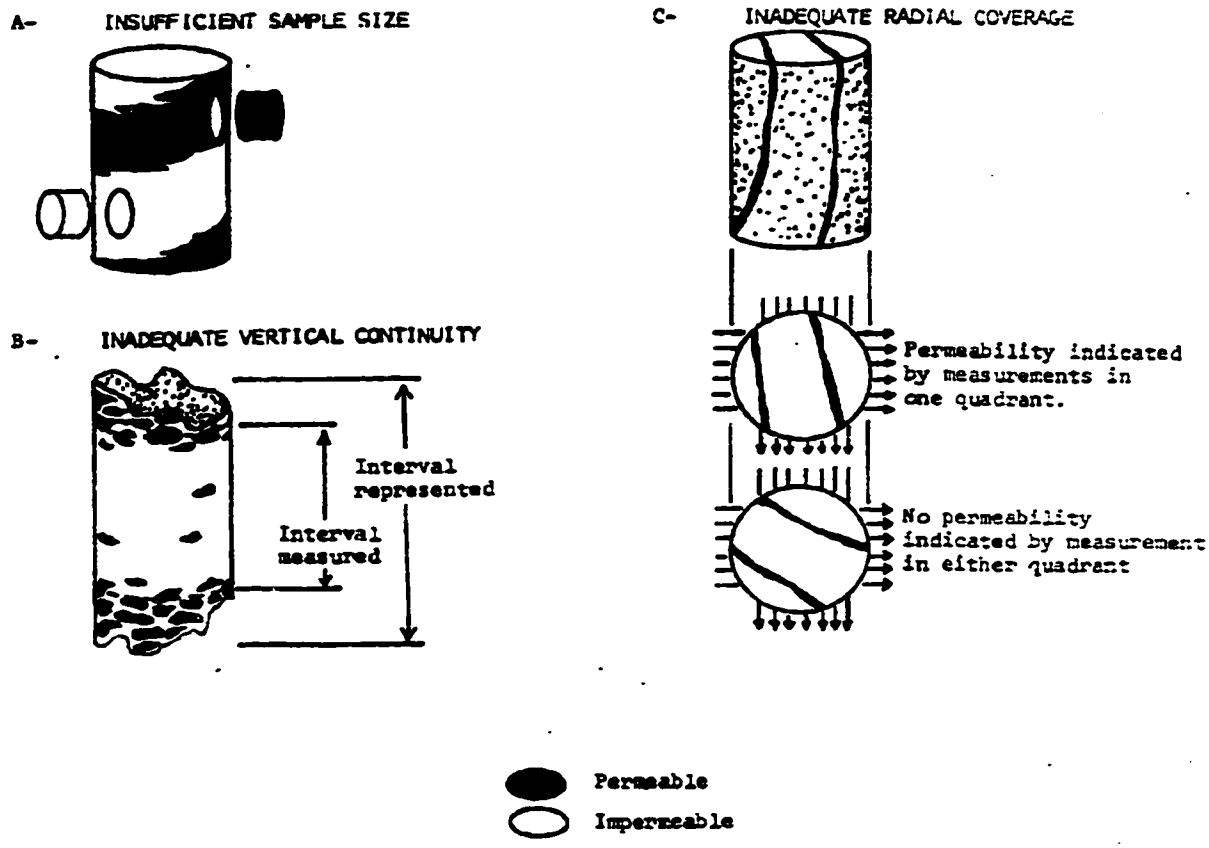

Figure 1.2: Defects in Existing Permeability Methods used on Inhomogeneous Cores [15]

CHAPTER 2

LITERATURE REVIEW

The desire to accurately characterize hydrocarbon reservoirs and to estimate the deliverability of very tight gas reservoirs has created a growing demand for reliable permeability measurements.

Various methods are used to determine the permeability of reservoir rocks. The conventional steady-state method is time-consuming and not particularly suited to low-quality rocks. If the permeability measurements are to be made on whole cores, the situation can become even more cumbersome as the stabilization/measurement time can be prohibitively long thus increasing error accumulations. Because of its usefulness in measuring very low-permeability, the pulse-decay technique has been discussed often in the literature. In this chapter, we review the work done by various researchers regarding the application of the pulse-decay technique in general, and permeability determination of whole cores, in particular.

Collins (1952)[21] presented the solution of the problem of determining the permeabilities of the petroleum reservoir rocks from measurements employing the steady-state flow of a gas through large cylindrical cores, transverse to the axis of the cores. This solution was obtained by solving the corresponding problem in potential theory and employing the method of conformal transformation of complex variable.

Brace, Walsh and Frangos (1968)[3] pioneered the pressure-pulse technique for performing laboratory permeability measurements on geologic materials having water permeabilities less than 10^{-18} m^2 or 10^{-6} darcy. They found it more convenient to use a transient method for permeability measurement, that is, to observe the decay of a small step change of pressure imposed at one end of a sample. Based on the assumptions that the compressibility of the rock matrix is negligible compared with that of the pore fluid, and that the pore volume of the sample is negligible compared to the volume of downstream vessel, Brace *et al.* gave an approximate solution to pulse-decay problem which leads to an exponential pressure vs. time decay. Permeability of the sample is obtained by comparing the observed pressure decay with the behavior predicted theoretically.

Jones (1972)[10] developed a simple, unsteady-state apparatus and appropriate theory for the rapid measurement of the core plug Klinkenberg

permeabilities ranging from about 0.001 md to 1000 md. The unsteady-state technique also determines one or two turbulence factors for cores that depart from Darcy flow behavior. The method reproduces the steady-state permeability determinations to within about ± 2 percent.

Yamada and Jones (1980)[17] showed, by both mathematical formulations and numerical analysis, that the Brace *et al.*'s solution can lead to significant errors in calculating permeability if the pore volume of the sample is not negligible compared with the upstream and the downstream vessel volumes. Exponential pressure decay is, thus, not always observed and various factors, such as upstream and downstream volume and specimen size control the pressure behavior.

Hsieh, Tracy, Neuzil, Bredehoeft and Silliman (1981)[23] proposed a general analytical solution for the transient pulse technique. They showed that the proposed general solution contains, as limiting cases, the analytical solutions that previous investigators had derived under more restrictive assumptions. Plots of dimensionless variables were used to illustrate the general nature as well as the limiting behavior of the solution.

Neuzil, Cooley, Silliman, Bredehoeft and Hsieh (1981)[25] presented in continuation of Hsieh *et al.*'s work, a graphical method utilizing type curves

for analyzing the time history data from a pulse decay test to obtain the hydraulic properties of the sample. They suggested that the ratio of the compressive storage in the sample to that in the upstream vessel should vary between 0.01 to 10 for simultaneous determination of hydraulic conductivity and specific storage. Similarly, for a sample with significant compressive storage, a large upstream vessel is required. Reasonable vessel volume values lie in the range of milliliters to 1-2 liters. Furthermore, they proposed that to minimize the time required for the test, the sample length should be kept as small as possible.

Lin (1982)[13] compared the Brace *et al.*'s simplified version of transient pulse-decay method with the numerical version suggested by Lin (1977). As discussed earlier, the Brace *et al.*'s solution assumes negligible pore volume, which leads to exponential pressure decay with time. Lin's (1977) numerical version used finite difference method to solve the differential equation of pressure decay and matched the observed pressure decay with the calculated decay curves which are not generally simple exponential function of time, as suggested by the simplified version. The comparison showed that the numerical version fits the observed data very well, whereas, the permeability value determined by the simplified version tends to be greater than that determined by the numerical version. The difference in the permeability between the two depends on many factors such as rock

properties (porosity and compressibility), sample size and vessel volumes. Both versions give close agreement provided the conditions for the simplified versions are met, i.e., small rock compressibility and porosity, which leads to small fluid storage capacity. Furthermore, the numerical version has its own limitations. The curve matching procedures used in the numerical version are not as convenient as the simplified version; the input data, especially, the porosity and compressibility should be close to that of the rock sample at experimental conditions.

Trimmer (1982)[16] also discussed the advantages and limitations of the two versions of the pulse technique, i.e., Brace *et al.*'s simplified analytical version and the modified and more general numerical version proposed by Trimmer (1980) and Lin (1982). He found that in designing permeability experiments, the technique described by Brace *et al.* should be used when possible because it is simple and fast. This requires that the sample pore volume should be small as compared to the vessel volume; otherwise, there is a systematic error attached with Brace *et al.*'s version, which is a function of the ratio of effective sample pore volume to the vessel volume. If this ratio is less than 0.25, then the associated error is less than 10%. If the experimental parameters cannot be adjusted to take advantage of the Brace *et al.*'s version, then the technique described by Trimmer (1980) and Lin (1982) may be used, which places no restriction on the ratio of the sample

pore volume to the reservoir size. Therefore, the time required for a measurement can also be adjusted by varying the reservoir size.

Bourbie and Walls (1982)[2] proposed a new analytical solution, known as the error-function solution for the laboratory pulse-decay permeability problem. The predicted decay curves obtained using this solution matched closely the ones obtained experimentally. Permeabilities calculated from their solution were within ± 5% of steady-state measurements over a wide range of permeability values.

Freeman and Bush (1983)[6] recommended the use of downstream pressure buildup data rather than the upstream pressure draw-down data. In their view, the downstream approach allowed the use of the smallest possible downstream volumes leading to the detection of very small flow rates in a relatively short time. Also, this helps in making the system temperature-insensitive. The pressure buildup data is used to determine the flow rate out of the sample, which is then used in Darcy's equation for one-dimensional flow, corrected by the Klinkenberg relation for slippage. They claimed that their method is not particularly sensitive to values for 'b' because of the relatively high mean pressures used. Values obtained were less than ± 5% of steady-state values.

Chen and Stagg (1984)[4] presented an alternative solution to the system of equations describing the pulse-decay technique of permeability measurements. In this solution, the sample pore volume is not ignored, and the experimental data is analyzed by using the slope of a semi-log plot to evaluate permeability. Chen *et al.* also pointed out that the error-function solution of Bourbie *et al.* is valid for a dimensionless time, t_D, of less than unity and a ratio of sample pore volume to downstream volume, γ, of less than 0.6. However, the proposed solution is not restricted by t_D or γ and, it reduces to an exponential-decay solution similar to that of Brace *et al.* when $t_D > 0.3$. Furthermore, they also found that the Brace *et al.*'s solution underestimates the permeability and the degree of underestimation is dependent on γ.

Amaefule, Wolfe, Walls, Ajufo and Paterson (1986)[1] reviewed the mathematical computational techniques and outlined proper experimental protocols for accurate determinations of effective liquid permeability in low-quality rocks. Effective oil and water permeabilities ranging in values from 0.5 to 2.9×10^{-4} md were determined by this technique with excellent reproducibility. They also investigated the effect of pore pressure depletion on effective oil and water permeabilities. They found out that effective oil and water permeabilities for some low-quality rocks were stress-sensitive, thus, making it necessary that these parameters are calculated at in-situ stress

conditions. Use of "zero porosity" approximation as suggested by Brace *et al.* was found to be susceptible to substantial error.

Haskett, Narahara and Holditch (1988)[9] presented an analytical model for unsteady-state gas-flow through a core. This analytical model can be used in conjunction with a history-matching technique (i.e., by history matching the analytical solution to the measured test data) to determine the porosity and permeability. In history-match, there are only two unknowns, i.e., porosity and permeability. A unique match of porosity for any given pressure decay is essentially ensured because the final pressure is solely dependent on porosity. Because the porosity is fixed, the single best value for permeability is also fixed. The results from this method showed good agreement with both numerically simulated and actual core data.

Dicker and Smits (1988)[5] analyzed the exact solution of the differential equation describing the decay curve resulting from a pressure-pulse measurement to study the effect of various parameters in the design of pressure-pulse permeameter. They re-wrote the solution of the differential equation in dimensionless form such that the symmetry of the experimental set-up was reflected in the equation. This was done by choosing the ratios of pore volume over upstream volume and the pore volume over downstream volume as independent parameters. In this way, the influence of the

experimental conditions on the pressure decay curve could be studied more easily. Dicker *et al.* found that fast and accurate measurements are possible when taking the upstream and downstream vessels in the equipment approximately equal to the pore volume of the sample. Also, a simple approximate solution was proposed which was accurate to within 0.3% of the exact solution.

Gilicz (1991)[7] applied the pulse-decay technique for radial cores. He described the experimental set-up, analytical solutions of the governing equation, and their applications to the measurements. The proposed analytical solution is general; no assumptions of negligible pore volume storage were made. To determine porosity and permeability, the core pressure response is to be matched with analytical solution. For determination of these unknowns, a stable direct search algorithm is also presented. The results obtained by this method were in agreement with conventionally obtained porosity and permeability values.

Kamath, Boyer and Nakagawa (1992)[12] developed new analytical methods and an experimental set-up to accurately and rapidly measure the permeability of homogeneous cores, matrix and fracture properties of fractured rocks and the individual properties of a butted core sample. They showed that the effective permeability calculated from a pressure-transient

test can be a function of the direction of the pressure disturbance and can differ significantly from the effective steady-state value. Also, the simplified analysis techniques (e.g., late-time solution) that are often used may yield erroneous values if the core is heterogeneous. They also found that the pressure-transient response of a heterogeneous core appears similar to that of a homogeneous core for small value of the ratio of compressive storage of core to that of upstream vessel. As this ratio increases, the response deviates, thus, revealing the core heterogeneity. It was also pointed out that the use of small vessels lead to need of increased frequency of pressure measurement because pressure decays quickly in small vessels.

Jones (1994)[11] suggested some ways to significantly reduce the total time required for pulse-decay experiments. He presented a modified experimental set-up, which can not only eliminate the time-consuming pressure equilibrium step but can also increase the permeability measurement range. By analyzing the existing mathematical formulations, he also suggested to use cores with large diameter and short length; the upstream and downstream reservoir volumes be equal to keep a constant mean pore pressure; the reservoir volumes be 2-10 times higher than that of the pore volume to reduce sensitivity to heterogeneity. He also pointed out that although, the early time behavior as treated by Kamath *et al.* is a powerful tool for

investigating heterogeneity in core plugs, more information is generally required to describe the heterogeneity fully.

Guo and Wong (1996)[8] presented an alternative method to conduct pressure decay tests without using upstream and downstream reservoirs. Mobility is calculated from the pressure decay in the sample using the finite difference method. Advantages of this technique include the elimination of reservoirs, high speed, and ability to analyze poorly controlled upstream and downstream pressures. The estimated values from this method are comparable to those obtained from steady-state measurements.

2.1 Statement of the Problem

It is apparent from the preceding literature review that significant work has been done in the development and application of pulse-decay technique for permeability measurements. However, most of the analytical, numerical and experimental work has been developed for linear core plugs only. For the case of whole cores, not much information is available; also apparently, only one experimental study for the permeability measurement using pulse-decay technique has been conducted on radial whole cores.[7] However, there are couple of problems associated with the radial whole core permeability measurements; first, the drilling of a hole in the center of the whole core sample may damage the sample and second, the measurements cannot be

carried out in different directions which can lead to unreliable permeability values if large permeability anisotropies exist. Furthermore, it requires elaborate sample preparation and more time and skill on the part of the analyst. It is thus more costly than the conventional methods.[15]

Measurement of permeability in core samples of inhomogeneous rocks using core plug analysis is susceptible to errors due to inadequate sample size. On the other hand, the whole core samples are much more representative of the formation since the sample is larger in volume and thus, the permeability measurements using transverse flow through whole core samples are more reliable.

Thus, there is a need to experimentally apply the pulse-decay technique on whole cores for permeability measurements and to compare the results with those from the conventional steady-state technique.

CHAPTER 3

OBJECTIVES OF THE STUDY AND ADOPTED APPROACH

3.1 Objectives of the Study

The objectives of this study were to

- Apply the pulse-decay technique for the permeability determination of tight whole core samples.
- Develop a procedure to analyze the test data to obtain permeability.

Results would enable a more accurate characterization of the tight and heterogeneous rocks.

3.2 Adopted Approach

In order to accomplish the objectives of this study, the following approach was adopted.

- An experimental set-up was constructed to perform pulse-decay tests on tight whole cores.
- Pulse-decay experiments were conducted on whole cores.
- A finite difference model (in curvilinear coordinate system) was developed to describe the transverse fluid flow through the whole core.

- The experimental data along with the numerical solution were used to determine the permeability using non-linear regression technique, i.e., by matching the observed decay curves with the numerically calculated curves.
- Steady-state experiments were conducted on whole cores to obtain permeability and results were compared with those obtained from the pulse-decay technique.

CHAPTER 4

MATHEMATICAL MODEL

In this chapter, detailed description of the mathematical model developed for this study is presented. The finite difference representation of the governing differential equation and the development of the grid system are also described. A brief account of the computer program developed for the analysis of experimental data using non-linear regression is also provided.

4.1 The Model Flow Equation

The forthcoming development of the equation governing the transient flow of compressible fluids in porous media is based upon the following assumptions:

1. Single-phase, isothermal gas flow
2. Two-dimensional flow
3. Isotropic and homogeneous incompressible medium
4. Rock properties such as permeability and porosity are constant

The fundamental equation describing the transient flow of real gases in porous medium was derived using the principle of conservation of mass,

Darcy' s law, Kilinkenberg equation and the equation of state. The model flow equation in radial coordinate system is given as,

$$\frac{1}{r}\frac{\partial}{\partial r}\left[r\frac{P}{\mu_g z}\left(1+\frac{b}{P}\right)\frac{\partial P}{\partial r}\right]+\frac{1}{r^2}\frac{\partial}{\partial \theta}\left[\frac{P}{\mu_g z}\left(1+\frac{b}{P}\right)\frac{\partial P}{\partial \theta}\right]=\left(\frac{\varphi c_g}{k_l}\right)\frac{P}{z}\left(\frac{\partial P}{\partial t}\right) \qquad (4.1)$$

where

k_l = *Liquid Permeability*

μ_g = *Gas Viscosity*

c_g = *Gas Compressibility*

z = *Gas Deviation Factor*

φ = *Porosity of whole core sample*

Figure 4.1 shows the schematic of a typical pulse-decay experimental set-up for transverse permeability measurement of whole core samples. Two mesh screens of equal width, covering a subtended angle θ, are placed on opposite ends of the core sample parallel to the axis of core and running the full length (Figure 4.2a). Fitted around the core and the screens is a rubber sleeve. The application of confining pressure seals the rubber sleeve to the core thus preventing any bypass flow around the core. Figure 4.2b shows the boundary conditions for transverse permeability problem. Here only one-half of the circle is considered because of the symmetry in flow geometry.

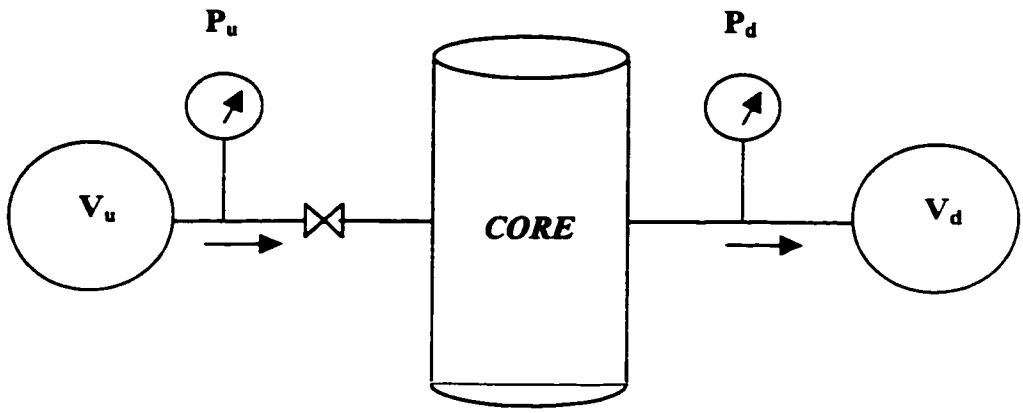

Figure 4-1: Pulse-Decay Experimental set-up for transverse permeability determination of whole cores

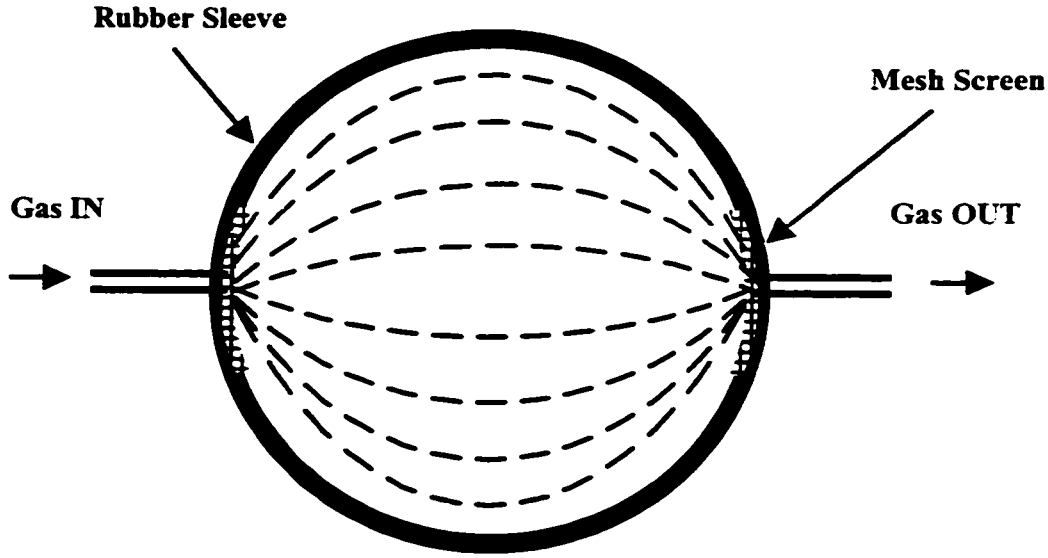

Figure 4.2a: Plan view of the transverse flow arrangement

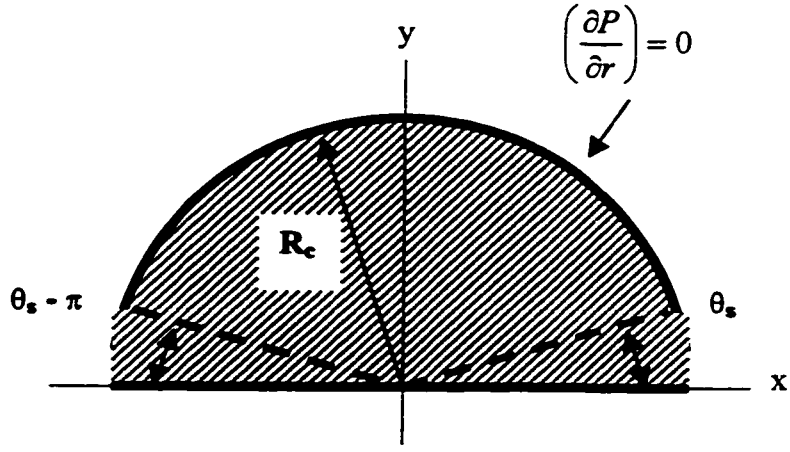

Figure 4.2b: Boundary conditions for transverse flow problem

4.2 Initial and Boundary Conditions

4.2.1 Initial Condition

At t = 0,

$$P_u(0) = P_U \qquad \textit{for upstream cell} \qquad (4.2)$$

$$P_d(0) = P_D \qquad \textit{for core and downstream cell} \qquad (4.3)$$

4.2.2 Boundary Conditions

At t > 0,

$$P(r,\theta,t) = P_u(t) \qquad \textit{for} \quad 0 \le \theta \le \theta_s \qquad (4.4)$$

$$P(r,\theta,t) = P_d(t) \qquad \textit{for} \quad (\pi - \theta_s) \le \theta \le \pi \qquad (4.5)$$

$$c_g V_u \frac{\partial P_u}{\partial t} = \frac{1}{CF}\frac{k_l h}{\mu}\left(1+\frac{b}{p}\right)\int_0^{\theta_s} r\frac{\partial p}{\partial r}d\theta\Big|_{r=R_c} \qquad \textit{for} \quad 0 \le \theta \le \theta_s \qquad (4.6)$$

$$c_g V_d \frac{\partial P_d}{\partial t} = \frac{1}{CF}\frac{k_l h}{\mu}\left(1+\frac{b}{p}\right)\int_{\pi-\theta_s}^{\pi} r\frac{\partial p}{\partial r}d\theta\Big|_{r=R_c} \qquad \textit{for} \quad (\pi - \theta_s) \le \theta \le \pi \qquad (4.7)$$

where

R_c = *Radius of whole core sample*

The remaining surface of the core sample, which is sealed by the rubber sleeve under confining pressure, is a no-flow boundary:

$$\left.\frac{\partial P}{\partial r}\right|_{r=R_c} = 0$$

Equation (4.2) states that at the start of the experiment, the pressure at the inlet lateral face is equal to upstream cell pressure whereas equation (4.3) states that the pressure in the sample is equal to the downstream cell pressure. Equations (4.4) and (4.5) indicate that the upstream and downstream faces of the sample are in direct contact with their respective cells. Equations (4.6) and (4.7) express mass conservation at the sample faces, for example, the volume of gas expansion in the upstream cell is equal to the volume that enters in the inlet end of the core sample.

4.3 The Numerical Model

4.3.1 Curvilinear Grid Generation

Various researchers[22,27] have proposed to use the Curvilinear coordinate system as an alternative to Cartesian and Radial coordinates for the simulation of the flow geometry. Hirasaki and O' Dell[22] suggested that the flow geometry for complex problems can be more accurately modeled by adopting curvilinear coordinates. They proposed that the cross-section of a reservoir could be represented by a system of curvilinear coordinates in such a way that the curvilinear surfaces coincide with the reservoir surfaces. The

finite difference equations presented by them were different from the standard formulation using Cartesian coordinates in that they include cross partial terms as well as a factor multiplying the pore volume and transmissibilities caused by the metric tensor. Sonier and Chaumet[27] proposed to use a system of curvilinear coordinates in the plane of the reservoir layer so as to obtain a mesh network and the elements required for directly writing the finite difference equations relating to the mass conservation equations without going through metric tensors because the latter would be too difficult to compute in general cases.

For our system, Curvilinear coordinates that coincide with the orthogonal network of streamlines and isopotential lines of a steady-state single-phase flow were developed. The isopotential lines and the streamlines, which are solution to the Laplace equation for homogeneous, isotropic system, are obtained by using the conformal mapping technique.[18] This involves combining a complex potential $w(z)$, with potential ϕ and the streamline ψ. Once $w(z)$ is obtained, ϕ is the real part of $w(z)$ and the streamline ψ is the imaginary part of $w(z)$.

Collins[18] presented conformal transformation equations for transverse permeability problem. The conformal mapping

$$w = -i \ln(\frac{z}{R}) \qquad (4.8)$$

yields the region of flow as semi-infinite strip in the w plane. Then a second conformal mapping

$$w' = \frac{\sin(w)}{K} \qquad (4.9)$$

transforms the region of flow to the whole upper half of the w' plane. Here

$$K = \sin\left(\frac{\pi}{2} - \theta_s\right) = \cos(\theta_s) \qquad (4.10)$$

Finally, by taking the inverse of the transformation

$$w' = \int_0^{w''} \frac{d\xi}{(1-\xi^2)^{1/2}(1-k^2\xi^2)^{1/2}} \qquad (4.11)$$

the flow domain is transformed from the upper half of the w' plane into the rectangle in w'' plane. The whole series of conformal mappings is depicted in Figure 4.2. Then, by applying the same transformations in reverse order, the grid system shown in Figure 4.3 is obtained.

If the isopotential lines and the streamlines are used as grid coordinates, then the governing partial differential equation is given as,

$$\frac{\partial}{\partial\phi}\left[F\frac{\partial P}{\partial\phi}\right] + \frac{\partial}{\partial\psi}\left[F\frac{\partial P}{\partial\psi}\right] = CF\sqrt{g}\frac{\varphi}{k_l}G\left(\frac{\partial P}{\partial t}\right) \qquad (4.12)$$

where

$$F = \frac{P+b}{\mu_g z}$$

$$G = \frac{Pc_g}{z}$$

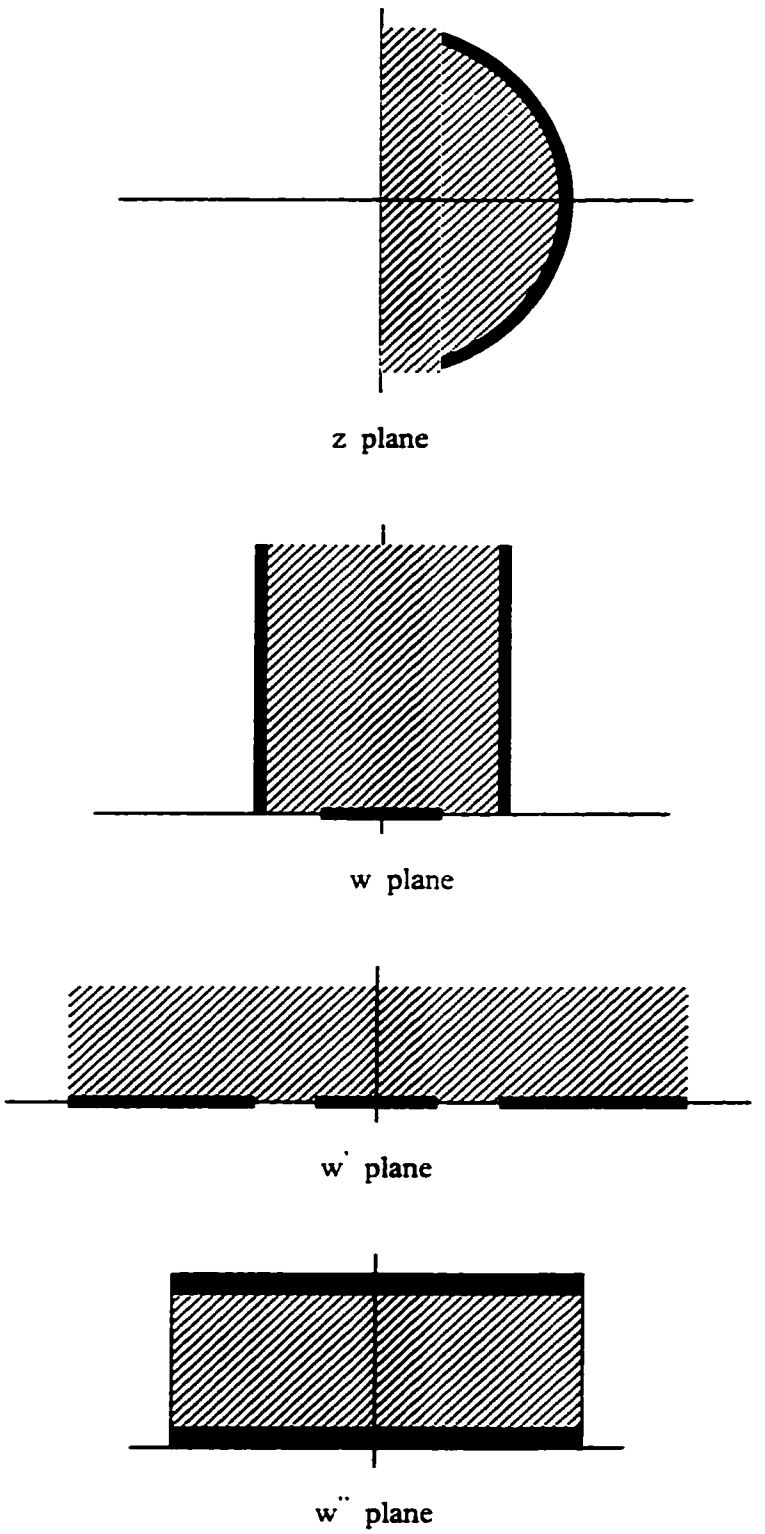

Figure 4.3: Conformal Mapping of transverse permeability problem

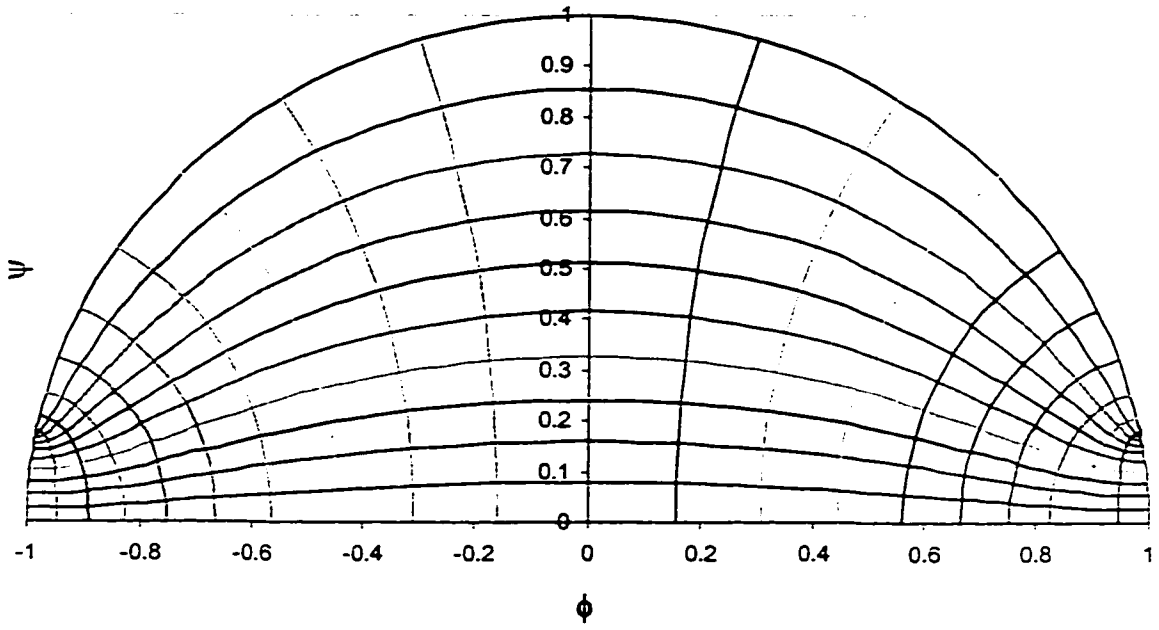

Figure 4.4: Grid System for Curvilinear Coordinates

CF = Units Conversion Factor

$\sqrt{g}$ = *Determinant of the metric tensor*

The matrix tensor relates increments of distance, area and volume to products of coordinate increments. It may be interpreted as "*shape operator*" which relates a curved grid block in a curvilinear coordinate system to a rectangular grid block in Cartesian coordinate system.[22]

Due to the non-linearity of equation (4.12), it is not possible to obtain an analytical solution for the transient compressible fluid flow equation. Thus, a numerical solution has been developed for the governing partial differential equation.

4.3.2 Finite Difference Equation

The equation describing the fluid flow in curvilinear coordinates system presented above was solved using the finite difference technique. A two-dimensional, single-phase, finite difference model, simulating the fluid flow was used to obtain the solution and compute the permeability from the measured experimental data. After incorporating the boundary conditions, the finite difference equations are given as,

Cell i = 1 , j *(Upstream cell)*

$$\left\{k\left(-\frac{\Delta\phi}{\Delta\psi}\right).F_{i,j-\frac{1}{2}}\right\}P^{n+1}_{i,j-1}+\left[k.F_{i,j-\frac{1}{2}}+k\left(\frac{2\Delta\psi}{\Delta\phi}\right).F_{i,j}+k.F_{i,j+\frac{1}{2}}+k\left(\frac{CF.V_{p_{i,j}}G}{\Delta t}\right)\right]P^{n+1}_{i,j}$$
$$+\left\{k\left(-\frac{2\Delta\phi}{\Delta\psi}\right).F_{i,j}\right\}P^{n+1}_{i+1,j}+\left\{-k.F_{i,j+\frac{1}{2}}\right\}P^{n+1}_{i,j+1}=\left(\frac{CF.V_{p_{i,j}}G}{\Delta t}\right)P^{n}_{i,j}$$

(4.13)

Cells i = 2 to N-1 , j *(Core)*

i = 2 , j

$$\left\{k\left(-\frac{\Delta\phi}{\Delta\psi}\right).F_{i,j-\frac{1}{2}}\right\}P^{n+1}_{i,j-1}+\left\{k\left(-\frac{2\Delta\psi}{\Delta\phi}\right).F_{i-\frac{1}{2},j}\right\}P^{n+1}_{i-1,j}+$$
$$\left[k\left(\frac{\Delta\phi}{\Delta\psi}\right).F_{i,j-\frac{1}{2}}+k\left(\frac{2\Delta\psi}{\Delta\phi}\right).F_{i-\frac{1}{2},j}+k\left(\frac{\Delta\psi}{\Delta\phi}\right).F_{i-\frac{1}{2},j}+k\left(\frac{\Delta\phi}{\Delta\psi}\right).F_{i,j-\frac{1}{2}}+\left(\frac{CF.V_{p_{i,j}}G}{\Delta t}\right)\right]P^{n-1}_{i,j}$$
$$+\left\{k\left(-\frac{\Delta\phi}{\Delta\psi}\right).F_{i+\frac{1}{2},j}\right\}P^{n+1}_{i+1,j}+\left\{k\left(-\frac{\Delta\psi}{\Delta\phi}\right).F_{i,j-\frac{1}{2}}\right\}P^{n+1}_{i,j+1}=\left(\frac{CF.V_{p_{i,j}}G}{\Delta t}\right)P^{n}_{i,j}$$

(4.14)

i = 3 to N-2 , j

$$\left\{k\left(-\frac{\Delta\phi}{\Delta\psi}\right).F_{i,j-\frac{1}{2}}\right\}P^{n+1}_{i,j-1}+\left\{k\left(-\frac{\Delta\psi}{\Delta\phi}\right).F_{i-\frac{1}{2},j}\right\}P^{n+1}_{i-1,j}+$$
$$\left[k\left(\frac{\Delta\phi}{\Delta\psi}\right).F_{i,j-\frac{1}{2}}+k\left(\frac{\Delta\psi}{\Delta\phi}\right).F_{i-\frac{1}{2},j}+k\left(\frac{\Delta\psi}{\Delta\phi}\right).F_{i+\frac{1}{2},j}+k\left(\frac{\Delta\phi}{\Delta\psi}\right).F_{i,j+\frac{1}{2}}+\left(\frac{CF.V_{p_{i,j}}G}{\Delta t}\right)\right]P^{n+1}_{i,j}$$
$$+\left\{k\left(-\frac{\Delta\phi}{\Delta\psi}\right).F_{i+\frac{1}{2},j}\right\}P^{n+1}_{i+1,j}+\left\{k\left(-\frac{\Delta\psi}{\Delta\phi}\right).F_{i,j+\frac{1}{2}}\right\}P^{n+1}_{i,j+1}=\left(\frac{CF.V_{p_{i,j}}G}{\Delta t}\right)P^{n}_{i,j}$$

(4.15)

i = N – 1 , j

$$\left\{k\left(-\frac{\Delta\phi}{\Delta\psi}\right)F_{i,j-\frac{1}{2}}\right\}P^{n+1}_{i,j-1}+\left\{k\left(-\frac{\Delta\psi}{\Delta\phi}\right)F_{i-\frac{1}{2},j}\right\}P^{n+1}_{i-1,j}+$$

$$\left[k\left(\frac{\Delta\phi}{\Delta\psi}\right)F_{i,j-\frac{1}{2}}+k\left(\frac{\Delta\psi}{\Delta\phi}\right)F_{i-\frac{1}{2},j}+k\left(\frac{2\Delta\psi}{\Delta\phi}\right)F_{i-\frac{1}{2},j}+k\left(\frac{\Delta\phi}{\Delta\psi}\right)F_{i,j-\frac{1}{2}}+\left(\frac{CF.V_{p_{i,j}}G}{\Delta t}\right)\right]P^{n+1}_{i,j}$$

$$+\left\{k\left(-\frac{2\Delta\phi}{\Delta\psi}\right)F_{i-\frac{1}{2},j}\right\}P^{n+1}_{i-1,j}+\left\{k\left(-\frac{\Delta\psi}{\Delta\phi}\right)F_{i,j-\frac{1}{2}}\right\}P^{n+1}_{i,j+1}=\left(\frac{CF.V_{p_{i,j}}G}{\Delta t}\right)P^{n}_{i,j}$$

(4.16)

i = N , j *(Downstream cell)*

$$\left\{k.F_{i,j-\frac{1}{2}}\right\}P^{n+1}_{i,j-1}+\left\{k\left(-\frac{2\Delta\psi}{\Delta\phi}\right)F_{i,j}\right\}P^{n+1}_{i-1,j}+$$

$$\left[k.F_{i,j-\frac{1}{2}}+k\left(\frac{2\Delta\psi}{\Delta\phi}\right)F_{i,j}+k.F_{i,j-\frac{1}{2}}+\left(\frac{CF.V_{p_{i,j}}G}{\Delta t}\right)\right]P^{n+1}_{i,j}$$

$$+\left\{-k.F_{i,j-\frac{1}{2}}\right\}P^{n+1}_{i,j+1}=\left(\frac{CF.V_{p_{i,j}}G}{\Delta t}\right)P^{n}_{i,j}$$

(4.17)

"*F*" is the Harmonic Mean of the values of function 'F'; for example, at the junction of cells (i , j) and (i , j+1), it is given as

$$F_{i,j-\frac{1}{2}}=\left(\frac{2F_{i,j}F_{i,j+1}}{F_{i,j}+F_{i,j+1}}\right)$$

k is the permeability and is equal to k_l, the liquid permeability, except for the first and last cell. To simulate the upstream and downstream cells, very large values of permeability are assigned to the first and last cell, i.e., in

equations (4.13) and (4.17), thus ensuring that there is no pressure variation in upstream and downstream cells.

The area of the grid cell is calculated by using the respective grid coordinates in the following equation:

$$\Delta A_{i,j} = \frac{1}{2}\left|(x_1 - x_2)(y_1 + y_2) + (x_2 - x_3)(y_2 + y_3) + (x_3 - x_4)(y_3 + y_4) + (x_4 - x_1)(y_4 + y_1)\right|$$

Subsequently, the pore volume of the grid cells is given by

$$V_{p_{i,j}} = \Delta A_{i,j} h \varphi$$

4.4 The Computer Model

Based on the above finite difference equations, a computer program was developed in Fortran Language for the simulation of the pulse-decay experiment and generation of pressure decay data with respect to time.

Using the same numerical scheme, two more computer programs, i.e., with and without slippage, were also developed for the analysis of the pulse decay experimental data using the non-linear regression technique. Subroutine DRNLIN from the IMSL library, which fits a non-linear regression model using least squares, has been used. A simplified flow chart of the data analysis program is shown in Figure 4.5. Complete listing of the computer programs is attached in Appendix. Before elaborating upon the data analysis program, a brief overview of the non-linear regression is given below.

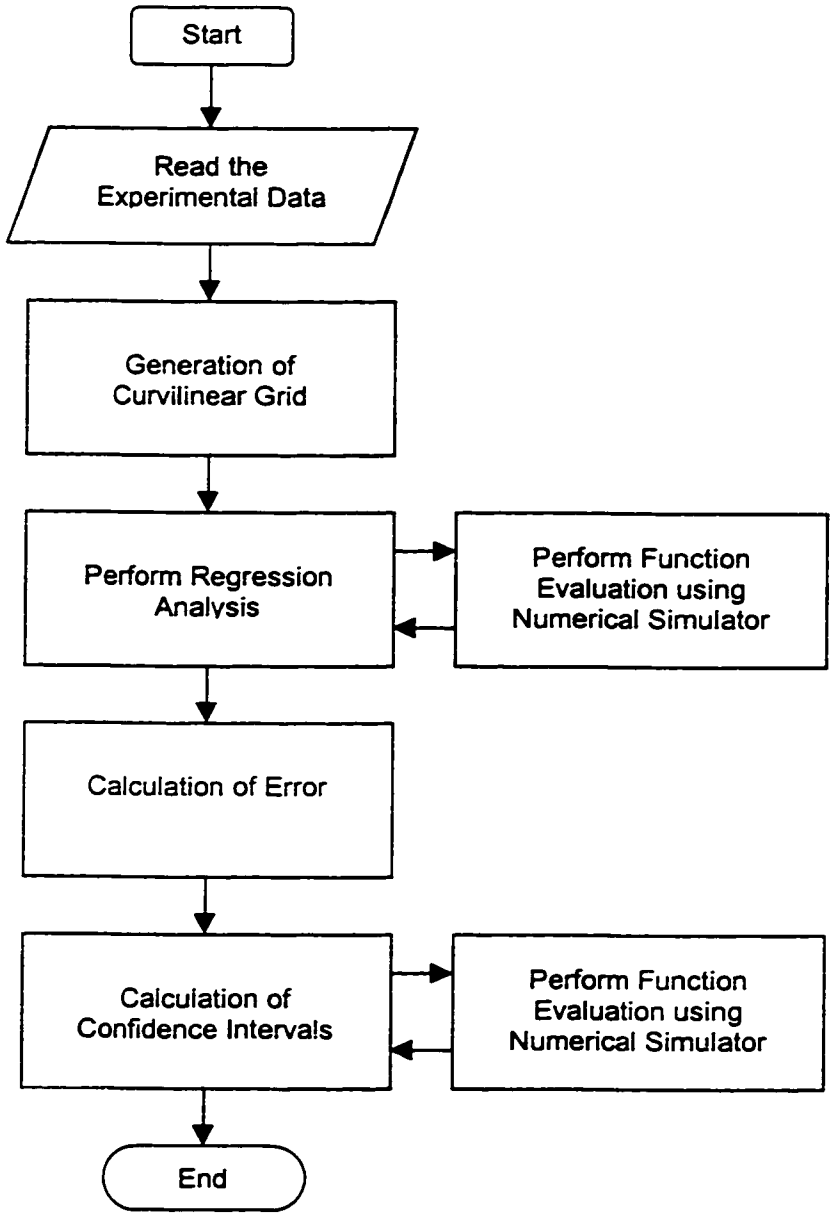

Figure 4.5: Simplified flow chart of the data analysis computer program

Nonlinear Regression is a powerful method for analyzing data described by models that are nonlinear in the parameters.

A nonlinear regression model is given as

$$y_i = f(x_i, \theta) + \varepsilon_i \qquad i = 1,2,3,\ldots n$$

where the observed values of y_i's constitute the responses or the value of the dependent variable, the x_i's are the known vectors of the independent variables, f is a known function of unknown regression parameters, θ, and the ε_i's are independently distributed normal errors with mean zero and variance σ^2.

The method of least squares is used to estimate the unknown parameters, θ, which requires the minimization of the residuals of the model, i.e.,

$$e_i(\theta) = y_i - f(x_i, \theta)$$

Values of θ that minimizes the sum of squares of the deviations of the observations from the regression model response, i.e.,

$$S = \sum_{i=1}^{n} [e_i(\theta)]^2 = \sum_{i=1}^{n} [y_i - f(x_i, \theta)]^2$$

is a least square estimate of θ. The least square estimates of θ, say $\hat{\theta}$ must satisfy

$$\frac{\partial S}{\partial \theta} = \sum_{i=1}^{n} -2[y_i - f(x_i, \theta)] \frac{\partial f(x_i, \theta)}{\partial \theta}$$

When this partial derivative is set equal to zero and the parameters, θ are replaced by the least square estimates $\hat{\theta}$, we obtain the normal equation as follows,

$$\sum_{i=1}^{n} y_i \left[\frac{\partial f(x_i,\theta)}{\partial \theta}\right]_{\theta=\hat{\theta}} - \sum_{i=1}^{n} f\left(x_i,\hat{\theta}\right)\left[\frac{\partial f(x_i,\theta)}{\partial \theta}\right]_{\theta=\hat{\theta}} = 0$$

In this study, pressure drop ΔP, is the response or dependent variable whereas time t, is the independent variable. In one of the data analysis programs, the permeability k, and Klinkenberg factor b are the unknown parameters while in the other program, only permeability k is the unknown parameter. For the single-parameter data analysis program, an initial guess for the permeability is supplied to the program and, after performing several iterations till convergence is reached, the program returns the final estimate of the unknown parameter, permeability in this case. For the two-parameter data analysis program, i.e., permeability and Klinkenberg factor, the same method is adopted. However, an initial estimate for the Klinkenberg factor is obtained by the following correlation that was suggested by Jones[10]:

$$b = 6.9\,(k_l)^{-0.36} \qquad 0.01 \text{ md} \le k_l \le 1000 \text{ md} \qquad (4.18)$$

4.5 Determination of the Physical Properties of Nitrogen

In order to accurately simulate the fluid flow, it is essential to properly estimate the physical properties of the flowing fluid, particularly if the fluid is

compressible. The reason is the fact that various gas properties like viscosity and compressibility are highly dependent on pressure and temperature.

In the following sections, the equations used in the computer program for the determination of these properties are given.

4.5.1 Gas Viscosity (μ_g)

The viscosity of nitrogen at a temperature of approximately 25 °C is calculated from the following equation:[20]

$$\mu_{N2}[T,P] = \mu_{N2}[T,1] - 0.12474 + 0.123688P + 1.05452\times10^{-3}P^2 - 1.5052\times10^{-6}P^3 \quad (4.19)$$

where $\mu_{N2}[T,1]$ is the viscosity of the nitrogen at one atmosphere pressure and is obtained using the following equation:[20]

$$\mu_{N_2}[T,1] = \frac{13.85T^{1.5}}{T+102} \quad (4.20)$$

The pressure in equation (4.19) is in atmosphere and the temperature in equation (4.20) is in degrees Kelvin.

4.5.2 Gas Deviation Factor (z_g)

To account for the real gas behavior, gas deviation factor is also included in the flow equation. For nitrogen, values of z-factor were obtained

as a function of pressure by fitting a 3-degree polynomial to the data given in API RP 40[20] for a temperature of 25 °C.

$$z = 1.0 - 1.96929\times10^{-3}P + 1.50321\times10^{-6}P^2 - 6.73225\times10^{-11}P^3 \qquad (4.21)$$

The pressure values used in equation (4.21) are in psia.

4.5.3 Gas Compressibility Factor (c_g)

Gas compressibility values have been calculated using the following equation:

$$c_g = \frac{1}{P} - \frac{1}{z}\frac{\partial z}{\partial P} \qquad (4.22)$$

where $\frac{dz}{dP}$ is obtained by differentiating equation (4.21). The pressure in equation (4.22) is in psia.

CHAPTER 5

EXPERIMENTAL APPARATUS AND PROCEDURES

In this chapter, the experimental set-ups and the experimental procedures used in the present study are presented.

5.1 Experimental Apparatus

A detailed description of the experimental apparatus used for both pulse-decay and steady-state experiments is given below. The experimental set-ups used for both methods are shown schematically in Figures 5.1 and 5.2 respectively.

5.1.1 Core Holder

The core holder (Figure 5.3) is constructed of a stainless steel cylinder threaded on one end for retaining the cap; the other end is closed, and is fitted with two ports. This core holder can accommodate 1-ft long and 4-inch diameter cores. Two mesh screens of equal width, covering a subtended angle θ, are placed on opposite ends of the core sample parallel to the axis of core and running the full length. Fitted around the core and the screens is

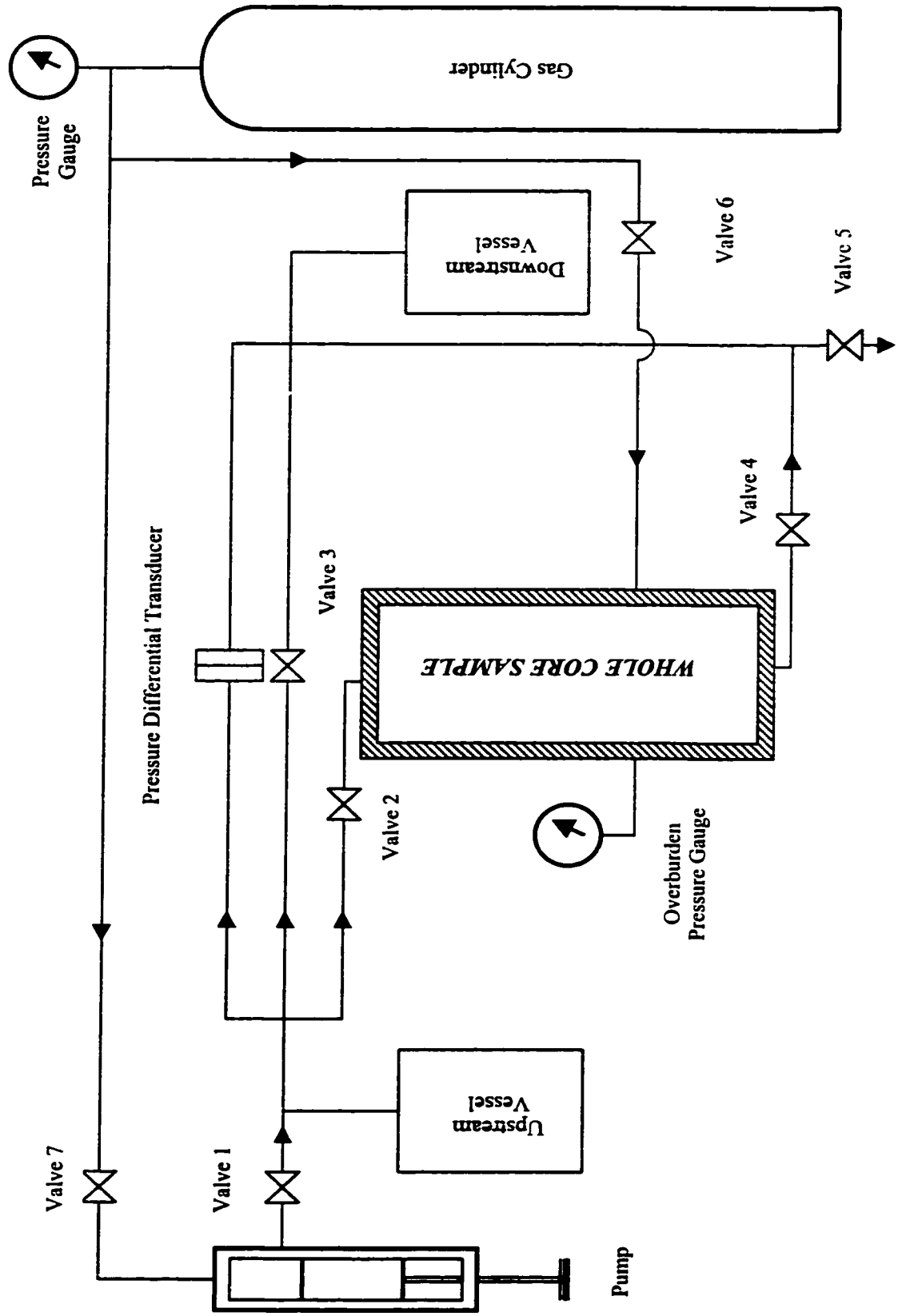

Figure 5.1: Schematic of the Experimental Set-Up for Pulse-Decay Experiments

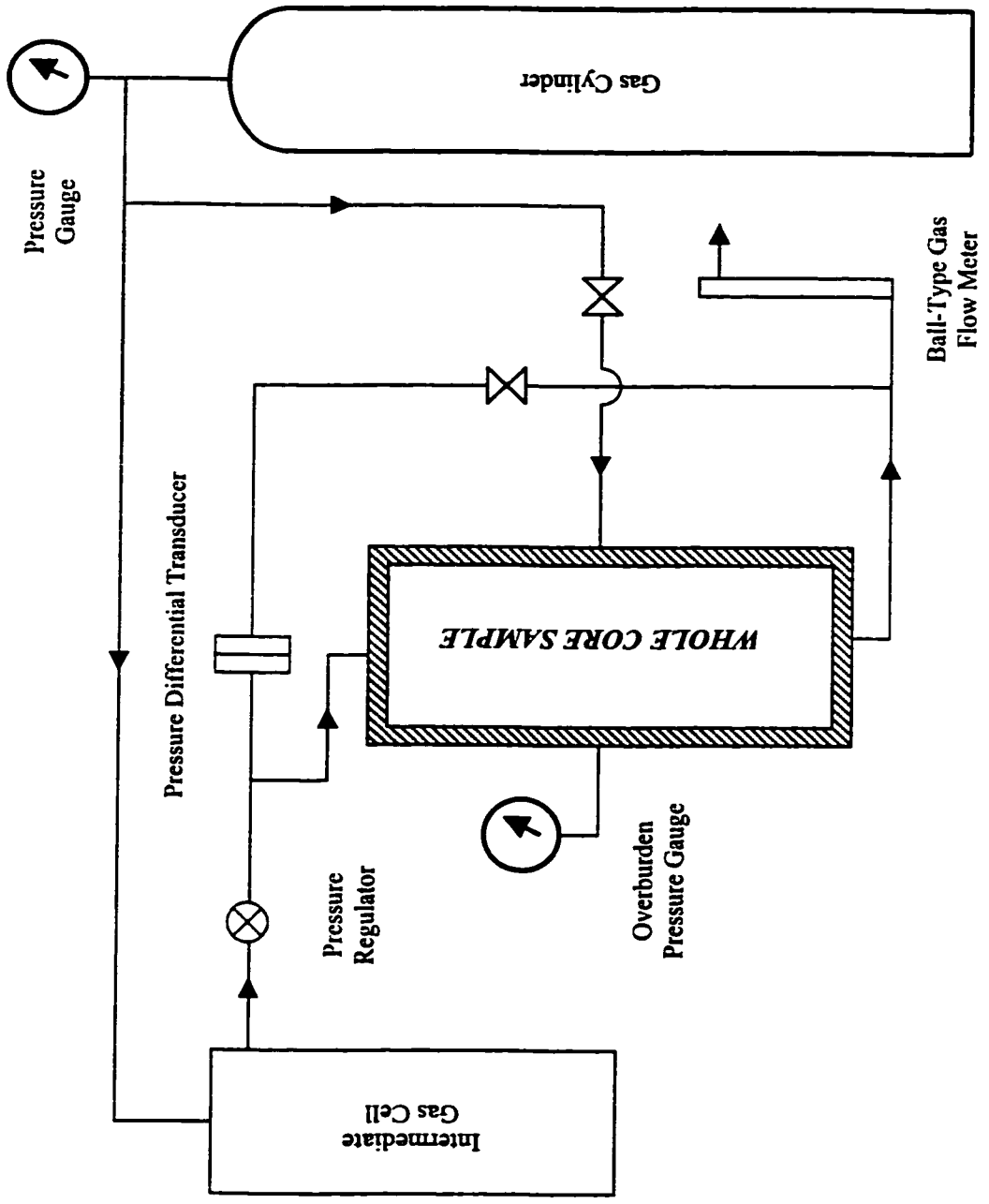

Figure 5.2: Schematic of the Experimental Set-Up for Steady-State Experiments

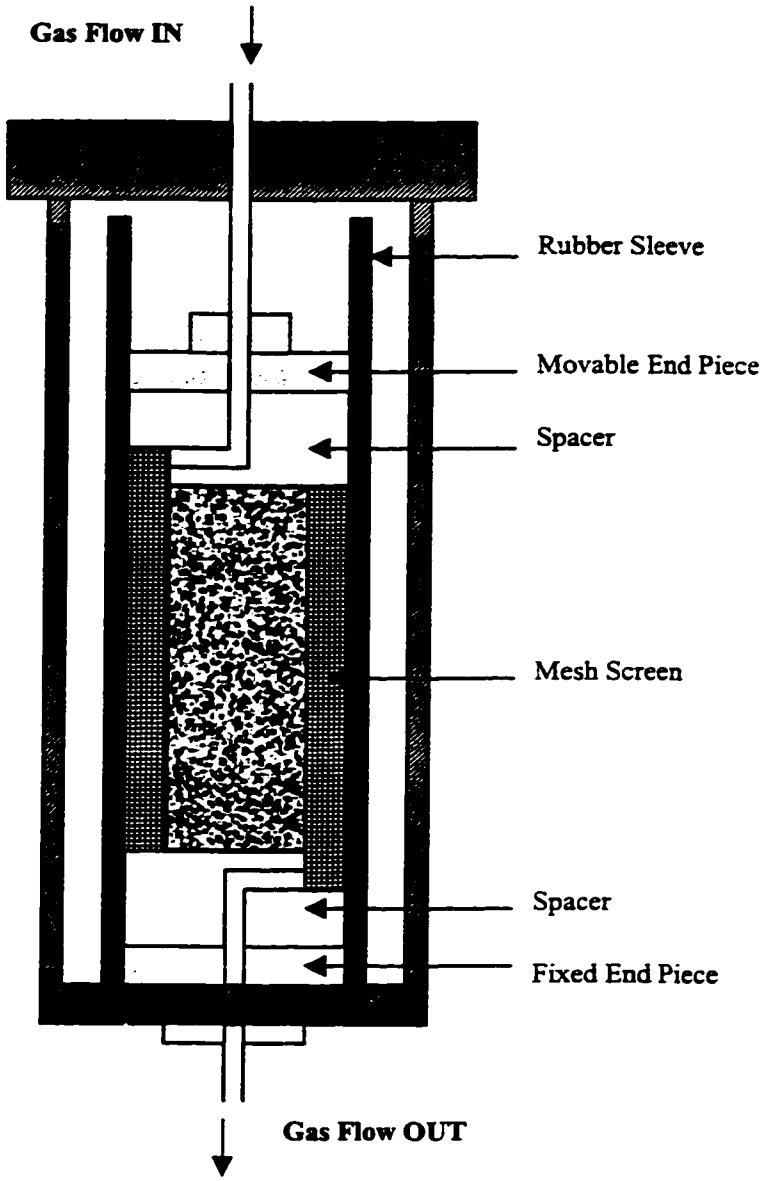

Figure 5. 3: Core Holder

a rubber sleeve. Two aluminum spacers are placed on either ends of the core. Each spacer has a 'L' shaped hole in the center. The whole assembly is then mounted within the core holder. On the closed end of the core holder, there is a built-in end-plug, while, on the other end, there is a movable end-plug to accommodate core samples of different lengths. Connected to the movable end-plug is a rigid tube leading out of the core holder. The fluid to be used in the experiments enters the core holder through this tube; the fluid then enters the spacer through the 'L' shaped hole, turns at an angle of 90° towards the side where one of the screens is fixed. The screen helps the fluid to spread evenly on one of the faces of the core. The annular space between the rubber sleeve and the metal cylinder is pressurized with nitrogen to a pressure in excess of the core pore pressure; this seals the rubber sleeve to the core thus preventing any by-pass flow around the core. The fluid leaves from the opposite face and out of the core holder by following the same *type* of route that was used for inlet except that this route is on the other closed end of the core holder. The whole route of travel is shown in the Figure 5.3.

5.1.2 Piston Pump

A manually operated piston pump is attached to the upstream side for creating the pressure pulse in pulse-decay experiments. This pump can be used to create pressure pulse of any desired magnitude. The system can be isolated once it has been brought to the test pressure.

5.1.3 Pressure Transducers, Digital Displays and Data Acquisition System

Two pressure transducers are used in the system for measuring the pressure. Both of them are differential type (Validyne DP303 with 32 psig diaphragm and 125 psig diaphragm respectively). The low range pressure transducer is used to measure the differential pressure between the upstream and downstream side. The other pressure transducer is used to measure the inlet pressure of the fluid. Each of the transducers is connected to a digital display. The electrical signals sent by the transducers are digitized by a data translation board and sent to data acquisition software in the computer where they are recorded every 0.1, 1 or any desired time interval in seconds, depending upon the rate of pressure decay.

5.1.4 Flow Meter

The gas flow rate is measured by gas bubble or floating ball gas flow meter in steady-state experiments.

5.1.5 Miscellaneous Items

Stainless steel tubing, fittings, valves, pressure gauges, screen, insulation and copper pressure cells were utilized to complete the experimental set-up. Nitrogen was used as the working fluid in the experiments.

5.2 Pre-Experimental Procedures

5.2.1 Testing and Calibration of the Experimental Set-Up

After constructing the whole set-up, it was tested for leaks. The system was pressurized up to 500 psi and was then left for one day to check for any leaks. Soap water bubble tester was used to instantly locate any major leak.

After ensuring that the system is leak-proof, it was calibrated to measure the total volume of the whole system, which includes the upstream and downstream cells, tubing, joints and valves. The gas was expanded from one volume to another volume and the resultant pressure drop was measured. Then, a solid cylinder of known volume was inserted in one of the cells thus reducing the total volume; the same procedure of gas expansion was repeated. The pressure-volume data was then used in conjunction with Boyle's Law to calculate the volume of the system.

5.2.2 Temperature Effects

In the development of the mathematical model, the fluid flow was assumed to be isothermal. However, in reality, as the pressure drops, the temperature also decreases. But, it is very difficult to accurately estimate this temperature variation with pressure. Therefore, in order to satisfy the restriction of isothermal flow, the upstream and downstream cells plus the entire tubing network were heavily insulated using glass wool. Furthermore, the upstream and downstream cells used in the experiment were made of

copper, which has a high heat capacity, thus keeping the temperature reasonably constant.

5.3 Experimental Procedures

Procedures for porosity measurements using Boyle's law gas expansion method and permeability measurements using pulse-decay and steady-state experiments are summarized in the following sub-sections.

5.3.1 Porosity Measurement

Porosity is defined as the ratio of pore volume to bulk volume of the core sample. The experimental set-up to be used for permeability measurements was also used to measure the porosity of the core samples.

5.3.1.1 *Principle*

Boyle's Law was used for measuring porosity. Using this law which is valid at constant temperature, the pressure-volume relationship for the proposed set-up is given as:

$$P_u V_u + P(V_t + V_P + V_d) = P_{fT} V_T$$

$$(P_{fT} - P) = \left(\frac{V_u}{V_t + V_P + V_d}\right)(P_u - P_{fT}) \qquad (5.1)$$

where

P_u = *Initial upstream pressure*

V_u = *Initial upstream volume*

P = *Atmospheric pressure*

V_t = *Dead volume*

V_P = *Pore volume of the rock sample*

V_d = *Downstream volume*

P_{fT} = *Final pressure of the total volume*

V_T = *Total volume*

Once the value of $\left(\frac{V_u}{V_t + V_P + V_d}\right)$ is measured, the pore volume of the rock specimen can be calculated easily. Finally, the porosity can be calculated as,

$$\varphi = \frac{V_P}{V_B} \qquad (5.2)$$

where

V_B = *Bulk volume of the rock sample*

5.3.1.2 *Procedure*

The procedure for measuring porosity can be described as:

- Initially, the system is accurately calibrated to know the exact volume of whole set-up.

- The sample is loaded into the core holder and a confining pressure of approximately 700 psi is applied.
- The upstream volume V_u is pressurized to a certain pressure P_u.
- The upstream volume V_u is then opened to the rock sample plus the attached downstream volume, and the final pressure P_{ff} of the upstream volume, rock sample and downstream volume is noted.
- Knowing the dead tubing volume V_t, upstream volume V_u and downstream volume V_d from initial calibration, the pore volume V_P is calculated.
- Porosity is calculated using the Equation (5.2).

5.3.2 Permeability Measurement Using the Pulse-Decay Method

Owing to the limited number of whole core samples, pulse-decay experiments were conducted on only two sandstone core samples. Another reason for fewer tests was the limitation of the experimental set-up, which could not sustain the high pore pressures that were required for testing very tight samples (<0.001 md). The dimensions, porosity and other relevant details of the two core samples are summarized in Table 5.1.

The following are the general steps of a typical pulse-decay experiment:

- After the placement of the core in the core holder and applying the confining pressure, the system, i.e., the upstream and downstream vessels and the core, is filled with nitrogen to a certain pressure.

TABLE 5.1: Dimensions & porosity of whole core samples

Sample Number	Length (cm)	Diameter (cm)	Porosity (%)	Angle Covered by the Screen (degrees)
CS-1	7.035	10.125	12.50	27.2
CS-2	7.035	10.140	10.50	27.2

- Time is allowed for the pressure to stabilize in and across the core. After reaching the equilibrium, valves 2 and 3 are closed (Figure 5.2).
- Next, the pressure in the upstream side of the system is increased slightly by manually turning the handle of the pump. Few minutes are allowed for the pressure in the upstream side to equilibrate.
- The test begins at time t = 0 with the simultaneous opening of valve 2 and starting of the data acquisition software. The gas in the upstream volume expands through the core into the downstream volume, thus, causing pressure decay in the upstream volume.
- Pressure is recorded as a function of time with a differential-pressure transducer and a computer. The pressure-time data is then analyzed using the developed data analysis computer program to calculate the permeability.

5.3.3 Permeability Measurement Using the Steady-State Method

5.3.3.1 *Theory*

The flow pattern in this transverse gas flow is complex, and the area normal to the streamlines is variable throughout the flow path. Using a conformal mapping transformation, Collins[18] computed a dimensionless geometrical factor G_θ. It is shown in Figure 5.4, and is a function of the angle subtended by the screens. The permeability was calculated using the following equation as:

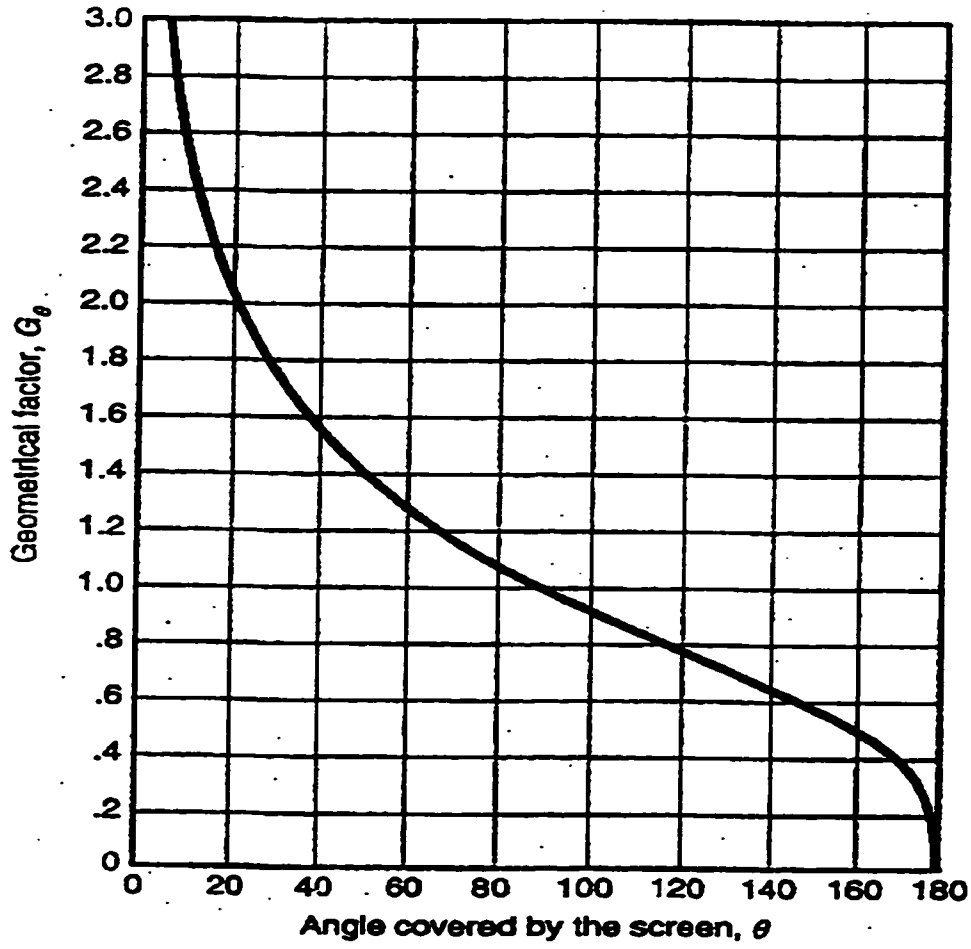

Figure 5.4: Dimensionless Geometric Factor for Transverse Flow[18]

$$k_g = \frac{p_{sc} q_{sc}}{p_m} \frac{\mu}{\Delta p} \frac{G_\theta}{L} \qquad (5.3)$$

where

p_{sc} = *Pressure at standard conditions*

q_{sc} = *Flow Rate measured at standard conditions*

p_m = *Mean pressure*

Δp = *Difference between upstream and downstream pressure*

L = *Length of the whole core sample*

5.3.3.2 *Procedure*

The procedure followed for measuring the permeability is as follows:

- The gas is passed through the rock specimen till steady-state condition is attained.
- The pressure difference across the two ends of the rock sample is noted.
- The gas flow rate is measured.
- Knowing the viscosity of the gas, length, and other parameters, the permeability can be calculated using Equation (5.3).

CHAPTER 6

RESULTS AND DISCUSSION

In this chapter, the simulation and experimental results are presented, analyzed and discussed.

As mentioned earlier, two versions of the numerical simulator were developed, i.e., with and without gas slippage effect. Based on these two versions of the numerical simulator, two data analysis computer programs were also developed. The simulators were used to study the effect of gas slippage on pressure decay curves. In addition, the error induced in the permeability estimates, by neglecting the gas slippage during the analysis of data with slippage effects, was also investigated.

The experimental results consist of two sets i.e.,

- Pressure Pulse-Decay Experimental Results, and
- Steady-State Experimental Results

The data analysis programs were used to analyze the simulated as well as the experimental pulse-decay data.

6.1 Effect of Gas Slippage on Pressure Decay Curve

Several simulation runs were performed with and without gas slippage effects for permeability values varying from 0.01 md to 1.0 md. Pressure pulses of 20 psi and 100 psi were used. The mean pore pressure ranged from 25 psi to 250 psi. Values of additional parameters like temperature, volume of upstream and downstream cells, porosity and dimensions of core sample used in the generation of synthetic pressure pulse-decay data are listed in Table 6.1. It was found from the simulation runs that the use of more than one grid cell in Y-direction did not significantly affect the accuracy of numerical solution, so only one grid cell was used in Y-direction. The results are presented in Figures 6.1 to 6.6. All the figures indicate that the pressure decays faster in the slippage case as compared to that in the no-slippage case, thus giving higher apparent permeability values as compared to the actual values. Furthermore, as the rock permeability increases, the slippage effects become less significant. Also, for a fixed value of permeability, the gas slippage effects diminish as the mean pore pressure increases.

The effect of neglecting the gas slippage effect was investigated by analyzing the synthetic data incorporating the slippage effects by using the data analysis program in which gas slippage effects are neglected. The results are tabulated in Table 6.2. It can be inferred from these results that for very low permeability samples (0.01 md), which are more prone to gas slippage effects, the error induced in the permeability estimation can be as

TABLE 6.1: Fixed parameters used in the generation of synthetic pulse-decay data

S. No.	Parameter	Value
1	Temperature (T)	25 °C
2	Upstream cell volume (V_u)	270.216 cc
3	Downstream cell volume (V_d)	274.381 cc
4	Height of the whole core sample (H)	7.035 cm
5	Radius of the whole core sample (R)	5.062 cm
6	Porosity (ϕ)	12.50%
7	Angle Covered by the Screen (θ)	27.2°
8	Number of grid cells in X-direction (N_x)	42
9	Number of grid cells in Y-direction (N_y)	1

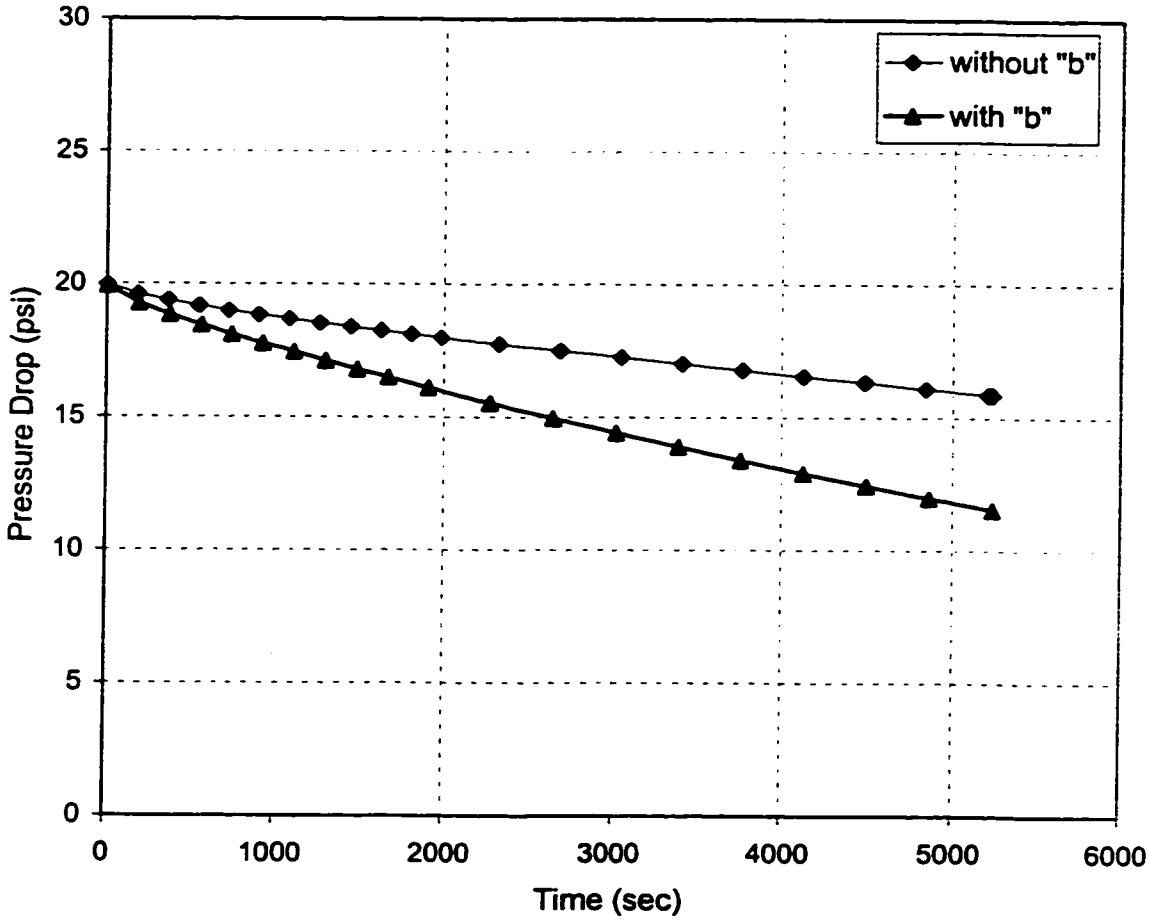

Figure 6.1: Effect of gas slippage on pressure decay curves
(k = 0.01 md, Δp = 20 psi and P_m = 25 psi)

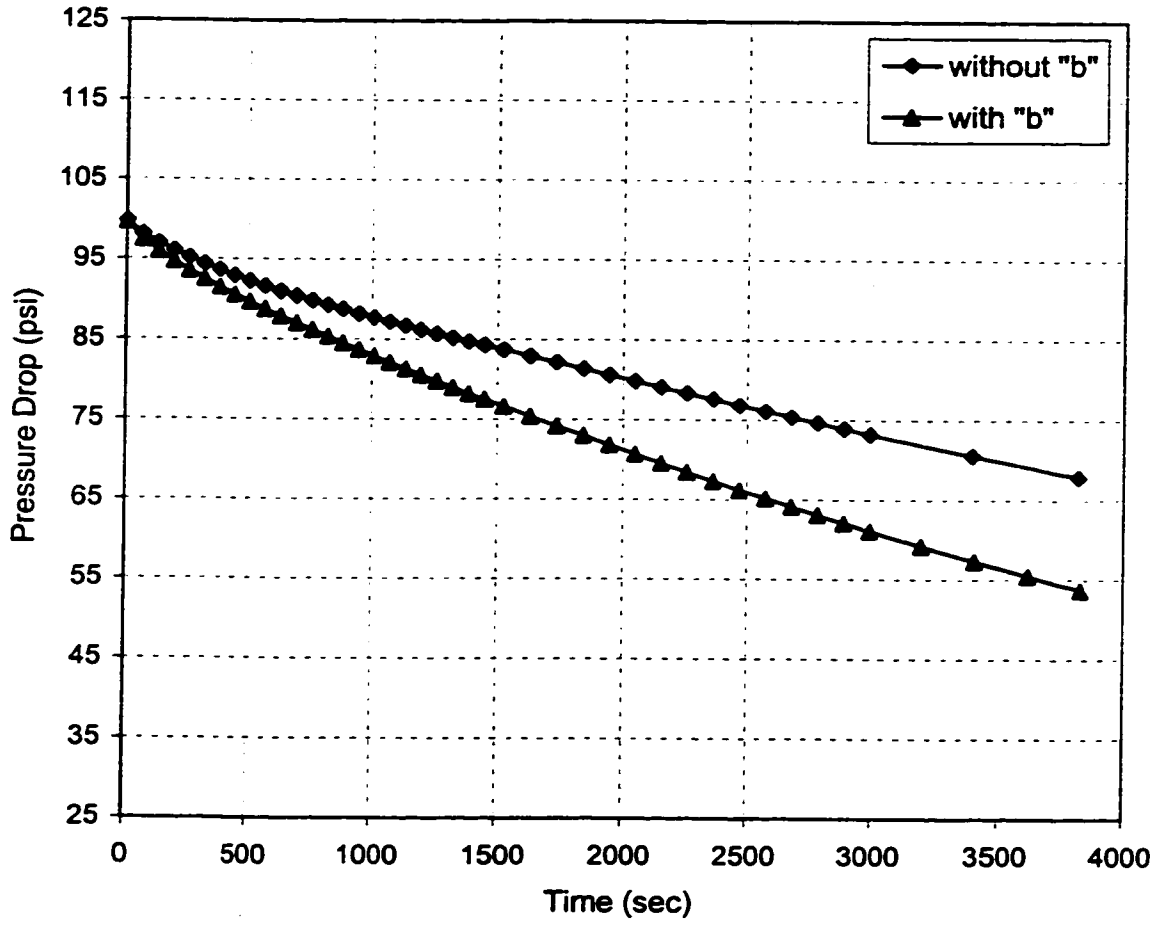

Figure 6.2: Effect of gas slippage on pressure decay curves
(k = 0.01 md, Δp = 100 psi and P_m = 65 psi)

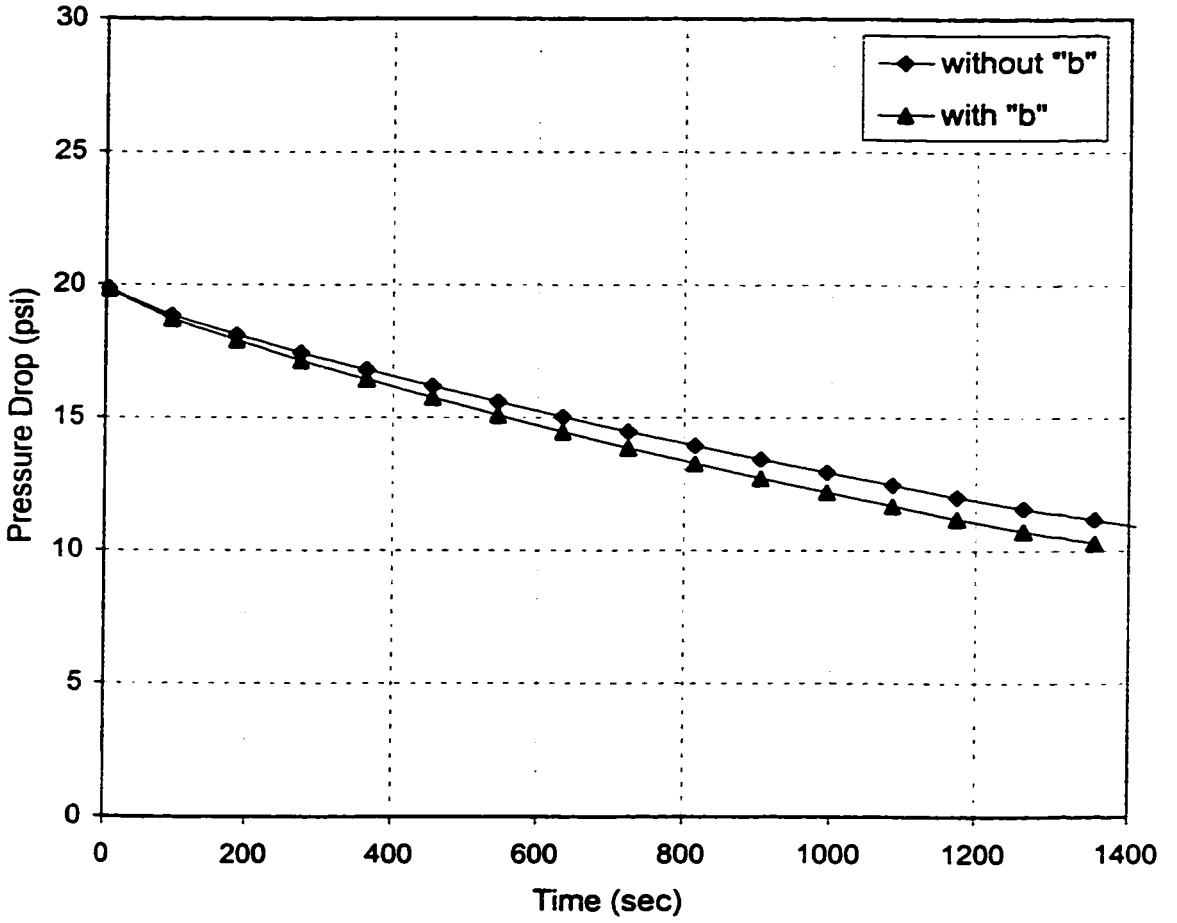

Figure 6.3: Effect of gas slippage on pressure decay curves
($k = 0.01$ md, $\Delta p = 20$ psi and $P_m = 250$ psi)

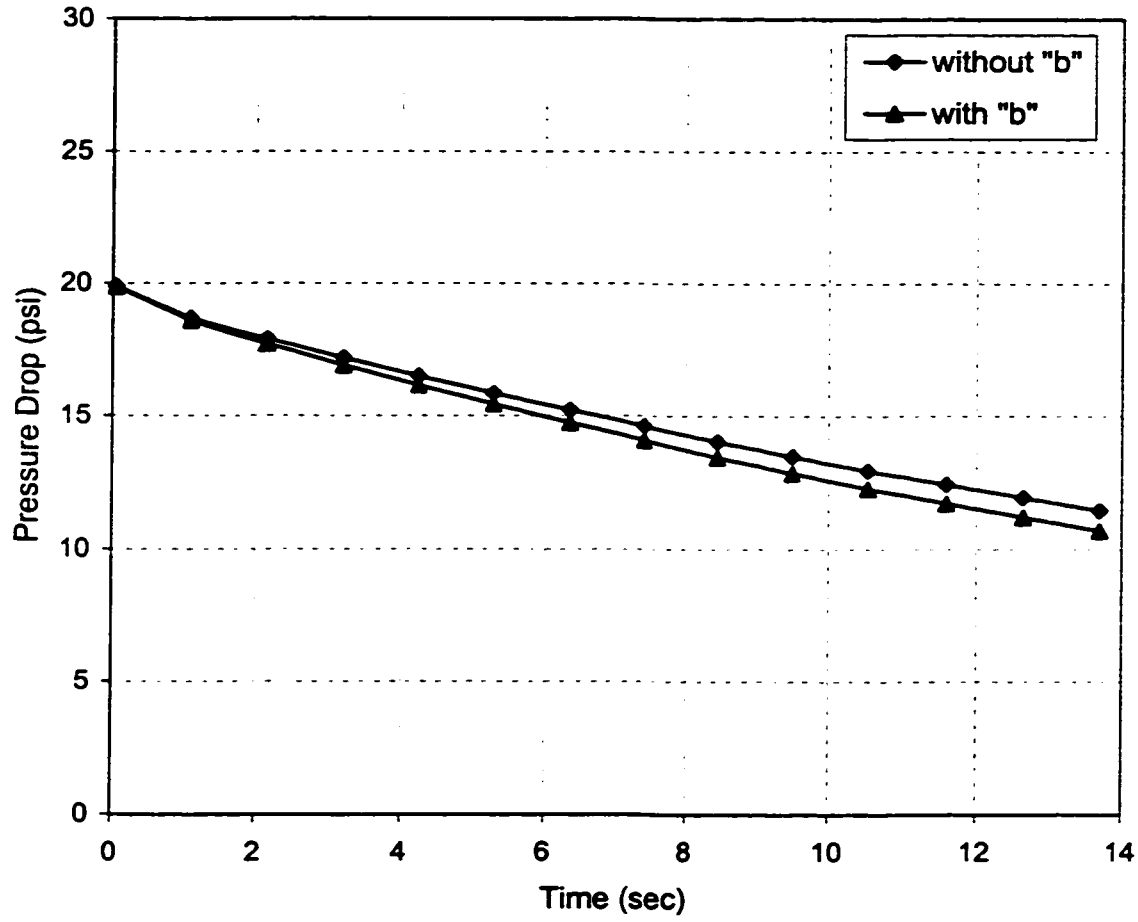

Figure 6.4: Effect of gas slippage on pressure decay curves
(k = 1.0 md, Δp = 20 psi and P_m = 25 psi)

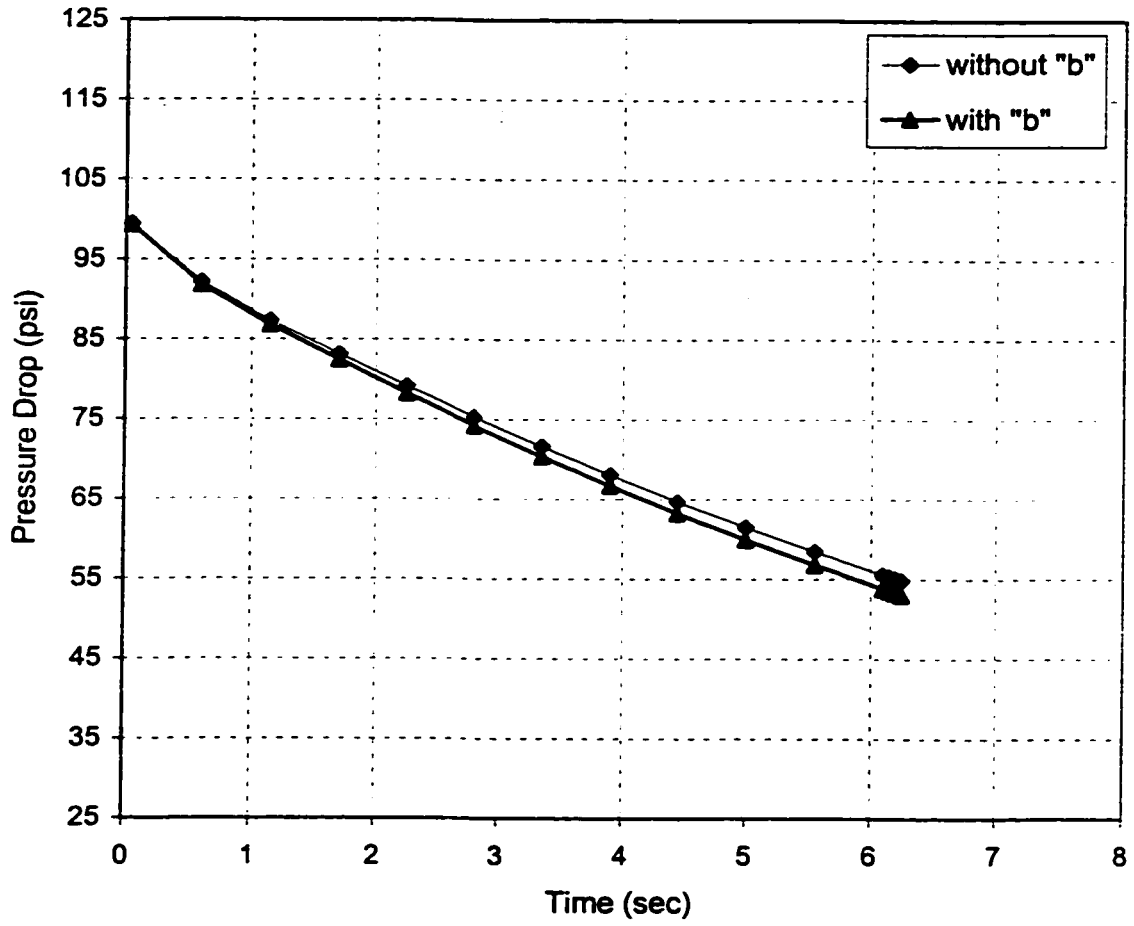

Figure 6.5: Effect of gas slippage on pressure decay curves
(k = 1.0 md, Δp = 100 psi and P_m = 65 psi)

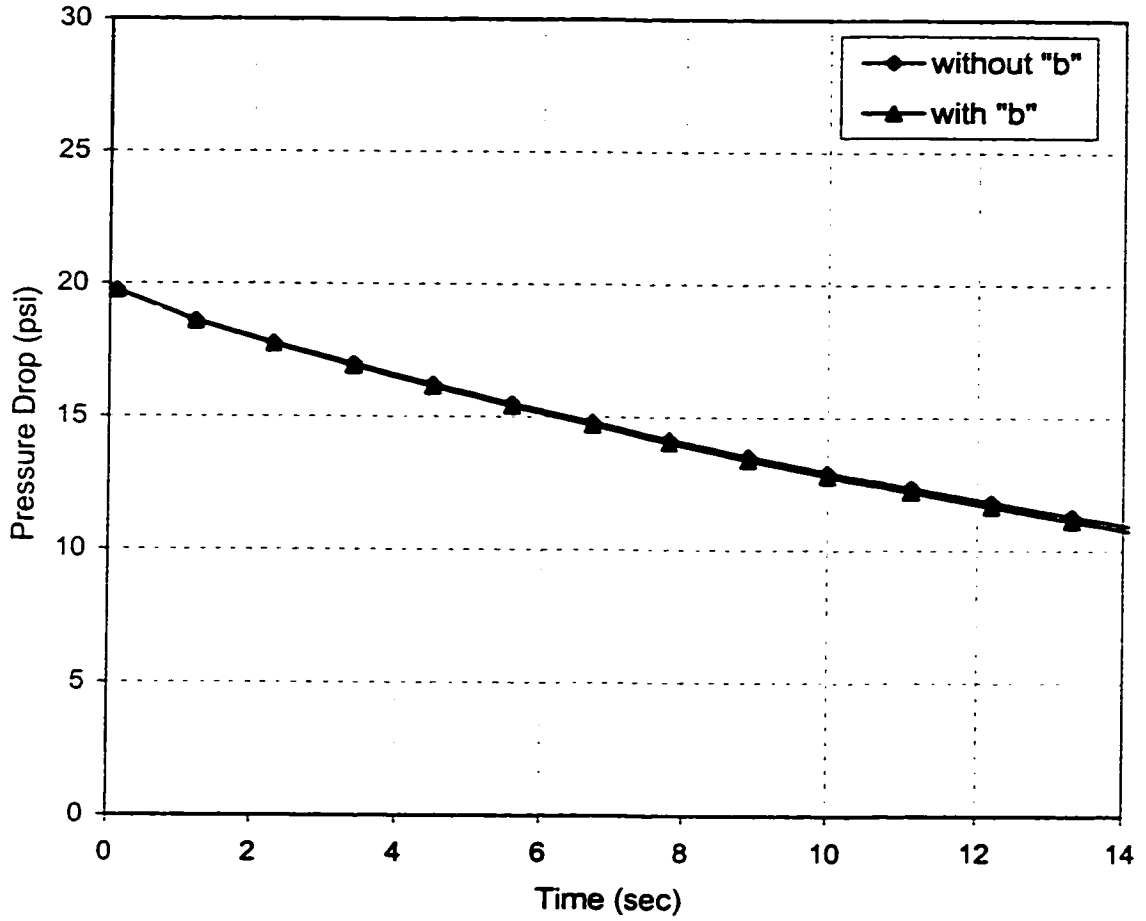

Figure 6.6: Effect of gas slippage on pressure decay curves
(k = 1.0 md, Δp = 20 psi and P_m = 250 psi)

TABLE 6.2: Effect of neglecting gas slippage on the estimation of permeability

Mean Pore Pressure (psia)	Simulator Input k_l (md)	Program Output k_g (md)	Error (%)
24.7	0.01	0.0255	155.26
34.7	0.01	0.0209	108.69
44.7	0.01	0.0184	83.53
54.7	0.01	0.0168	67.85
24.7	1.00	1.2976	29.76
34.7	1.00	1.2077	20.77
44.7	1.00	1.1595	15.95
54.7	1.00	1.1295	12.95

large as +155%. However, for the relatively high permeable samples (1.0 md), the error is not very large but is still very significant.

The results also indicate that at a relatively higher mean pore pressure (55 psi), the error for very low permeability samples is reduced from +155% to +67% while for relatively high permeable samples (1.0 md), the error is reduced from +29% to +13%. The use of larger pressure pulse size (100 psi) appears to reduce the error because it tends to increase the mean pore pressure. However, the use of larger pressure pulse size may lead to non-Darcy flow effects, specially for high permeability samples. The non-Darcy flow effects tend to slow the pressure decay, thus resulting in the underestimation of permeability values.

6.2 Analysis of Simulated Pulse-Decay Data Using the Developed Computer Program

The performance of the data analysis computer program was evaluated by analyzing the synthetic pulse-decay data generated for the conditions where gas slippage effects exist. Permeability values varying from 0.01 md to 1.0 md, and pressure pulses of 20 psi and 100 psi, were used. The mean pore pressure values ranged from 25 psi to 250 psi. The experimental conditions for the simulation runs were such that the mean pore pressure remained nearly constant during the experiments.

6.2.1 Estimation of k and b from single test data using the two-parameter program

The synthetic data incorporating the gas slippage effects were analyzed by using two-parameter data analysis program, which returns the estimates of two unknown parameters, i.e., permeability and Klinkenberg factor. The results are tabulated in Table 6.3. The results indicate that the program is giving almost exact estimates as compared to the values for which the data was generated from the simulator.

6.3 Analysis of Experimental Pulse-Decay Data Using the Developed Computer Programs

The estimation of permeability and Klinkenberg factor for whole cores was the primary objective of this study. So, based on the findings from the preceding simulation results, it was decided to perform the pulse decay experiments at low mean pore pressures where slippage effects exist. To maintain low mean pore pressures, a low value of pressure pulse, i.e., 20 psi was selected. The reasons for avoiding the use of larger pressure pulse size, were, first, it may result in the onset of non-Darcy flow effects and second, gas expansion from a high pressure may result in cooling effects.

Several pulse-decay experiments were performed under different experimental conditions on the two sandstone whole core samples. During some runs, the size of pressure pulse was varied to experimentally verify the

TABLE 6.3: Analysis of the synthetic pulse-decay data using two-parameter analysis program

Pulse Size	Pressure		Simulator Input		Program Output		Error	
ΔP (psi)	P_u (psia)	P_d (psia)	k_l (md)	b (psi)	k_l (md)	b (psi)	k_l (%)	b (%)
20	34.7	14.7	0.01	36.21	0.01	36.212	0.00	0.01
100	114.7	14.7	0.01	36.21	0.01	36.212	0.00	0.01
20	34.7	14.7	1.00	6.90	1.00	6.900	0.00	0.00
100	114.7	14.7	1.00	6.90	1.00	6.900	0.00	0.00

findings of the simulation results. Furthermore, the orientation of the mesh screens was also changed to check for the existence of any permeability anisotropy. Table 6.4 summarizes the experimental conditions for all the pulse-decay experiments.

6.3.1 Estimation of k and b from single test experimental data using the two-parameter program

For each of the two cores, pulse-decay experiments were conducted for the conditions where the slippage effects exist. Upstream and downstream cells of approximately equal volume were used in the experimental set-up, thus leading to nearly constant mean pore pressure during the experiments. The experimental data for both samples were then analyzed by using the two-parameter data analysis program, which returns the estimates of two unknown parameters, i.e., permeability and Klinkenberg factor. The results are tabulated in Table 6.5. The results indicate that the program is giving negative values for Klinkenberg factor. The values of permeability are also not reliable. In order to investigate the reason for these negative values, the Klinkenberg's correlation was analyzed.

$$k_g = k_l\left(1+\frac{b}{P_m}\right)$$

Investigation of the relationship indicates that for a fixed value of mean pore pressure, there could be various combinations of liquid permeability, k_l, and Klinkenberg factor, b, that would yield same value of gas permeability, k_g,

TABLE 6.4: Summary of experimental conditions for pulse-decay experiments

Test #	Pulse Size	Pressure	
	ΔP (psi)	P_u (psia)	P_d (psia)
10-1	10	24.7	14.70
10-2	10	29.7	19.70
10-3	10	34.7	24.70
10-4	10	39.7	29.70
10-5	10	44.7	34.70
20-1	20	34.7	14.70
20-2	20	44.7	24.70
20-3	20	54.7	34.70
20-4	20	64.7	44.70
20-5	20	74.7	54.70
30-1	30	44.7	14.70
30-2	30	54.7	24.70
30-3	30	64.7	34.70
30-4	30	74.7	44.70
30-5	30	84.7	54.70
100-1	100	114.7	14.70
100-2	100	124.7	24.70
100-3	100	134.7	34.70
100-4	100	144.7	44.70
100-5	100	154.7	54.70

TABLE 6.5: Analysis of the experimental pulse-decay data using two-parameter analysis program

Test #	Pulse Size	Pressure		Program Output	
	ΔP (psi)	P_u (psia)	P_d (psia)	k_l (md)	b (psi)
1	20	85.93	64.77	0.8487	-58.14
2	20	55.76	35.13	2.267	-21.04
3	20	45.26	25.02	1.507	-0.16

thus indicating the non-uniqueness of the solution. In other words, it is possible to get a good regression fit for test data at more than one set of k_l and b (Figure 6.7). So, this could probably be one of the reasons for getting negative values of Klinkenberg factor. To adjust this, the data analysis program was returning higher values of liquid permeability.

Another reason for these erroneous results could be that the data might have some experimental errors. Although, there can be various sources of the experimental errors, here only the effect of error in the initial upstream pressure measurement and porosity measurement on parameter estimation was investigated.

6.3.2 Effect of error in initial upstream pressure measurement

In order to investigate the effect of error in the initial upstream pressure measurement, synthetic pulse-decay data incorporating slippage effects were generated for permeability values of 0.01 md and 1.0 md. Then the initial upstream pressure value was varied by ± 0.5% and the data were analyzed by the two-parameter program which returns the values of liquid permeability k_l and Klinkenberg factor b. The results are tabulated in Table 6.6. Using Klinkenberg's relationship, the values of gas permeability k_g were also calculated from k_l and b values obtained from the two-parameter program and are tabulated in the Table 6.6. The data was then analyzed by one-parameter program that ignores the slippage effects in the analysis of pulse-decay data

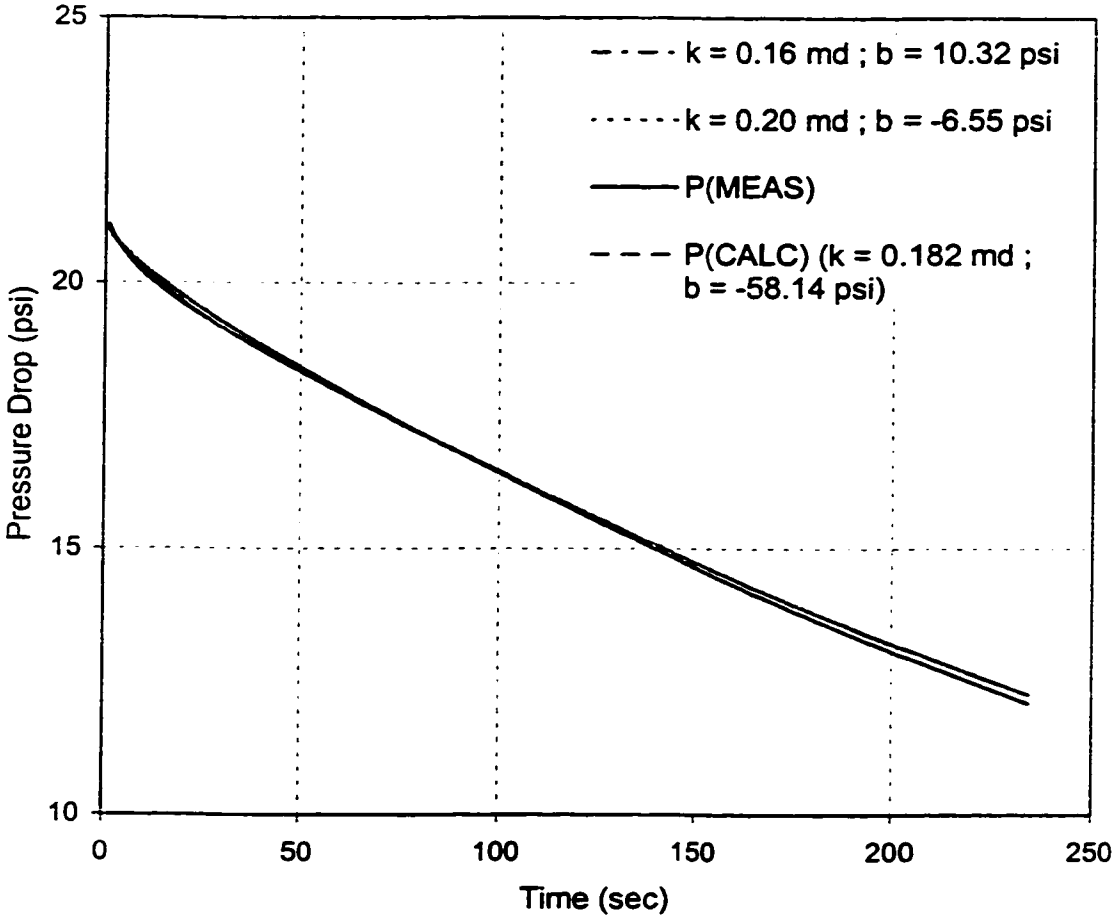

Figure 6.7: Comparison of pressure decay curves generated using different sets of 'k_l' and 'b' for a fixed value of 'k_g' for core sample CS-1 ($\theta = 0^\circ$ and $\Delta p = 20$ psi)

TABLE 6.6: Effect of error in the initial upstream pressure measurement on parameter estimation

Program Output (Without Error)				"P_{ui}" varied by + 0.5%				"P_{ui}" varied by - 0.5%			
k_l	b	k_g (Klink.)	k_g	k_l	b	k_g (Klink.)	k_g	k_l	b	k_g (Klink.)	k_g
0.0100	36.212	0.0162	0.0164	0.0166	0.209	0.0167	0.0167	0.0029	264.25	0.0158	0.0162
1.0000	6.900	1.1178	1.1257	1.4042	-10.242	1.1597	1.1385	0.4899	70.57	1.0827	1.1128

and thus, only returns the value of gas permeability k_g. The results are presented in Table 6.6. The results indicate that the values of Klinkenberg factor are much more sensitive to the error in the initial upstream pressure measurement as compared to permeability values. It is also evident from the results that the values of gas permeability as calculated from Klinkenberg's relationship are almost the same for the data with and without error. Similarly, the values of gas permeability as obtained from the one-parameter program are also not sensitive to the error in the initial upstream pressure measurement.

6.3.3 Effect of error in porosity measurement

Simulation data incorporating slippage effects were generated for permeability values of 0.01 md and 1.0 md. Then the porosity value was varied by ± 0.5% and the data were analyzed by using both two-parameter and one-parameter programs. The results obtained from both the programs are tabulated in Table 6.7. By using the values of k_l and b as obtained from the two-parameter program in Klinkenberg's relationship, the values of k_g were also calculated and are tabulated in the Table 6.7. The results indicate that the values of Klinkenberg factor b are again very sensitive to the error in the porosity measurement. Similarly, the values of liquid permeability k_l are also sensitive to the error in the porosity measurement. However, the values of gas permeability k_g as calculated from Klinkenberg's relationship are

TABLE 6.7: Effect of error in the porosity measurement on parameter estimation

Program Output (Without Error)				"φ" varied by + 0.5%				"φ" varied by - 0.5%			
k_l	b	k_g (Klink.)	k_g	k_l	b	k_g (Klink.)	k_g	k_l	b	k_g (Klink.)	k_g
0.0100	36.212	0.0254	0.0256	0.0091	41.990	0.0254	0.0255	0.0109	31.27	0.0254	0.0255
1.0000	6.900	1.1178	1.1257	0.9690	8.899	1.1162	1.1262	1.0317	4.98	1.1194	1.1253

relatively insensitive to this error. Moreover, the values of k_g as obtained from the one-parameter program are also not sensitive to the error in the porosity measurement.

Since both k_l and b values are related to each other, i.e., when one increases the other decreases, it is difficult to quantify the effect of error in initial upstream pressure and porosity measurement on each of the parameters, individually. However, it is clear from Table 6.6 and 6.7 that the output values from the two-parameter data analysis program are very sensitive to these measurement errors. On the other hand, the output values from the one-parameter data analysis program are relatively insensitive to these errors. Hence, it was decided to use another approach for the analysis of the experimental data to determine the liquid permeability, k_l and Klinkenberg factor, b.

6.3.4 NLR-Graphical Technique for the estimation of k and b from multiple test data

As mentioned earlier, if we ignore the gas slippage effects in the analysis of data incorporating the gas slippage effects, the permeability values obtained are larger than the actual permeability values. The permeability values thus obtained are actually gas permeability values. However, the difference between the gas permeability values and the liquid

permeability values becomes progressively smaller with increasing mean pore pressure.

To avoid the problem of obtaining pore-pressure-dependent gas permeabilities, Klinkenberg[24] presented a method in which gas permeability values are determined at different mean pore pressures and are then plotted against the reciprocal of mean pressure as a straight line. When this line is extrapolated to infinite mean pressure ($1/P_m$) intercept, the liquid permeability is obtained, while by dividing the slope of the line by the intercept, one can get the Klinkenberg factor, b. This method is generally used for steady-state permeability measurements, when gas is the pore fluid.

However, this graphical method may also be used for the determination of liquid permeability and Klinkenberg factor using unsteady-state or pulse-decay technique. In order to verify this, several runs of the simulator, which incorporates the gas slippage effects, were made at various mean pore pressures. Permeability values varying from 0.01 md to 1.0 md, and pressure pulses of 20 psi and 100 psi, were used. The resultant pulse-decay data sets were then analyzed by using the one-parameter data analysis program, which ignores the slippage effects. The permeability values obtained after the analysis, which were actually gas permeability values, were plotted against the reciprocal of respective mean pressures as a straight line. Figures 6.8, 6.9 and 6.10 show the resultant graphs. The values of liquid permeability, k_l and Klinkenberg factor, b found from the graph are in close

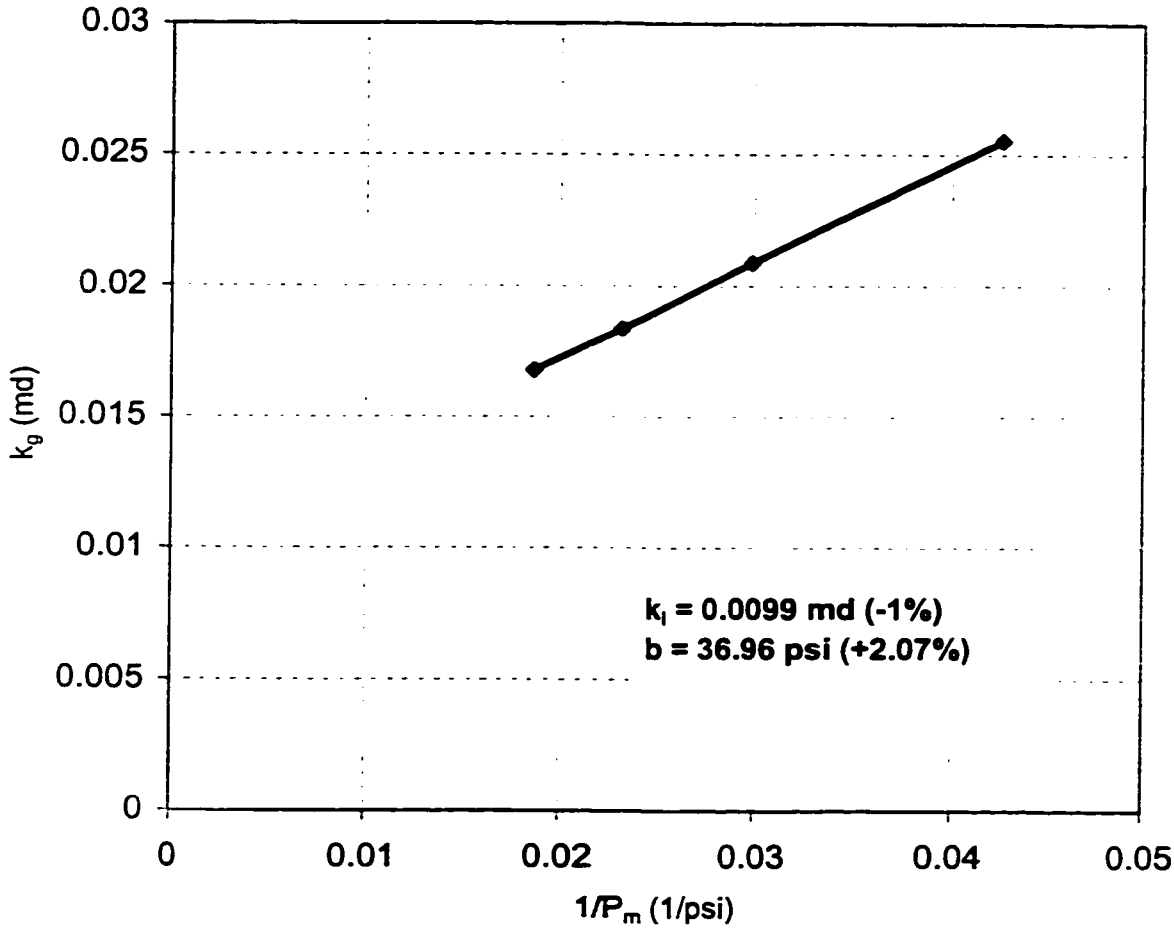

Figure 6.8: Verification of the NLR-Graphical Method for the determination of 'k_l' and 'b' from synthetic pulse-decay data (k_l = 0.01 md, b = 36.21 psi and Δp = 20 psi)

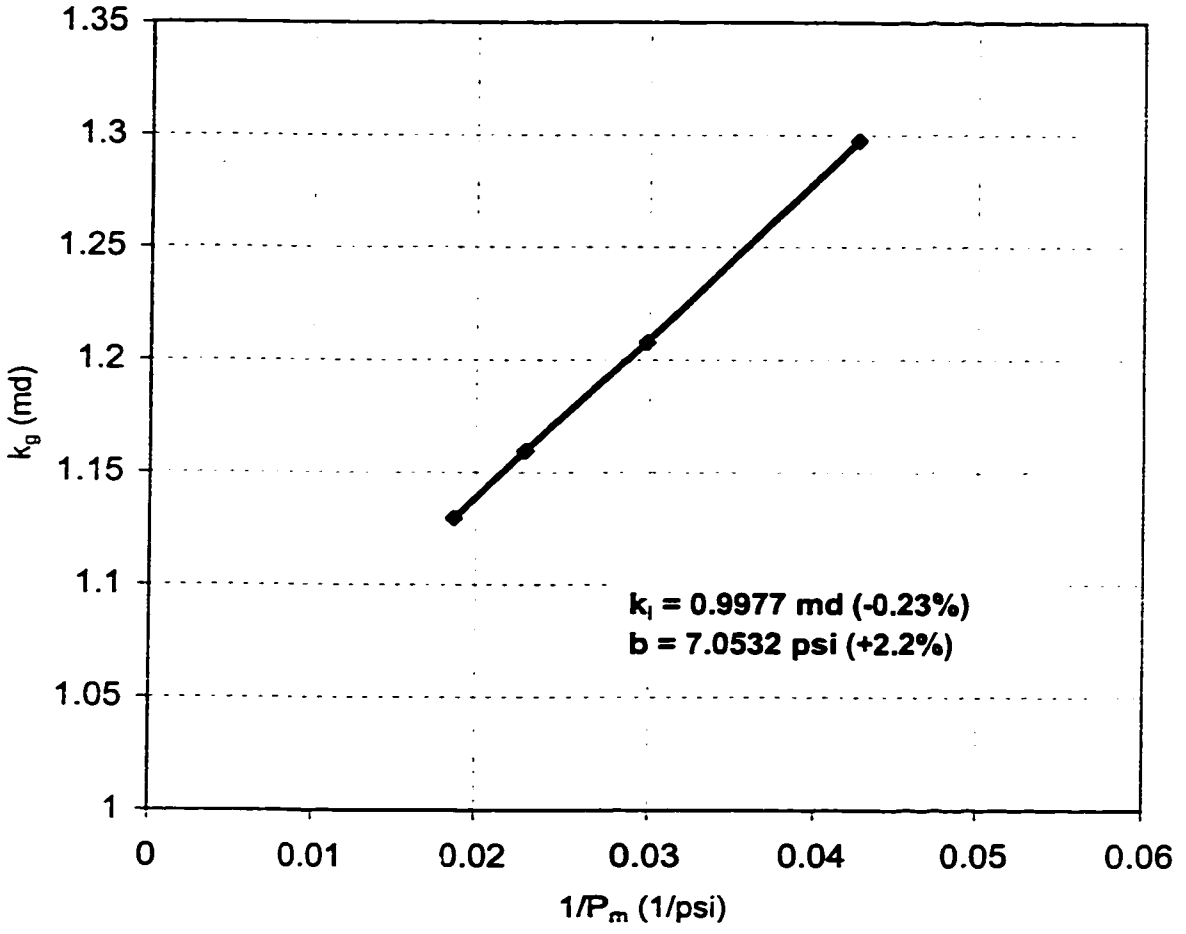

Figure 6.9: Verification of the NLR-Graphical Method for the determination of 'k_l' and 'b' from synthetic pulse-decay data (k_l = 1.0 md, b = 6.9 psi and Δp = 20 psi)

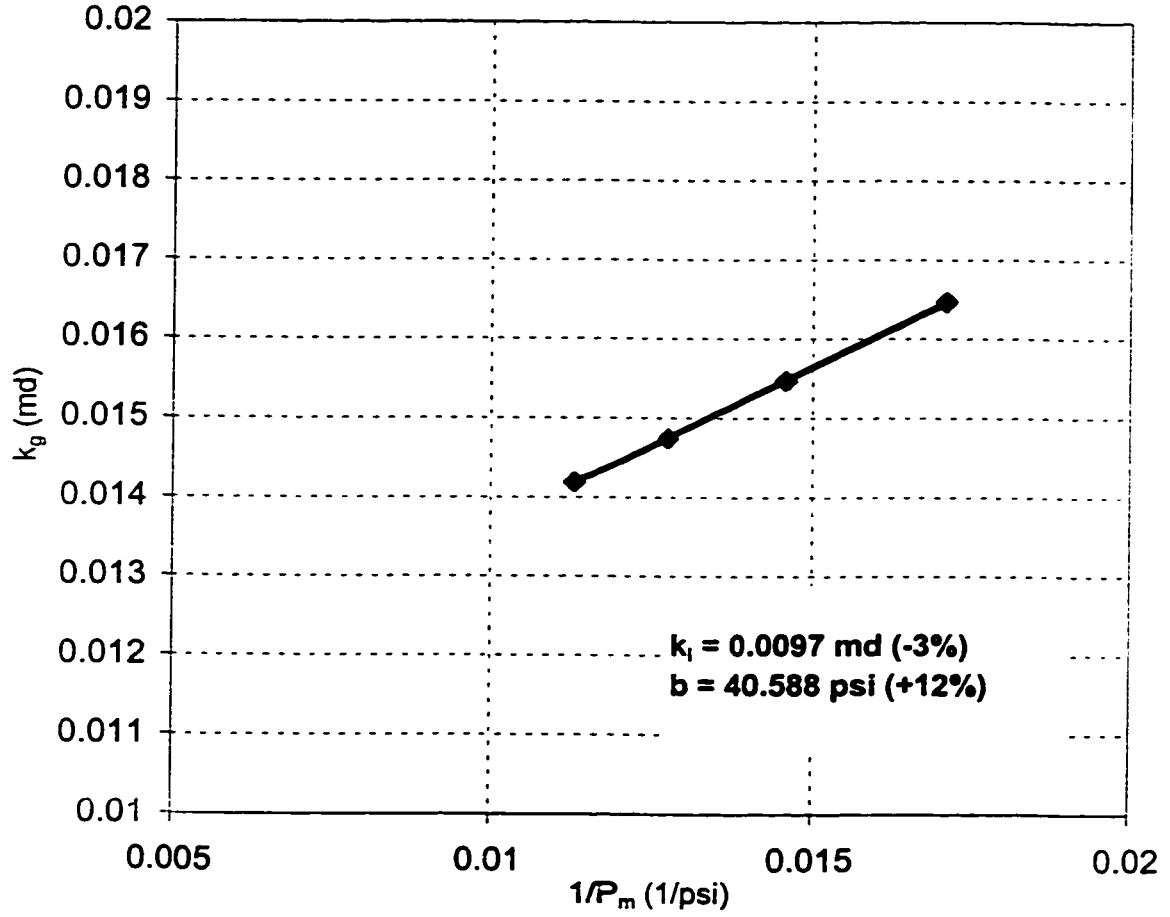

Figure 6.10: Determination of 'k_i' and 'b' from synthetic pulse-decay data using NLR-Graphical Method (k_i = 0.01 md, b = 36.21 psi and Δp = 100 psi)

agreement with the values used to generate the synthetic data. However, there is a difference of -3% in permeability value and +12% in Klinkenberg factor value obtained from the analysis of data generated using large pulse size. This could be attributed to the fact that the use of large pulse size leads to sudden change in the mean pore pressure whereas it was assumed to be constant during the experiment.

6.3.5 Estimation of k and b from multiple test data using the one-parameter program (NLR-Graphical Method)

The proposed technique was then used to analyze the same experimental data, which were earlier analyzed by the two-parameter program. The experimental data were first analyzed by using the computer program that does not include the gas slippage effects, to obtain the permeability. The permeability values thus obtained were gas permeability values. The gas permeability values obtained at various mean pore pressures were then plotted against the reciprocal of the respective mean pore pressures as a straight line. The y-intercept of this line was the liquid permeability whereas the Klinkenberg factor 'b' was obtained by dividing the slope of the line by its y-intercept.

6.3.6 Determination of Permeability Anisotropy

In order to check for the existence of any permeability anisotropy, pulse-decay experiments were carried out at three different transverse flow directions, i.e., 0°, 45° and 90° by changing the location of mesh screens along the circumference of the core.

Figures 6.11 to 6.13 show the results of core sample CS-1. All the runs for sample CS-1 using a common pressure pulse value of 20 psi show the same permeability, thus indicating the absence of any anisotropy. The values of the Klinkenberg factor for all these runs were about 13% to 35% less than that obtained from Jones' empirical correlation. The difference between the values of the Klinkenberg factor could be attributed to the fact that in Jones' correlation, the Klinkenberg factor is a function of only permeability whereas it also depends upon the type of gas and rock.

Figures 6.14 to 6.16 present the results of pulse-decay runs conducted on core sample CS-2. Pulse-decay experiments were carried out using Δp equal to 10 psi and 20 psi, respectively for each of the three locations. The permeability values for the three locations were different from each other thus indicating the existence of some heterogeneity in the core sample. In order to verify this finding, some runs were repeated but the results were still the same. The values of the Klinkenberg factor were also calculated for all the runs. Results of all the pulse-decay runs are summarized in Table 6.8.

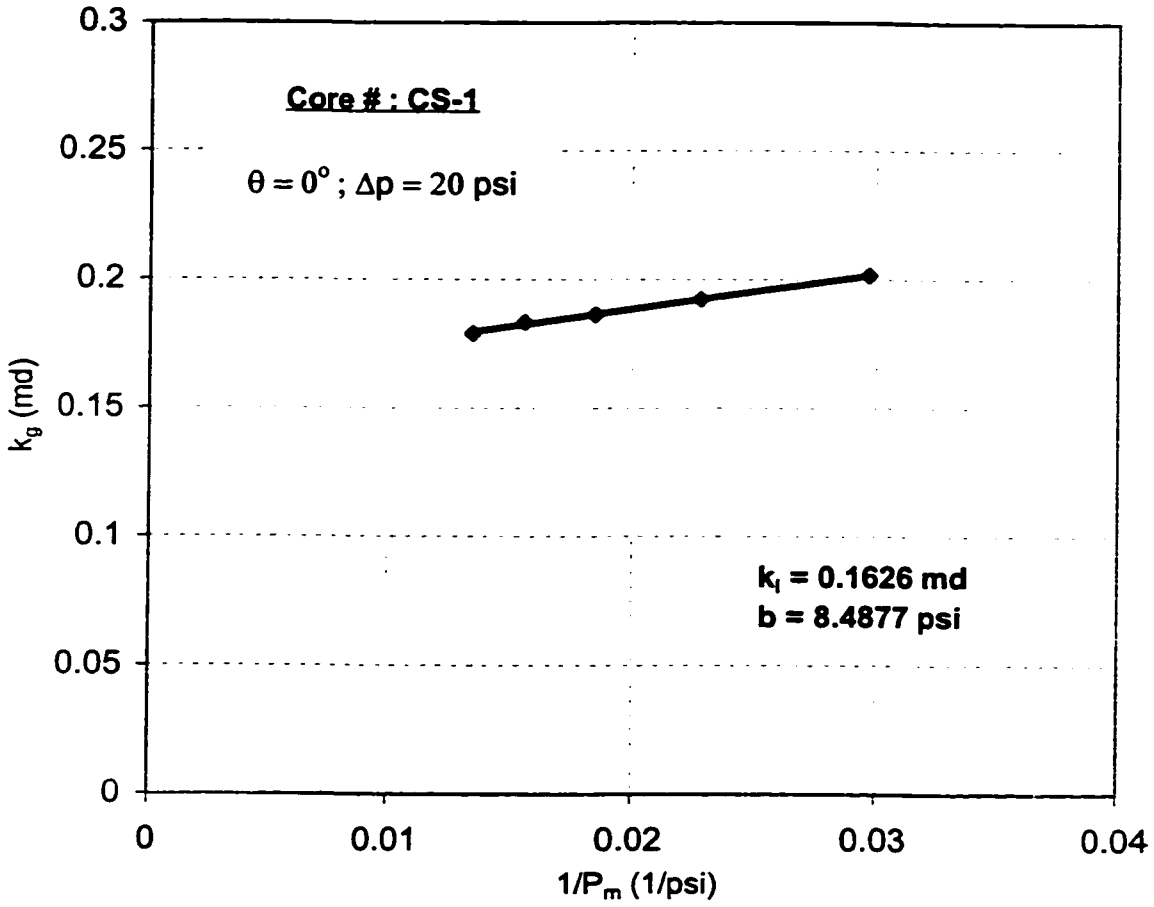

Figure 6.11: Determination of 'k_l' and 'b' from experimental pulse-decay data using NLR-Graphical Method for core sample CS-1 ($\theta = 0^\circ$ and $\Delta p = 20$ psi)

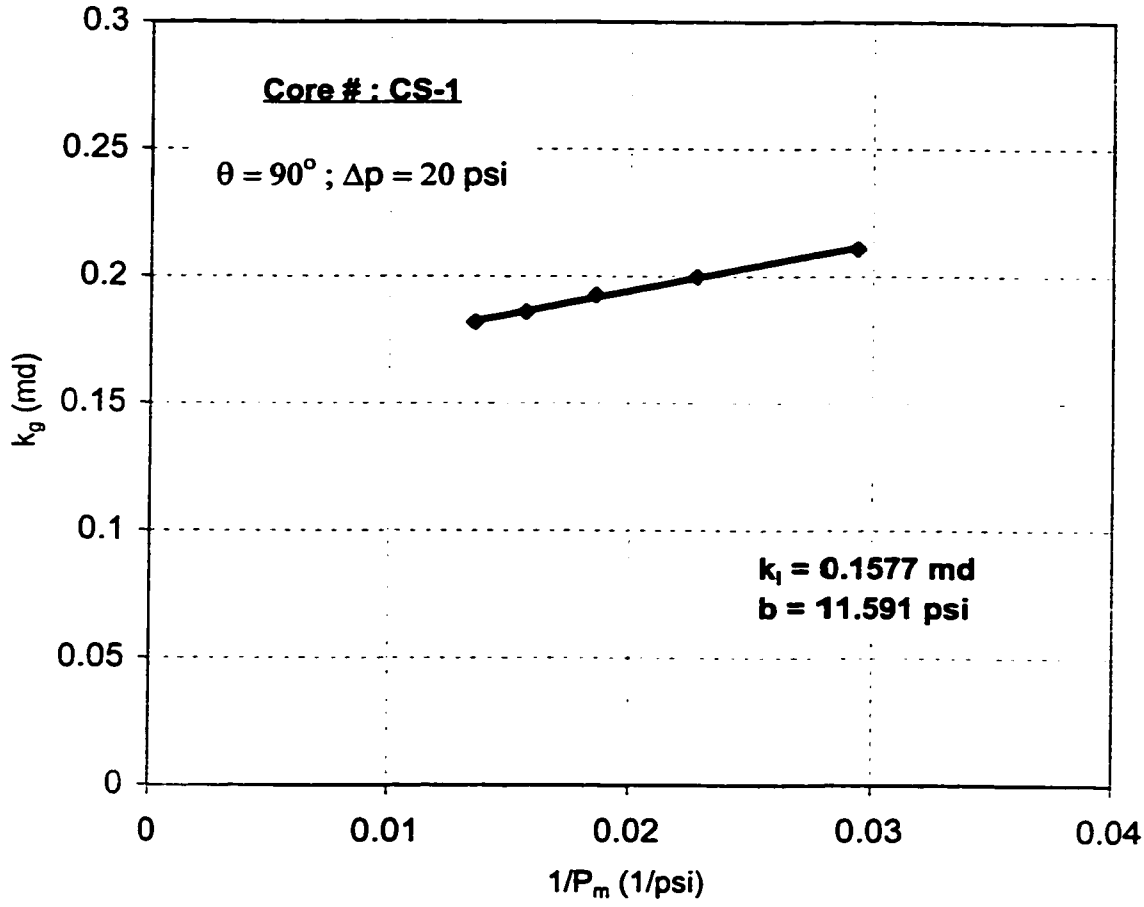

Figure 6.12: Determination of 'k_i' and 'b' from experimental pulse-decay data using NLR-Graphical Method for core sample CS-1 ($\theta = 90^\circ$ and $\Delta p = 20$ psi)

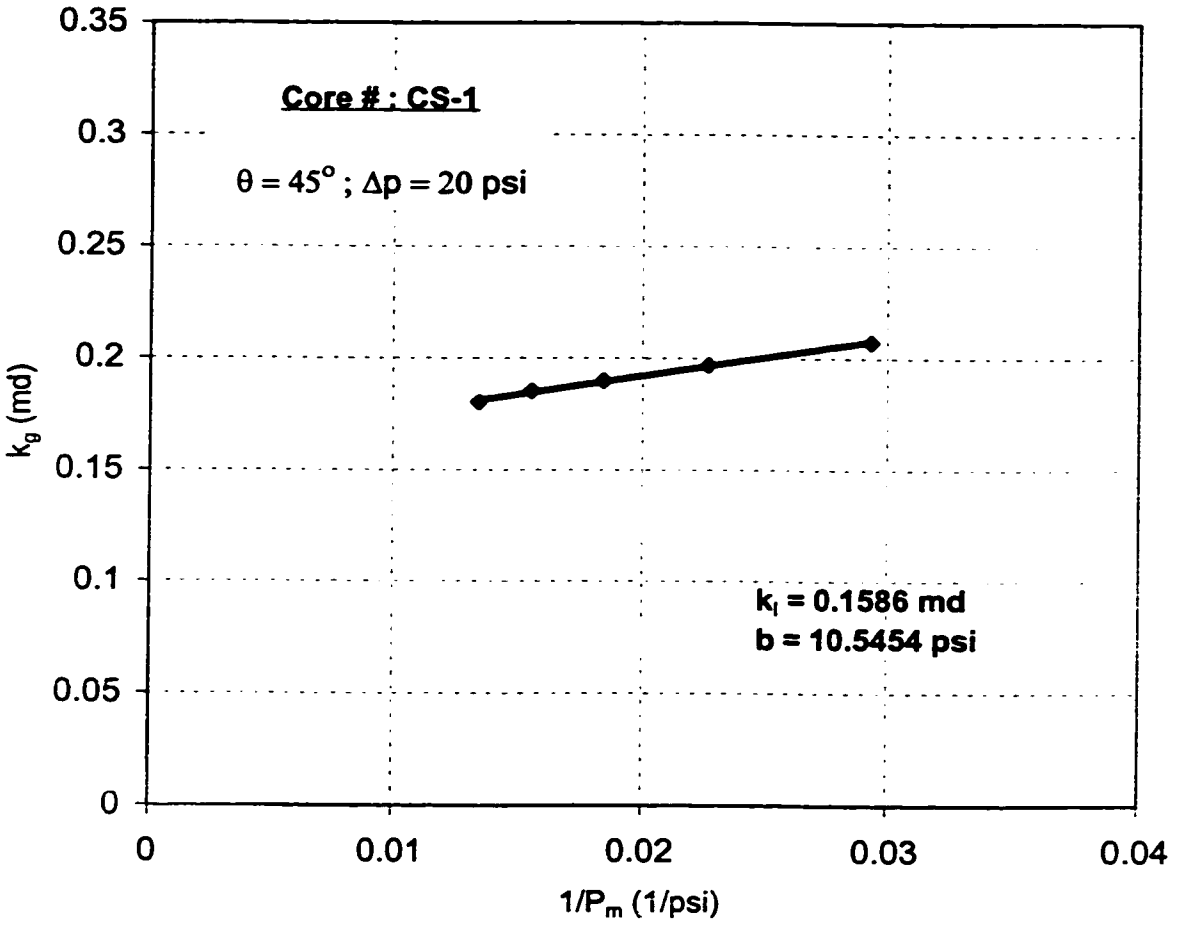

Figure 6.13: Determination of 'k_l' and 'b' from experimental pulse-decay data using NLR-Graphical Method for core sample CS-1 ($\theta = 45^\circ$ and $\Delta p = 20$ psi)

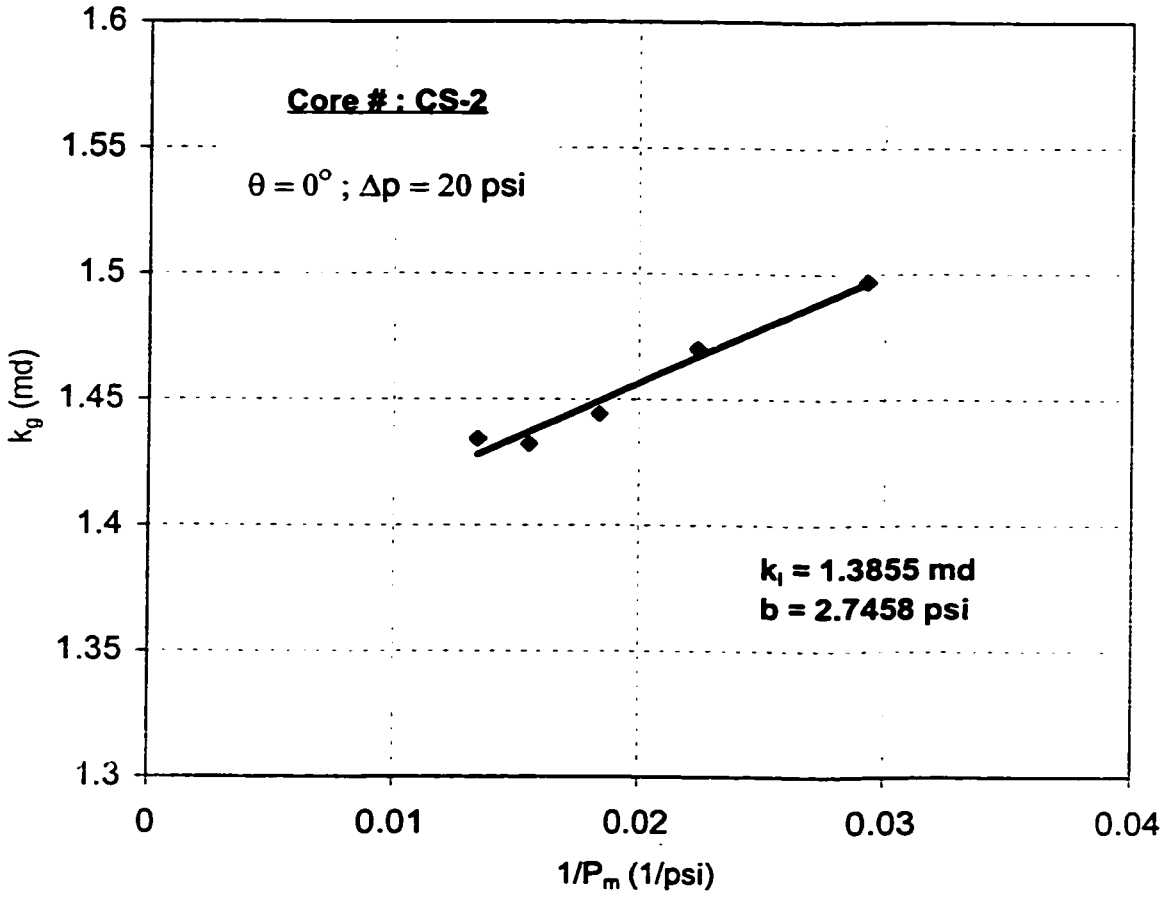

Figure 6.14: Determination of 'k_l' and 'b' from experimental pulse-decay data using NLR-Graphical Method for core sample CS-2 ($\theta = 0^\circ$ and $\Delta p = 20$ psi)

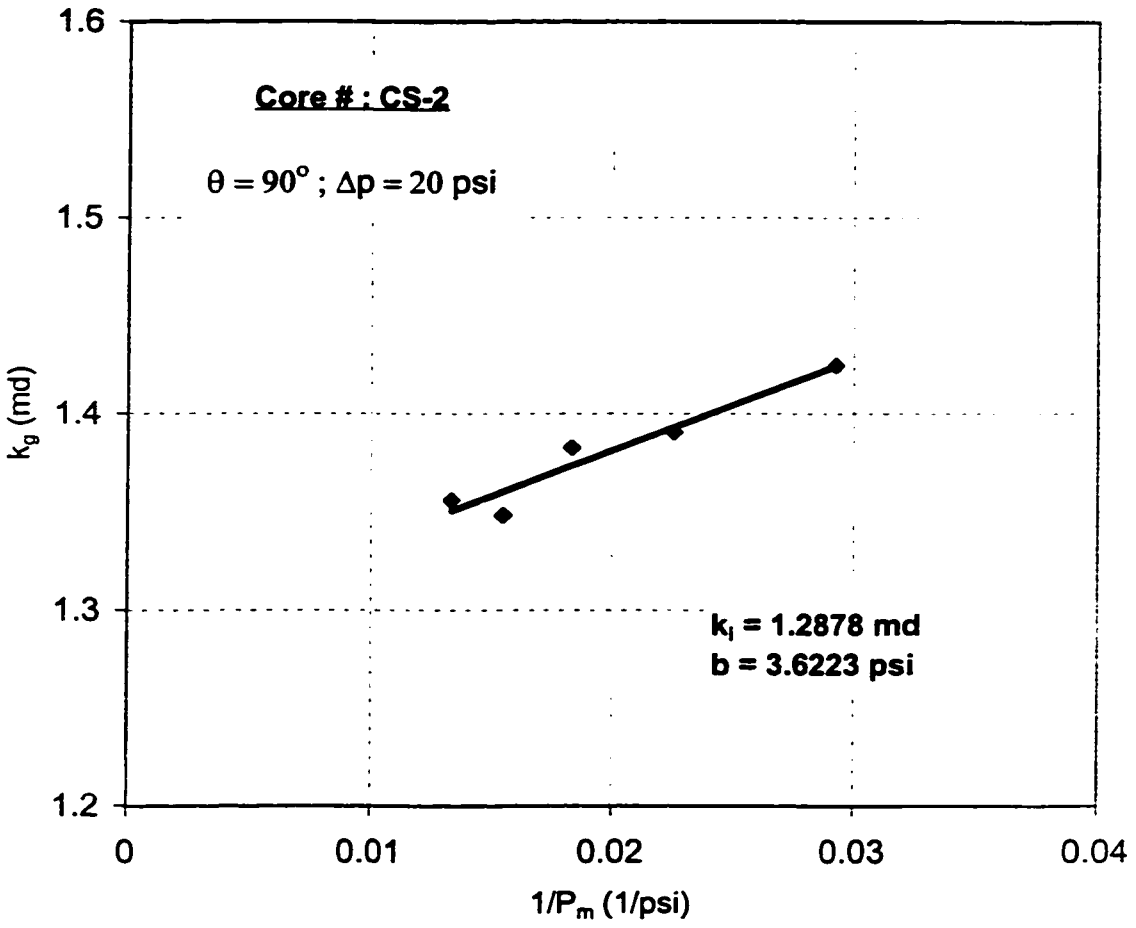

Figure 6.15: Determination of 'k_i' and 'b' from experimental pulse-decay data using NLR-Graphical Method for core sample CS-2 ($\theta = 90^\circ$ and $\Delta p = 20$ psi)

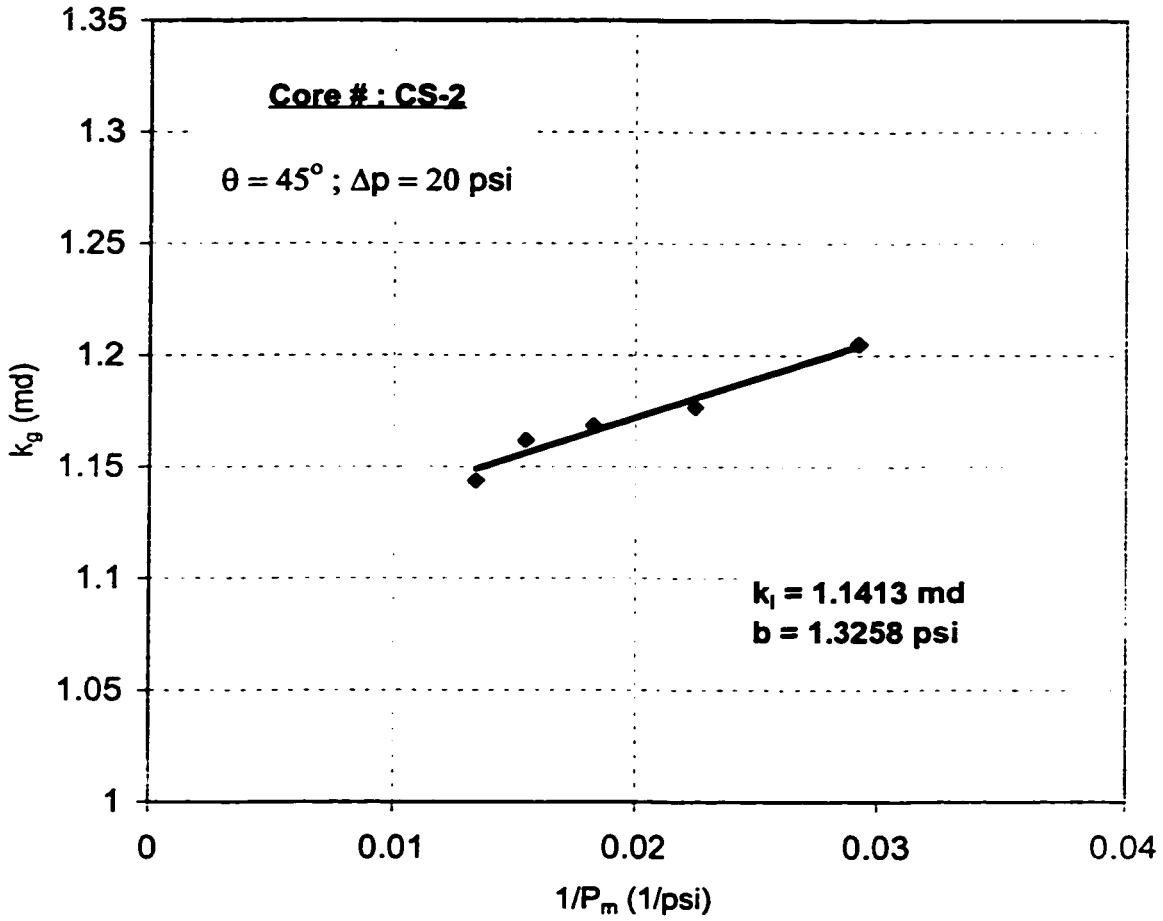

Figure 6.16: Determination of 'k_l' and 'b' from experimental pulse-decay data using NLR-Graphical Method for core sample CS-2 ($\theta = 45^\circ$ and $\Delta p = 20$ psi)

TABLE 6.8: Summary of Pulse-Decay Experimental Results

Sample Number	ΔP (psi)	Permeability (md)			Klinkenberg Factor (psi)			Klinkenberg Factor (Jones) (psi)		
		Location			Location			Location		
		$\theta = 0^o$	$\theta = 90^o$	$\theta = 45^o$	$\theta = 0^o$	$\theta = 90^o$	$\theta = 45^o$	$\theta = 0^o$	$\theta = 90^o$	$\theta = 45^o$
CS-1	21	0.1626	0.1577	0.1586	8.49	11.59	10.54	13.26	13.42	13.39
CS-1	30	0.1583	-	-	9.08	-	-	13.40	-	-
CS-1	100	0.1303	0.1325	-	21.07	22.20	-	14.37	14.28	-
CS-2	10	1.3654	1.3176	1.1147	3.28	1.85	3.59	6.30	6.41	6.78
CS-2	20	1.3855	1.2878	1.1413	2.75	3.62	1.33	6.14	6.40	6.58

6.3.7 Effect of Pressure Pulse Size

During some experimental runs, the pressure pulse size was varied to experimentally verify the simulation findings.

For sample CS-1, three runs of pulse-decay experiments were performed at $\theta=0^{\circ}$, using pulse size of 20, 30 and 100 psi (Figures 6.11, 6.17 and 6.18). The results indicate that as pulse size increases, the measured value of permeability decreases. The reason, as discussed earlier in the previous sections, could either be the introduction of non-Darcy flow effects or sudden variation in the mean pore pressure. A similar trend was also observed for $\theta=90^{\circ}$ (Figures 6.12 and 6.19).

6.4 Analysis of Steady-State Experimental Results

To verify the results of the-pulse decay experiments, several runs of steady-state experiments were carried out for the two core samples. By using Equation 5.3, gas permeabilities were calculated at different mean pore pressures and were then plotted against the reciprocal of mean pore pressures as a straight line. As discussed earlier, the y-intercept of the line is the liquid permeability whereas the Klinkenberg factor is obtained by dividing the slope of the line by its y-intercept. The results are plotted in Figures 6.20 to 6.22.

Since, the results of pulse-decay experiments for sample CS-1 showed that the core sample has almost the same permeability at the three different

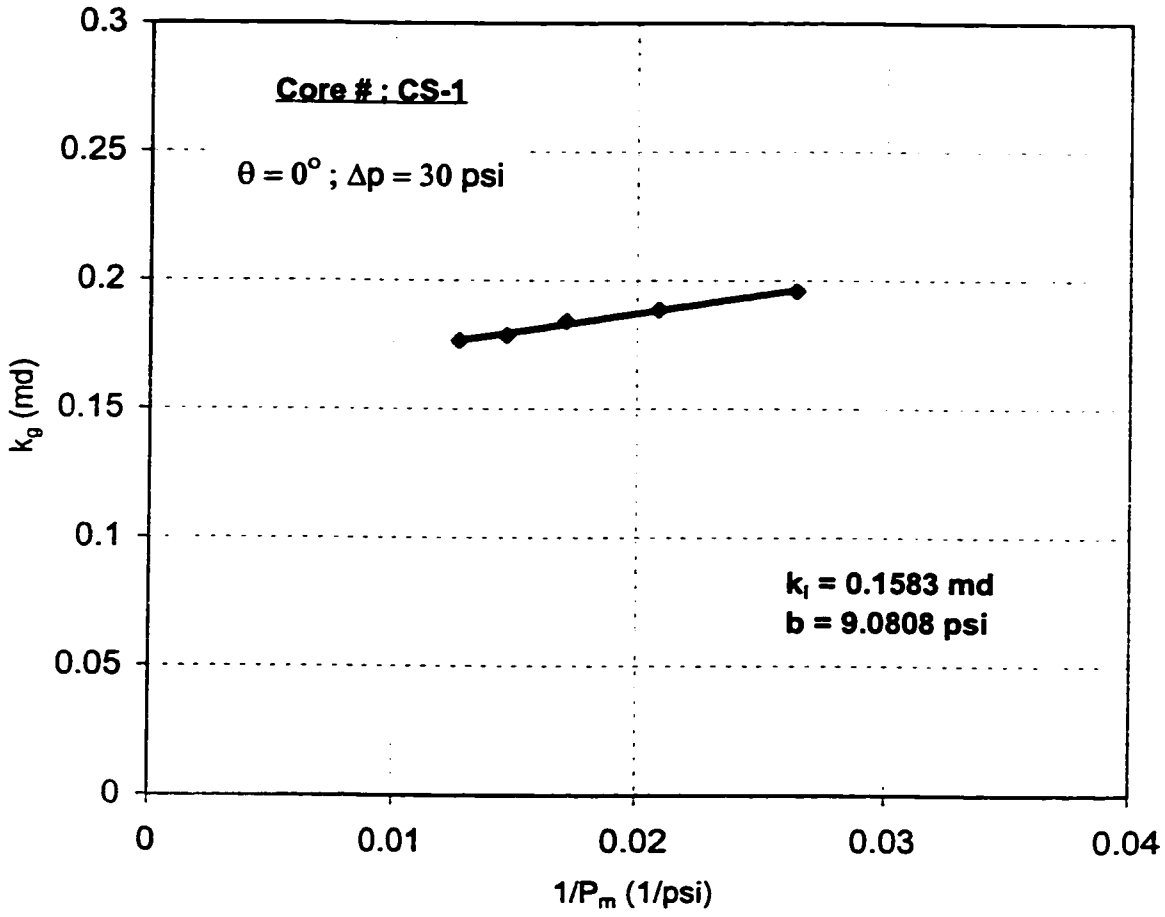

Figure 6.17: Determination of 'k_l' and 'b' from experimental pulse-decay data using NLR-Graphical Method for core sample CS-1 ($\theta = 0^\circ$ and $\Delta p = 30$ psi)

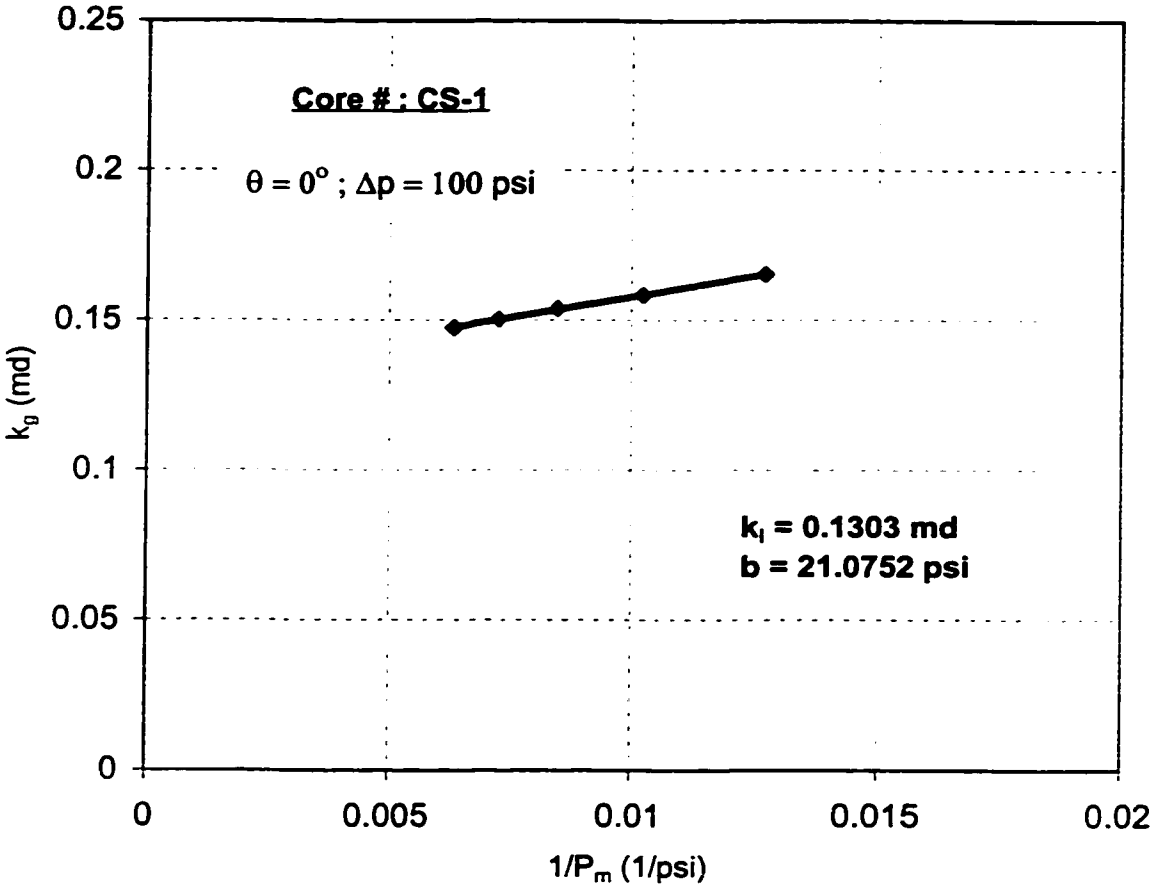

Figure 6.18: Determination of 'k_l' and 'b' from experimental pulse-decay data using NLR-Graphical Method for core sample CS-1 ($\theta = 0^\circ$ and $\Delta p = 100$ psi)

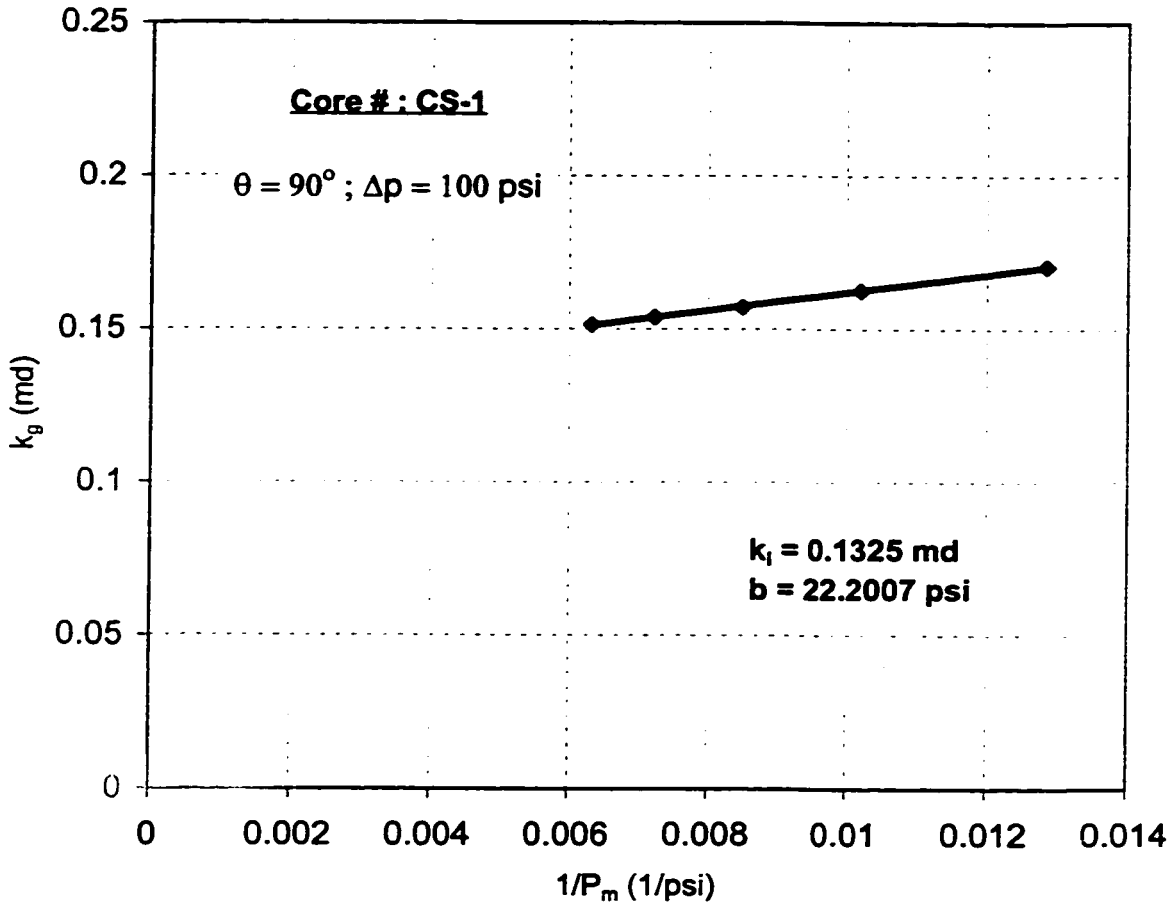

Figure 6.19: Determination of 'k_l' and 'b' from experimental pulse-decay data using NLR-Graphical Method for core sample CS-1 ($\theta = 90^\circ$ and $\Delta p = 100$ psi)

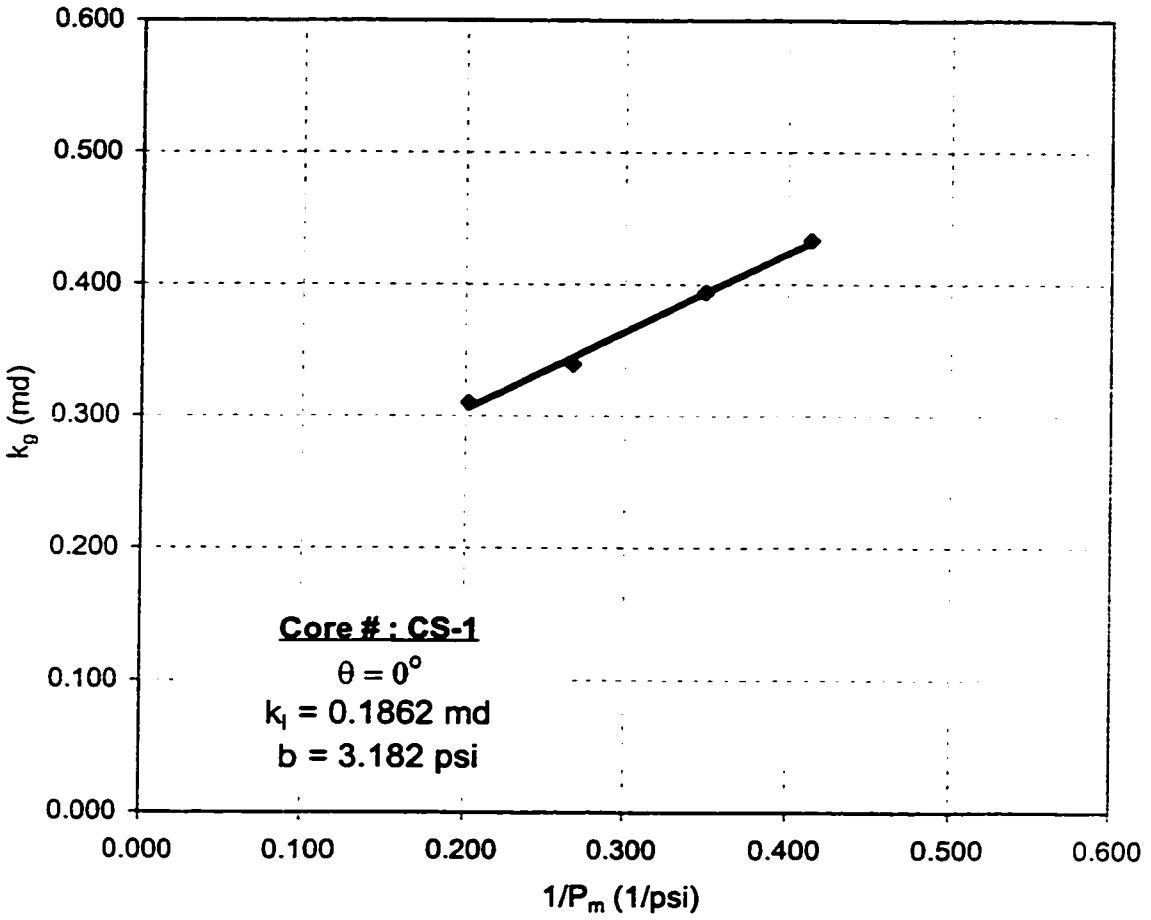

Figure 6.20: Determination of 'k_l' and 'b' from steady-state experimental data using Graphical Method for core sample CS-1 (θ = 0°)

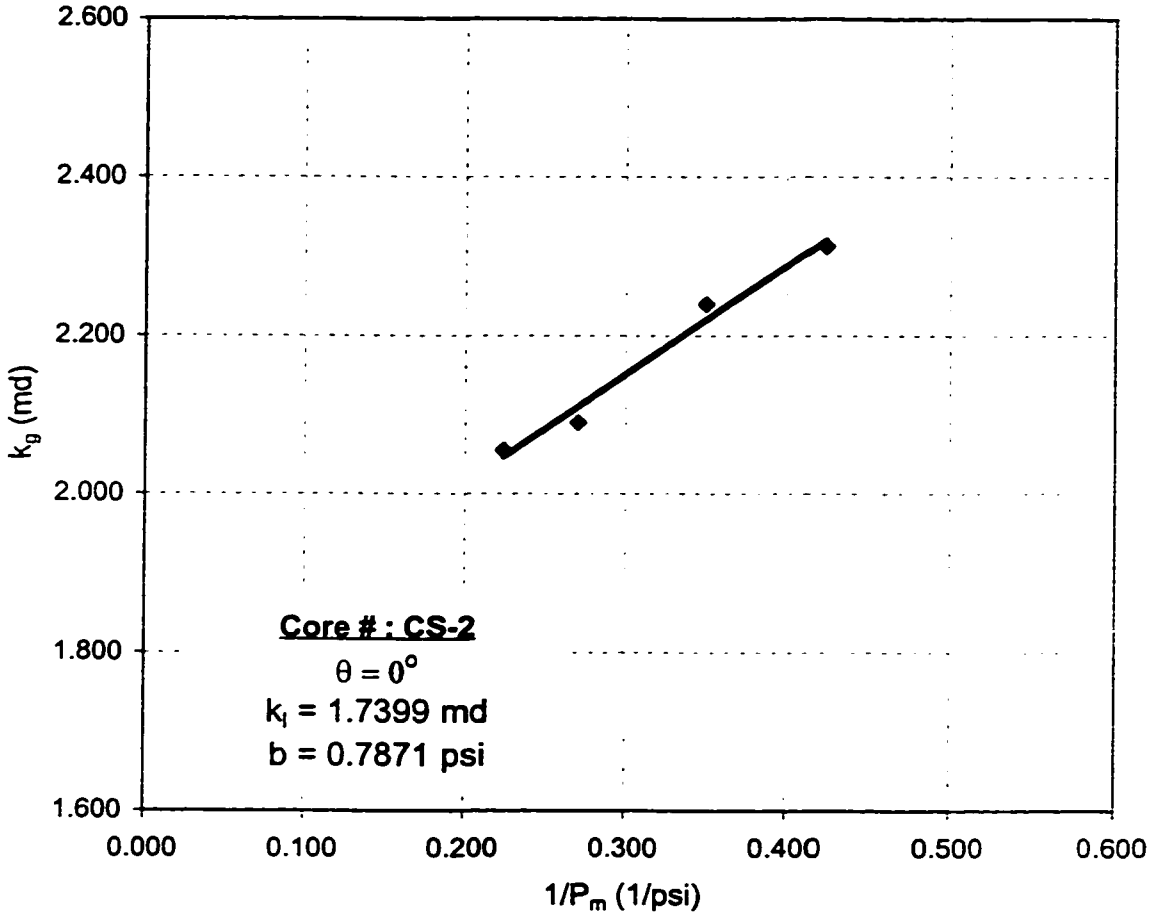

Figure 6.21: Determination of 'k_l' and 'b' from steady-state experimental data using Graphical Method for core sample CS-2 ($\theta = 0^\circ$)

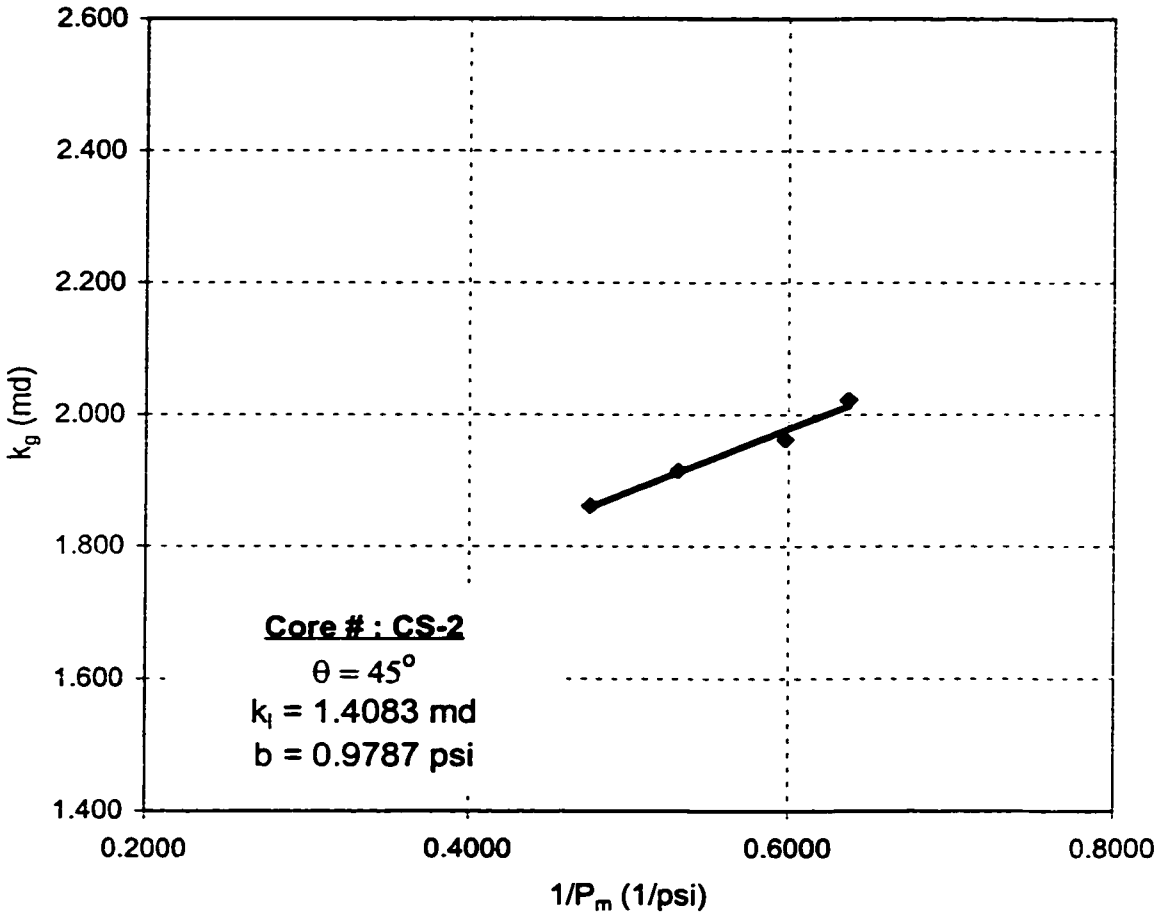

Figure 6.22: Determination of 'k_i' and 'b' from steady-state experimental data using Graphical Method for core sample CS-2 (θ = 45°)

directions of transverse flow across the core, it was decided to carry out the experiment in only one direction. The results are shown in Figure 6.20. On the other hand, for core sample CS-2, different values of permeability were obtained across the core for different directions. Therefore, two experiments, each consisting of 4 to 5 runs of various mean pore pressures, were performed and the results are shown in Figures 6.21 and 6.22.

A comparison of the pulse-decay values and steady-state values for permeability and Klinkenberg factor is shown in Table 6.9. The values of Klinkenberg factor obtained by using the Jones' empirical correlation are also tabulated in the Table 6.9. It is clear from the comparison that permeability values obtained through pulse-decay experiments are lower than that obtained by steady-state experiments. The difference ranges from 12 to 20%. Similarly, a comparison of the Klinkenberg factor values clearly indicates a significant difference between the values obtained from both methods. However, the values obtained by the pulse-decay experiments appear to be in close agreement with the values obtained from Jones' empirical correlation. Therefore, based on this and also keeping in view the problems associated with the steady-state experiments such as attainment of steady-state, accurate measurement of the flow rate and longer stabilization times, it seems appropriate to assume that the pulse-decay values are more reliable.

TABLE 6.9: Comparison of Pulse-Decay and Steady-State Results

	Pulse-Decay Values		Steady-State Values			% Difference b/w PD & SS Values	
Sample Number	k (md)	b (psi)	k (md)	b (psi)	b (Jones Correlation)* (psi)	k	b
CS-1 ($\theta = 0^o$)	0.163	8.488	0.186	3.182	13.269	-12.67	166.74
CS-2 ($\theta = 0^o$)	1.386	2.746	1.740	0.787	6.136	-20.37	248.85
CS-2 ($\theta = 45^o$)	1.141	1.326	1.408	0.674	6.579	-18.96	96.71

* ***Jones' Correlation***

$b = 6.9(k_l)^{(-0.36)}$

CHAPTER 7

SUMMARY, CONCLUSIONS AND RECOMMENDATIONS

In this chapter, the results of the work carried out in this study concerning the application of pulse-decay method for the permeability determination of whole core samples is summarized and concluded.

7.1 Summary

1. Experimental set-up was constructed to perform pulse-decay experiments on whole cores.

2. Mathematical model, which incorporates the slippage effects, has been developed to solve the problem of unsteady transverse flow through whole cores.

3. A numerical simulator is developed to solve the two-dimensional, single-phase, transient compressible fluid flow equation incorporating the gas-slippage effects, to describe pressure pulse-decay in whole cores.

4. Based on the numerical simulator, a computer program is developed that analyzes the pressure pulse-decay data of whole cores to estimate permeability and Klinkenberg factor using non-linear regression.

5. Pressure pulse-decay method has been applied on full diameter whole cores for permeability determination.

7.2 Conclusions

1. A technique is proposed for the simultaneous estimation of permeability (k) and Klinkenberg factor (b) of whole core samples from multiple pressure pulse-decay tests.

2. Pressure pulse-decay method can also be used to detect permeability anisotropy by making pressure measurements at different directions after changing the orientation of core sample.

3. Experimental errors can significantly affect the correct estimation of permeability (k) and Klinkenberg factor (b) of whole core samples from single pressure pulse-decay test.

4. Use of large pressure pulse in pulse-decay experiments can introduce non-Darcy flow effects, thus leading to underestimation of permeability. Furthermore, it also causes a sudden variation in mean pore pressure,

which violates our assumption of constant mean pore pressure in the proposed technique. However, the selection of the optimum pulse size depends upon the permeability of the sample and the size of the upstream and downstream cells.

5. The permeability values obtained from pulse-decay method differed by 12-20% from the steady-state values. Similarly, the values of Klinkenberg factor obtained from both methods differ quite significantly.

7.3 Recommendations

1. Pressure pulse-decay method is faster and easier to perform as compared to conventional steady-state method. Therefore, as a new alternative, it could be introduced as a standard lab permeability measurement.

2. Work is suggested to incorporate the non-Darcy flow effects in the governing flow equation.

REFERENCES

[1] Amaefule, J. O., Wolfe, K., Walls, J. D., Ajufo, A. O., and Peterson, E., "Laboratory Determination of Effective Liquid Permeability in Low-Quality Reservoir Rocks by the Pulse Decay Technique", paper SPE 15149 presented at The 56th California Regional Meeting of the SPE held in Oakland, CA, April 2-4, 1986, pp. 493-502.

[2] Bourbie, T. and Walls, J., "Pulse Decay Permeability : Analytical Solution and Experimental Test", Society of Petroleum Engineers Journal, October 1982, pp. 719-721.

[3] Brace, W. F., Walsh, J. B. and Frangos, W. T., "Permeability of Granite under High Pressure", Journal of Geophysical Research, Vol. 73, No. 6, March 15, 1968, pp. 2225-2336.

[4] Chen, T. and Stagg, P. W., "Semi-log Analysis of the Pulse-Decay Technique of Permeability Measurement", Society of Petroleum Engineers Journal, December 1984, pp. 639-642.

[5] Dicker, A. I. and Smits, R. M., "A Practical Approach for Determining Permeability from Pressure-Pulse Decay Measurements", paper SPE 17578 presented at the SPE International Meeting on Petroleum Engineering, held in Tianjin, China, November 1-4, 1988, pp. 285-292.

[6] Freeman, D. L. and Bush, D. C., "Low-permeability Laboratory Measurements by Nonsteady-state and Conventional Methods", Society of Petroleum Engineers Journal, December 1983, pp. 928-936.

[7] Gilicz, A., "Application of the Pulse Decay Technique", paper SPE 22688 presented at the 66th Annual Technical Conference and Exhibition of the SPE held in Dallas, TX, October 6-9, 1991, pp. 305-317.

[8] Guo, F. and Wong, K., "A New Pressure Decay Technique – Measurement of Live Heavy Oil Mobility in Unconsolidated Oil Sand Cores", The Journal of Canadian Petroleum Technology, Vol. 35, No. 1, January 1996, pp. 60-62.

[9] Haskett, Steven E., Narahara, Gene M. and Holditch, Stephen A., "A Method of Simultaneous Determination of Permeability and Porosity in Low-Permeability Cores", SPE Formation Evaluation, September 1988, pp. 651-658.

[10] Jones, S. C., "A Rapid Accurate Unsteady-state Klinkenberg Permeameter", Society of Petroleum Engineers Journal, October 1972, pp. 383-397.

[11] Jones, S. C., "A Technique for Faster Pulse-Decay Permeability Measurements in Tight Rocks", paper SPE 28450 presented at the 69th Annual Technical Conference and Exhibition of the SPE held in New Orleans, LA, September 25-28, 1994, pp. 907-914.

[12] Kamath, J., Boyer, R. E., and Nakagawa, F. M., "Characterization of Core-Scale Heterogeneities using Laboratory Pressure Transients", SPE Formation Evaluation, September 1992, pp. 219-227.

[13] Lin, W., "Parametric Analyses of the Transient Method of Measuring Permeability", Journal of Geophysical Research, Vol. 87, No. B2, February 10, 1982, pp. 1055-1060.

[14] Narahara, G. M., Holditch, S. A. and Moore, K. R., "A New Method for the Measurement of Gas Relative Permeability and Water Saturation Simultaneously in Low-Permeability Cores", paper SPE 18318 presented at the 63rd Annual Technical Conference and Exhibition of the SPE held in Houston, TX, October 2-5, 1988, pp. 551-557.

[15] Rudd, Neilson, "Pressure Decay Measurements", paper SPE 1604 presented at SPE Gas Technology Symposium held in Omaha, Nebraska, September 15-16, 1966, pp. 1-6.

[16] Trimmer, Donald A., "Design Criteria for Laboratory Measurements of Low-Permeability rocks", Geophysical Research Letters, Vol. 8, No. 9, September 1981, pp. 973-975.

[17] Yamada, S. E. and Jones, A. H., "A Review of a Pulse Technique for Permeability Measurements", Society of Petroleum Engineers Journal, October 1980, pp. 357-358.

[18] Collins, R. E., "Flow of Fluids through Porous Materials", The Petroleum Publishing Company, 1976, pp. 88-98.

[19] Kelton, Frank C., "Analysis of Fractured Limestone Cores", T.P. 2913, Petroleum Transactions, AIME, Vol. 189, 1950, pp. 225-234.

[20] American Petroleum Institute, "Recommended Practices for Core Analysis", RP 40, Second Edition, February 1998.

[21] Collins, R. E., "Determination of the Transverse Permeabilities of Large Core Samples from Petroleum Reservoirs", Journal of Applied Physics, Vol. 23, No. 6, June 1952, pp. 681-684.

[22] Hirasaki, G.J. and O' Dell, P.M., "Representation of Reservoir Geometry for Numerical Simulation", Society of Petroleum Engineers Journal, December 1970, pp. 393-404; Trans., AIME, Vol. 249.

[23] Hseih, P. A., Tracy, J. V., Neuzil, C. E., Bredehoeft, J. D. and Silliman, S.E., "A Transient laboratory Method for Determining the Hydraulic Properties of 'Tight' Rocks – I. Theory", Intl. Journal Rock Mech. Min. Sci. and Geomech. Abstracts, Vol. 18, 1981, pp. 245-252.

[24] Klinkenberg, L.J., "The Permeability of Porous Media to Liquids and Gases", Drilling and Production Practices, American Petroleum Institute, pp. 200, 1941.

[25] Neuzil, C. E., Cooley, C., Silliman, S. E., Bredehoeft, J. D. and Hseih, P. A., "A Transient laboratory Method for Determining the Hydraulic Properties of 'Tight' Rocks – II. Application", Intl. Journal Rock Mech. Min. Sci. and Geomech. Abstracts, Vol. 18, 1981, pp. 253-258.

[26] Robertson, G. E. and Woo, P.T., "Grid-Orientation Effects and the Use of the Orthogonal Curvilinear Coordinates in Reservoir Simulation", Society of Petroleum Engineers Journal, February 1978, pp. 13-19.

[27] Sonier, F. and Chaumet, P., "A Fully Implicit Three-Dimensional Model in Curvilinear Coordinates", Society of Petroleum Engineers Journal, August 1974, pp. 361-370; Trans., AIME, Vol. 257.

APPENDIX

```
************************************************************************
**    TWO-PARAMETER COMPUTER PROGRAM FOR THE ANALYSIS OF PRESSURE    **
**    PULSE DECAY DATA FOR THE ESTIMATION OF LIQUID PERMEABILITY &   **
**     KLINKENBERG FACTOR USING NON-LINEAR REGRESSION TECHNIQUE      **
************************************************************************


                        ====================
                            MAIN Program
                        ====================

      USE MSIMSLMS
      USE MSIMSLSD

C     DESCRIPTION OF PARAMETERS :
C
C     NX     = NUMBER OF GRID BLOCKS IN THE X-DIRECTION
C     NY     = NUMBER OF GRID BLOCKS IN THE Y-DIRECTION
C     NW     = NUMBER OF WELLS IN THE SYSTEM
C     AREA   = AREA OF GRID BLOCK, FT**2
C     VPD    = PORE VOLUME OF GRID BLOCK, CU FT
C     TX     = TRANSMISSIBILITY AT THE FACE IN THE X-DIRECTION, MD-FT
C     TY     = TRANSMISSIBILITY AT THE FACE IN THE Y-DIRECTION, MD-FT
C     P      = PRESSURE, PSI
C     IW     = WELL LOCATION IN THE X-DIRECTION
C     JW     = WELL LOCATION IN THE Y-DIRECTION
C     PWF    = CALCULATED FLOWING BOTTOM HOLE PRESSURE, PSI
C     TD     = ELAPSED TIME, SEC
C     DTr    = TIME STEP SIZE, SEC
C     DTD    = CONSTANT
C     DT     = TIME STEP SIZE (EXP), SEC
C     NDT    = NUMBER OF TIME STEPS (Exp)
C     NP     = NUMBER OF EXPERIMENTAL DATA POINTS

C     INPUT DATA :
C
C     THE PROGRAM REQUIRES THE DATA TO BE SUPPLIED FROM A FILE
C     AS SPECIFIED IN THE READING FORMATS. THE FOLLOWING FILES
C     ARE REQUIRED:
C
C           (1) PDSR-E1.DAT     : CONTAINS EXPERIMENTAL INPUT DATA.
C           (2) PDSR-G1.DAT     : CONTAINS BASIC INPUT GRID DATA.
C
C     OUTPUT DATA :
C
C           (1) .ARE    : CONTAINS AREA OF GRID CELLS.
C           (2) .DEC    : CONTAINS UPSTREAM & DOWNSTREAM PRESSURES & DECAY.
C           (3) .DIS    : CONTAINS PRESSURE DISTRIBUTION.
C           (4) .PAR    : CONTAINS FINAL ESTIMATES OF NON-LINEAR PARAMETERS.
C           (5) .FIN    : CONTAINS ERROR B/W MEASURED & CALCULATED DECAY.
C
      INCLUDE 'PDSR-C1.COP'
      DIMENSION PM(LDX),PC(LDX)
      DIMENSION A(NCOEF),R(NCOEF,NCOEF)
      COMMON /BLK6/ V(LDX,NCOL),NP
C
```

```
      EXTERNAL EVAL
      DATA IDERIV/1/
C
      OPEN(UNIT=6,FILE='PDSR-G1.DAT')
      OPEN(UNIT=11,FILE='PD.ARE')
      OPEN(UNIT=12,FILE='PD.DEC')
      OPEN(UNIT=13,FILE='PD.DIS')
      OPEN(UNIT=16,FILE='PDSR-E1.DAT')
      OPEN(UNIT=17,FILE='PDSR.PAR')
      OPEN(UNIT=18,FILE='PDSR.FIN')
C
C     Read Experimental Data
      CALL EXPDATA(PERM,BEE,PM)
C
      A(1)=PERM
      A(2)=BEE
C
C     Generate Grid Cells and Calculate Transmissibilities & Areas
      CALL GENGRID
C
      WRITE(17,100)
      WRITE(17,110) PERM,BEE
      WRITE(17,120) NP
  100 FORMAT(/,5X,'INITIAL ESTIMATE OF THE UNKNOWN PARAMETERS')
  110 FORMAT(5X,'PERMEABILITY=',E12.5,3X,'BEE=',E12.5)
  120 FORMAT(/,5X,'NUMBER OF DATA POINTS READ =',I4)
  140 FORMAT(/,5X,'FINAL ESTIMATE OF THE UNKNOWN PARAMETERS')
  220 FORMAT(/,5X,'INITIAL ESTIMATE OF THE NON-LINEAR PARAMETERS')
  230 FORMAT(5X,'A(',I1,')=',E12.5)
  240 FORMAT(/,5X,'FINAL ESTIMATE OF THE NON-LINEAR PARAMETERS')
C
  300 FORMAT(5X,'SAE =',F10.2,3X,'NO. OF ITER =',I3)
  340 FORMAT(11X,'TIME     P(MEAS)    P(CALC)    ERROR %')
  350 FORMAT(5X,F10.2,3F10.2)
  400 FORMAT(5X,'AVERAGE ABSOLUTE RELATIVE ERROR =',F10.3)
  500 FORMAT(/,3X,'ESTIMATE OF THE PARAMETERS AT ITERATION NUMBER =',I2)
  600 FORMAT(5X,'SUM OF THE SQUARES OF THE ERROR =',F12.3)
C
C     PRINT THE INITIAL ESTIMATES OF THE NON-LINEAR PARAMETERS
      WRITE(17,220)
      WRITE(17,230) (I,A(I),I=1,NCOEF)
C     MESSAGE ON THE SCREEN
      WRITE(*,*)
      WRITE(*,*)' Please Wait !  Program is Running.'
      WRITE(*,*)
C
C     NON-LINEAR REGRESSION - LEAST SQUARE METHOD
      CALL DRNLIN(EVAL,NCOEF,IDERIV,A,R,LDX,IRANK,DFE,SSE)
C
C     PRINT THE FINAL ESTIMATES OF THE NON-LINEAR PARAMETERS
      WRITE(17,240)
      WRITE(17,230) (I,A(I),I=1,NCOEF)
C
      PERM = A(1)
      BEE  = A(2)
      WRITE(17,140)
      WRITE(17,110) PERM,BEE
      WRITE(18,340)
C
C     COMPUTE THE CALCULATED PRESSURES
      CALL FUNEVL(PERM,BEE,NP,PC)
C     CALCULATE ERRORS AND PRINT THE RESULTS
      CALL ERROR(PM,PC,NP,NCOEF,SSE)
C     CALCULATE CONFIDENCE
      CALL CONF(A,SSE)
C
      DO 765 K=1,NP
```

```
      ERR=100.*(PM(K)-PC(K))/PM(K)
      WRITE(18,350) V(K,1),PM(K),PC(K),ERR
  765 CONTINUE
      STOP
      END

                        ------------------------
                             Subroutine EXPDATA
                        ------------------------

      SUBROUTINE EXPDATA(PERM,BEE,PM)
C
C     THIS SUBROUTINE READS THE EXPERIMENTAL DATA
C
      IMPLICIT REAL*8 (A-H,O-Z)
      PARAMETER (NCOL=2,NOBS=600,LDX=NOBS)
      DIMENSION PM(LDX)
      COMMON /BLK1/ TEMP,PU,PD,VU,VD,RAD,H,POR,Vp
      COMMON /BLK2/ DT(NOBS),NDT(NOBS)
      COMMON /BLK6/ V(LDX,NCOL),NP
C
C     READ THE EXPERIMENTAL PARAMETERS
      READ(16,*)
      READ(16,*) TEMP,PU,PD,VU,VD,RAD,H,POR
C     READ THE INITIAL ESTIMATE OF THE PARAMETERS
      READ(16,*)
      READ(16,*) PERM,BEE
C     CALCULATE BEE FROM CORRELATION IF NOT GIVEN IN FILE
      IF(BEE.LT.0.) BEE=6.9/PERM**.36
C     READ PRESSURE DROP EXPERIMRNTAL DATA
      READ(16,*)
      K=0
   10 K=K+1
      READ (16,*,END=15) V(K,1),DP,DT(K),NDT(K)
      V(K,2)=DP
      PM(K)=DP
      GO TO 10
   15 NP=K-1
      RETURN
      END

                        ------------------------
                             Subroutine GENGRID
                        ------------------------

      SUBROUTINE GENGRID
C
C     THIS SUBROUTINE GENERATES THE GRID DATA
C
      INCLUDE 'PDSR-C1.COP'
      REAL    AD,AM,AMP,AK,XM,YM,DXX,DYY,TOL,X(MX,MY),Y(MX,MY),
     &        A1,A2,A3,A4
      REAL    ELK
      COMPLEX CEJSN,CASIN
      COMPLEX XI,XK,WPP,WP,WK,W,ZXM,ZYM,DZX,DZY,ZP(MX,MY),Z(MX,MY)
C
      XI = (0.,1.)
      READ(6,*)
      READ(6,*) AD,NPL,NSL,TOL
C     Generation of Rectangular Grid
      AK=COSD(AD) - TOL
      AM=AK*AK
      AMP=1.-AM
      XM=ELK(AM) - TOL
      YM=ELK(AMP) - TOL
      ZXM=CMPLX(XM)
      ZYM=CMPLX(0.,YM)
```

```
      XK=CMPLX(AK)
      DXX=XM/(NPL-1)
      DYY=YM/(NSL-1)
      DZX=CMPLX(DXX)
      DZY=CMPLX(0.,DYY)
      ZP(1,1) = (0.,0.)
      DO 10 I=2,NPL-1
      ZP(I,1) = ZP(I-1,1) + DZX
 10   CONTINUE
      ZP(NPL,1)=ZXM
      DO 20 I=1,NPL
      DO 25 J=2,NSL-1
 25   ZP(I,J) = ZP(I,J-1) + DZY
 20   ZP(I,NSL)=ZP(I,1) + ZYM
C
C     Conversion of Rectangular Grid into Quarter-Circular Grid
      DO 35 I=1,NPL
      DO 30 J=1,NSL
      WPP= ZP(I,J)
      WP = CEJSN (WPP, AM)
      WK = XK*WP
      W  = CASIN (WK)
      Z(I,J) = -XI*CEXP (XI*W)
 30   CONTINUE
 35   CONTINUE
C
C     Compute the Coordinates of the Grid Points in a Semi-Circle
      DO 40 JJ=1,NSL
      J=NSL-JJ+1
C
      DO 42 II=1,NPL
      I=NPL-II+1
      X(II,JJ)=REAL(Z(I,J))
      Y(II,JJ)=-AIMAG(Z(I,J))
 42   CONTINUE
      DO 44 I=2,NPL
      II=NPL+I-1
      X(II,JJ)=-REAL(Z(I,J))
      Y(II,JJ)=-AIMAG(Z(I,J))
 44   CONTINUE
C
 40   CONTINUE
C
      NX2=2*NPL-1
      NX=NX2+1
      NY=NSL-1
C
C     Compute the Transmissibilities
      DO 51 J=1,NY
      TX(1,J)=0.
      TX(NX,J)=2.*DYY/DXX
      IF(J .GT. 1) THEN
               TY(1,J)=1.0D6
               TY(NX,J)=1.0D6
      ELSE
               TY(1,J)=0.
               TY(NX,J)=0.
      ENDIF
      DO 50 I=1,NX-2
      II=I+1
      IF(I .GT. 1) THEN
               TX(II,J)=DYY/DXX
      ELSE
               TX(II,J)=2.*DYY/DXX
      ENDIF
      IF(J .GT. 1) THEN
               TY(II,J)=DXX/DYY
```

```
      ELSE
            TY(II,J)=0.
      ENDIF
 50   CONTINUE
 51   CONTINUE
C     COMPUTATION OF AREAS
      DO 54 J=1,NY
C
C     Compute the Areas of the Upstream & Downstream Reservoir Grid Cells
      Vp=(3.14159)*(RAD**2)*H*POR
      ALFA=Vp/Vu
      BEETA=Vp/Vd
      AREA(1,J)=(1./ALFA)/NY
      AREA(NX,J)=(1./BEETA)/NY
C     Compute the Areas of the REMAINING Middle Grid Cells
      DO 53 I=1,NX-2
      II=I+1
      A1=(X(I,J)-X(I+1,J))*(Y(I,J)+Y(I+1,J))
      A2=(X(I+1,J)-X(I+1,J+1))*(Y(I+1,J)+Y(I+1,J+1))
      A3=(X(I+1,J+1)-X(I,J+1))*(Y(I+1,J+1)+Y(I,J+1))
      A4=(X(I,J+1)-X(I,J))*(Y(I,J+1)+Y(I,J))
      AREA(II,J)=0.5*ABS(A1+A2+A3+A4)
 53   CONTINUE
 54   CONTINUE
C
      SUM=0.
      WRITE(11,*) '   I','    J','   CELL AREA','        TX','
     *   TY'
      WRITE(11,*)
      DO 55 J=1,NY
      DO 55 I=1,NX
      IF(I .GT. 1 .AND. I .LT. NX) SUM=SUM+AREA(I,J)
      WRITE(11,200) I,J,AREA(I,J),TX(I,J),TY(I,J)
 200  FORMAT(2I5,4E14.6)
 55   CONTINUE
      WRITE(11,*)
      WRITE(11,*) 'TOTAL AREA   = ',SUM
      RETURN
      END

                    ----------------------
                        Subroutine EVAL
                    ----------------------

      SUBROUTINE EVAL(NPAR,A,IOPT,IOBS,FRQ,WT,E,DE,IEND)
C
      IMPLICIT REAL*8 (A-H,O-Z)
      PARAMETER (NCOEF=2,NCOL=2,NOBS=600,LDX=NOBS)
      DIMENSION A(NPAR),DE(NPAR)
      DIMENSION PP(LDX),PP1(LDX),PP2(LDX)
      COMMON /BLK6/ V(LDX,NCOL),NP
C
      PERM=A(1)
      BEE=A(2)
      IF(IOBS .EQ. 1 .AND. IOPT .EQ. 0) THEN
            CALL FUNEVL(PERM,BEE,NP,PP)
      ENDIF
      IF(IOBS .EQ. 1 .AND. IOPT .EQ. 1) THEN
            PERM=1.001*A(1)
            CALL FUNEVL(PERM,BEE,NP,PP1)
           PERM=A(1)
            BEE=1.001*A(2)
            CALL FUNEVL(PERM,BEE,NP,PP2)
      ENDIF
      IF(IOBS .LE. NP) THEN
            K=IOBS
            WT=1.0
```

```
                FRQ=1.0
                IEND=0
                IF(IOPT .EQ. 0) THEN
                        E=V(K,2)-PP(K)
                ELSE
                        DE(1)=-(PP1(K)-PP(K))/(0.001*A(1))
                        DE(2)=-(PP2(K)-PP(K))/(0.001*A(2))
                ENDIF
        ELSE
                IEND=1
        ENDIF
        RETURN
        END

                        -------------------------
                            Subroutine FUNEVL
                        -------------------------

        SUBROUTINE FUNEVL(PERM,BEE,NP,PC)
C
        INCLUDE 'PDSR-C1.COP'
        DIMENSION PC(LDX)
C
C       Initialize Pressure Distribution and Calculate Pore Volumes
        CALL INITAL
C       Print Input Data in .DIS file
        WRITE (13,100) NX,NY
 100    FORMAT(5X,'NUMBER OF GRID BLOCKS IN THE X-DIRECTION=',I3,
       &/,5X,'NUMBER OF GRID BLOCKS IN THE Y-DIRECTION=',I3)
C
C       Print Input Data & Titles in .DEC file
        WRITE(12,400)
        WRITE(12,450) TEMP,PU,PD,VU,VD,Vp,RAD,H,POR
        WRITE(12,*)
        WRITE(12,460)
        WRITE(12,470) PERM,BEE
        WRITE(12,*)
        WRITE(12,500)
        WRITE(12,*)
C
        NXY=NX*NY
        NX1=NX-1
        NY1=NY-1
        TD=0.
        NTS=0
C
C       TIME Loop Starts  H E R E
        DO 15 K=1,NP
        IFRST=0
        DO 10 L=1,NDT(K)
        DTr=DT(K)
        TD=TD+DTr
        NTS=NTS+1
C
        DO 5 J=1,NY
        DO 5 I=1,NX
        POLD(I,J)=P(I,J)
 5      CONTINUE
C
C       Calculate Properties
        CALL FUNC(DTr,PERM,BEE,DTD)
C       Compute Non-Zero Elements of the Matrices & RHS
        CALL COEFPO(DTD)
C       Solve for Pressure Distribution
        CALL SOLVEP(IFRST)
        IFRST=0
 10     CONTINUE
```

```
C     Compute Flowing Pressures
      CALL PWELL
      DPD=(PWF(1)-PWF(2))
      WRITE(12,200) TD,PWF(1),PWF(2),DPD
      NCTR=NCTR+1
      PC(K)=DPD
 15   CONTINUE
C     TIME Loop ends  H E R E
C
      WRITE(12,*)
C     Print Pressure Distribution
      CALL PRNT(NTS,TD)
C
 200  FORMAT (4F14.7)
 300  FORMAT (4I5,3F10.4)
 350  FORMAT (I5,2F10.4)
 400  FORMAT (2X,' Temp ',2X,' Pu ',4X,' Pd ',4X,' Vu ',7X,' Vd ',
     *7X,' Vp ',2X,' Rad ',2X,' H ',1X,' Por ')
 450  FORMAT (1X,F6.2,2F8.2,F9.2,e12.5,F8.2,2F6.2,F5.2)
 460  FORMAT (3X,'Permeability',3X,'Slip Factor')
 470  FORMAT (4X,F6.2,10X,F6.2)
 500  FORMAT (8X,' TD ',8X,' Pwf(1) ',5X,' Pwf(2) ',6X,' DPD ')
      NCTR=0
      RETURN
      END
```

Subroutine INITAL

```
      SUBROUTINE INITAL
C
C     THIS SUBROUTINE COMPUTES THE INITIAL PRESSURE DISTRIBUTION
C     & PORE VOLUMES
C
      INCLUDE 'PDSR-C1.COP'
C
C     Determine Initial Pressure Distribution
      DO 20 I=1,NX
      DO 20 J=1,NY
      IF(I .EQ. 1) THEN
               P(I,J)=PU
      ELSEIF(I .EQ. NX) THEN
               P(I,J)=PD
      ELSE
               P(I,J)=PD
      ENDIF
 20   CONTINUE
C     Calculate Pore Volumes of the Grid Blocks
      DO 40 I=1,NX
      DO 40 J=1,NY
      VPD(I,J)=AREA(I,J)
 40   CONTINUE
      RETURN
      END
```

Subroutine FUNC

```
      SUBROUTINE FUNC(DTr,PERM,BEE,DTD)
C
C     THIS SUBROUTINE CALCULATES THE PROPERTIES
C
      INCLUDE 'PDSR-C1.COP'
      DATA CZ1/-.196929D-04/,CZ2/.150321D-07/,CZ3/-.673225D-12/
      T=TEMP+273.
```

```
      V1=13.85*T**1.5/(T+102.)
C     Calculate Gas Viscosity, Compressibility Factor
C     & Gas Compressibility
C
      DO 20 I=1,NX
      DO 10 J=1,NY
      PR=P(I,J)
      PATM=PR/14.7
      DV=-0.12474+0.123688*PATM+1.05452E-3*PATM**2-1.5052E-6*PATM**3
      VG=1.E-4*(V1+DV)
      PZ=PR
      ZG=1.0+CZ1*PZ+CZ2*PZ**2+CZ3*PZ**3
      DZ=CZ1+2.*CZ2*PZ+3.*CZ3*PZ**2
      CG=1./PR-DZ/ZG
      F(I,J)=(P(I,J)+BEE)/(VG*ZG)
      G(I,J)=CG*P(I,J)/ZG
 10   CONTINUE
 20   CONTINUE
C     Calculation of Constants
      CF=1.47D4
      DTD=PERM*DTr/(CF*POR*(RAD**2))
      RETURN
      END
```

Subroutine COEFPO

```
      SUBROUTINE COEFPO(DTD)
C
C     THIS SUBROUTINE COMPUTES THE NON-ZERO ELEMENTS
C     OF THE MATRIX FROM THE GAS FLOW EQUATION
C
      INCLUDE 'PDSR-C1.COP'
C
      DO  5 I=1,NX
      DO  5 J=1,NY
      BXL(I,J)=0.0
      BYL(I,J)=0.0
      CXY(I,J)=0.0
      BXU(I,J)=0.0
      BYU(I,J)=0.0
 5    CONTINUE
C
      IF(NX .EQ. 1) GO TO 15
      DO 10 I=1,NX1
      DO 10 J=1,NY
      I1=I+1
      IF(I.EQ.1)THEN
               FH=F(I,J)
      ELSEIF(I.EQ.NX1)THEN
               FH=F(I1,J)
      ELSE
               FH=(2*(F(I,J)*F(I1,J))/(F(I,J)+F(I1,J)))
      ENDIF
      TT=-TX(I1,J)*FH
      BXL(I1,J)=TT
      CXY(I1,J)=CXY(I1,J)-TT
      CXY(I,J)=CXY(I,J)-TT
      BXU(I,J)=TT
 10   CONTINUE
C
 15   IF(NY .EQ. 1) GO TO 25
      DO 20 I=1,NX
      DO 20 J=1,NY1
      J1=J+1
      FH=(2*(F(I,J)*F(I,J1))/(F(I,J)+F(I,J1)))
```

```
      TT=-TY(I,J1)*FH
      BYL(I,J1)=TT
      CXY(I,J1)=CXY(I,J1)-TT
      CXY(I,J)=CXY(I,J)-TT
      BYU(I,J)=TT
 20   CONTINUE
C
C     Compute the RHS
 25   DIV=1.0/DTD
      DO 70 J=1,NY
      DO 70 I=1,NX
      TT=DIV*VPD(I,J)*G(I,J)
      TTP=TT*POLD(I,J)
      BXY(I,J)=CXY(I,J)+TT
      RHS(I,J)=TTP
 70   CONTINUE
      RETURN
      END
```

Subroutine SOLVEP

```
      SUBROUTINE SOLVEP(IFRST)
C
C     THIS SUBROUTINE SOLVES FOR THE PRESSURE DISTRIBUTION
C     USING STANDARD ORDERING WHEN IMPES METHOD IS USED
C
      INCLUDE 'PDSR-C1.COP'
      COMMON /BAND/A(MBLK),X(MXY),D(MXY),LOC(MXY)
      DATA NPASS/0/,EPS/.0001/
C
      IF(NPASS.EQ.1) GO TO 111
      NPASS=1
      NW1=NY
      NW2=2*NW1+1
      NN1=NXY-NW1
      NN2=NXY+NW1+2
      NBL=NXY*NW2-NW1*(NW1+1)
      LOC(1)=1
      DO 10 N=2,NXY
      N1=N-1
      IF(N .GT. NW1) GO TO 12
      LOC(N)=LOC(N1)+NW1+N
      GO TO 10
 12   IF(N .GT. NN1) GO TO 14
      LOC(N)=LOC(N1)+NW2
      GO TO 10
 14   LOC(N)=LOC(N1)+NN2-N
 10   CONTINUE
C     INITIALIZE MATRIX A TO ZERO
 111  CONTINUE
      IF(IFRST .GT. 0) GO TO 222
      DO 15 I=1,NBL
 15   A(I)=0.0
 222  CONTINUE
C     SET UP MATRIX A
      N=0
      DO 20 I=1,NX
      DO 20 J=1,NY
      N=N+1
      D(N)=RHS(I,J)
      IF(IFRST .GT. 0) GO TO 20
      L=LOC(N)
      A(L)=BXY(I,J)
      IF(I .EQ. 1) GO TO 21
      A(L-NW1)=BXL(I,J)
```

```
 21   IF(I .EQ. NX) GO TO 22
      A(L+NW1)=BXU(I,J)
 22   IF(J .EQ. 1) GO TO 23
      A(L-1)=BYL(I,J)
 23   IF(J .EQ. NY) GO TO 20
      A(L+1)=BYU(I,J)
 20   CONTINUE
C     SOLVE FOR A*X=D
      CALL GBAND (NXY,NW1,EPS,IERR,IFRST)
      N=0
      DO 70 I=1,NX
      DO 70 J=1,NY
      N=N+1
      P(I,J)=X(N)
 70   CONTINUE
      RETURN
      END
```

Subroutine GBAND

```
      SUBROUTINE GBAND(N,M,EPS,IERR,IFRST)
C
      INCLUDE 'PDSR-C1.COP'
      COMMON /BAND/A(MBLK),X(MXY),D(MXY),LOC(MXY)
C
      IERR=0
      J=1
      DO 10 I=1,N
      IE=M
      IF(I+M-N)21,21,22
 22   IE=N-I
 21   IEAUX=M
      IF(I-M)23,23,24
 23   IEAUX=I
 24   IE1=IE+IEAUX
      MBIG=IE
      J1=J+IE1
      J2=J1
      IF(IFRST.GT.0)GO TO 27
      IF(DABS(A(J))-EPS)25,25,27
 25   IERR=IERR+1
C     WRITE(2,*) J,A(J)
 27   IF(MBIG)10,10,26
 26   DO 20 J0=1,MBIG
      SS=A(J1)/A(J)
      IF(IFRST.GT.0)GO TO 35
      DO 30 K=1,MBIG
      J1K=J1+K
      JK=J+K
 30   A(J1K)=A(J1K) -A(JK)*SS
 35   CONTINUE
      IAUX=J0+I
      D(IAUX)=D(IAUX)-D(I)*SS
      IE=M
      IF(IAUX+M-N)31,31,32
 32   IE=N-IAUX
 31   IEAUX=M
      IF(IAUX-M)33,33,34
 33   IEAUX=IAUX
 34   IE1=IE+IEAUX
 20   J1=J1+IE1
 10   J=J2+1
      J=J-M-1
      NP1=N+1
      DO 40 IINV=1,N
```

```
      I=NP1-IINV
      IE=M
      IF(I+M-N)41,41,42
 42   IE=N-I
 41   MBIG=IE
      X(I)=D(I)
      IF(MBIG)44,44,43
 43   DO 50 K=1,MBIG
      IK=I+K
      JK=J+K
 50   X(I)=X(I)-X(IK)*A(JK)
 44   X(I)=X(I)/A(J)
      IE=M
      IF(I+M-NP1)51,51,52
 52   IE=NP1-I
 51   IEAUX=M
      IF(I-1-M)53,53,54
 53   IEAUX=I-1
 54   IE1=IE+IEAUX
      J=J-IE1-1
 40   CONTINUE
      RETURN
      END
```

Subroutine PWELL

```
      SUBROUTINE PWELL
C
C     THIS SUBROUTINE COMPUTES THE FLOWING PRESSURE IN FIRST
C      AND LAST CELL IN X-DIRECTION
C
      INCLUDE 'PDSR-C1.COP'
      DATA NW/2/
C
      NC(1)=NY
      NC(2)=NY
C     Setting the Location of Wells
      DO 5 J=1,NY
      L=1
      IW(L,J)=1
      JW(L,J)=J
      L=2
      IW(L,J)=NX
      JW(L,J)=J
 5    CONTINUE
C     Computation of Pwf(1) & Pwf(2)
      DO 10 L=1,NW
      SUMF=0.
      DO 20 N=1,NC(L)
      I=IW(L,N)
      J=JW(L,N)
      SUMF=SUMF+P(I,J)
 20   CONTINUE
      PWF(L)=SUMF/NC(L)
 10   CONTINUE
      RETURN
      END
```

```
                    ----------------------
                        Subroutine PRNT
                    ----------------------

      SUBROUTINE PRNT (NTS,TDP)
C
C     THIS SUBROUTINE PRINTS THE PRESSURE DISTRIBUTION
C
      INCLUDE 'PDSR-C1.COP'
      WRITE (13,100) NTS,TDP
      WRITE (13,200)
      I1=0
      I2=0
 10   I1=I2+1
      I2=I2+15
      IF (I2 .GT. NX) I2=NX
      WRITE (13,300) (I,I=I1,I2)
      DO 20 J=1,NY
      WRITE (13,400) J,(P(I,J),I=I1,I2)
 20   CONTINUE
      IF (I2 .LT. NX) GO TO 10
      WRITE (13,300)
      WRITE (13,300)
C
 100  FORMAT (/,5X,'TIME STEP NUMBER = ',I3,5X,'TIME = ',F14.5)
 200  FORMAT (/,15X,'PRESSURE DISTRIBUTION')
 300  FORMAT (/,7X,I2,14(5X,I3))
 400  FORMAT (1X,I2,15(1X,F7.3))
      RETURN
      END

                    ------------------------
                        Subroutine ERROR
                    ------------------------

      SUBROUTINE ERROR(XM,XC,N,M,SSE)
C
      IMPLICIT REAL*8 (A-H,O-Z)
      PARAMETER (NOBS=600)
      DIMENSION  XM(1),XC(1),E(NOBS)
      SUMER=0.0
      SUMEA=0.0
      SS=0.0
      SSR=0.0
      SSE=0.0
      SST=0.0
      SUMXM=0.0
      EMAX=0.0
      EMIN=1.0D9
      DO  10  K=1,N
 10   SUMXM    =SUMXM+XM(K)
      XMAVG    =SUMXM/N
      DO  20  I=1,N
      E(I)=0.0
      IF(XC(I) .NE. 0.) E(I)=100.0
      IF(XM(I) .NE. 0.) E(I)=100.0*(XM(I)-XC(I))/XM(I)
      SUMER=SUMER+E(I)
      SUMEA=SUMEA+DABS(E(I))
      SS   =SS   + E(I)*E(I)
      SSE  =SSE  +(XM(I)-XC(I))**2
      SSR  =SSR  +(XC(I)-XMAVG)**2
 20   SST  =SST  +(XM(I)-XMAVG)**2
      ER =SUMER/N
      EA =SUMEA/N
      NM = N-M-1
      SD=DSQRT(SS /NM)
      R2=1.0-SSE/SST
```

```
      F0=((SST-SSE)/M)/(SSE/NM)
      DO 30     K=1,N
      IF(DABS(E(K)).LT.EMIN ) EMIN = DABS(E(K))
      IF(DABS(E(K)).GT.EMAX ) EMAX = DABS(E(K))
 30   CONTINUE
      WRITE(17,700)
 700  FORMAT(/,7X,'ER',10X,'EA',6X,'MIN ER-',4X,'MAX ER+',4X,'SSE')
      WRITE(17,750)ER,EA,EMIN,EMAX,SSE
 750  FORMAT(4(1X,F10.3),1X,E10.3)
      WRITE(17,800)
 800  FORMAT(/,6X,'SSR',8X,'SST',10X,'SD',7X,'R**2',7X,'F0')
      WRITE(17,850)SSR,SST,SD,R2,F0
 850  FORMAT(2(1X,E10.3),2(1X,F10.4),1X,E12.4)
      RETURN
      END
```

Subroutine CONF

```
      SUBROUTINE CONF(A,SSE)
C
      IMPLICIT REAL*8 (A-H,O-Z)
      PARAMETER (NCOEF=2,NCOL=2,NOBS=600,LDX=NOBS)
      DIMENSION A(NCOEF),F(LDX,NCOEF),R(NCOEF,NCOEF)
      DIMENSION PP(LDX),PP1(LDX),PP2(LDX)
      COMMON /BLK6/ V(LDX,NCOL),NP
C
      PERM=A(1)
      BEE=A(2)
      CALL FUNEVL(PERM,BEE,NP,PP)
      PERM=1.001*A(1)
      CALL FUNEVL(PERM,BEE,NP,PP1)
      PERM=A(1)
      BEE=1.001*A(2)
      CALL FUNEVL(PERM,BEE,NP,PP2)
      SUMX=0.
      DO 10 K=1,NP
      SUMX=SUMX+V(K,1)
      F(K,1)=(PP1(K)-PP(K))/(0.001*A(1))
      F(K,2)=(PP2(K)-PP(K))/(0.001*A(2))
 10   CONTINUE
      XAVG=SUMX/(NP-1)
      SGMX=0.
      DO 20 I=1,NP
 20   SGMX=SGMX+(V(I,1)-XAVG)**2
C     CALCULATE THE CONFIDENCE LIMITS
      CALL DMXTXF (NP,NCOEF,F,LDX,NCOEF,R,NCOEF)
      CALL DLINRG (NCOEF,R,NCOEF,R,NCOEF)
      PROB=1.0 - 0.05/2.0
      DF = NP - NCOEF
      TSTAT=DTIN(PROB,DF)
      WRITE(17,100)
      DO 50 I=1,NCOEF
 50   WRITE(17,400) I,(R(I,J),J=1,NCOEF)
      WRITE(17,200)
      RMS=DSQRT(SSE/DF)
      DO 55 I=1,NCOEF
      DELA=RMS*DSQRT(DABS(R(I,I)))*TSTAT
      PERC=100.*DELA/DABS(A(I))
 55   WRITE(17,400) I,A(I),DELA,PERC
 100  FORMAT(/,5X,'INVERSE OF THE SENSITIVITY MATRIX')
 200  FORMAT(/,2X,'NO',5X,'PARAMETER    CONF. INTERVAL  CONF. INT.%')
 400  FORMAT(I4,5E15.6)
      RETURN
      END
```

Vita

Name:	**Hamid Jalal**
Address:	**8-G Rafah-e-Aam Housing Society Malir Halt, Karachi-75210, Pakistan.**
E-mail Address:	**hamid_jalal@yahoo.com**
Date of Birth:	**August 4, 1970**
Nationality:	**Pakistani**
Education:	**MS Petroleum Engineering King Fahd University of Petroleum & Minerals, Dhahran, Saudi Arabia BE Mechanical Engineering NED University of Engineering & Technology, Karachi, Pakistan.**
Graduation Dates:	**MS in Petroleum Engineering in April 2000 BE in Mechanical Engineering in January 1995**